OFFICE OF CIVILIAN RADIOACTIVE WASTE MANAGEMENT
ANALYSIS/MODEL COVER SHEET
Complete Only Applicable Items

1. QA: QA

2. ☒ Analysis — Check all that apply

Type of Analysis	☐ Engineering ☒ Performance Assessment ☐ Scientific
Intended Use of Analysis	☐ Input to Calculation ☒ Input to another Analysis or Model ☐ Input to Technical Document ☐ Input to other Technical Products

Describe use:

Abstracts CSNF rod failure for TSPA

Abstracts CSNF rod unzipping for TSPA

3. ☐ Model — Check all that apply

Type of Model	☐ Conceptual Model ☐ Abstraction Model ☐ Mathematical Model ☐ System Model ☐ Process Model
Intended Use of Model	☐ Input to Calculation ☐ Input to another Model or Analysis ☐ Input to Technical Document ☐ Input to other Technical Products

Describe use:

4. Title:

Clad Degradation – Summary and Abstraction

5. Document Identifier (including Rev. No. and Change No., if applicable):

ANL-WIS-MD-000007 REV 00

6. Total Attachments:

2

7. Attachment Numbers - No. of Pages in Each:

I-2, II-21

	Printed Name	Signature	Date
8. Originator	E. Siegmann	Eric R. Siegmann	4/25/00
9. Checker	H. Anderson	Robert Mockinnon for HA	4/25/00
10. Lead/Supervisor	R. Rechard	Robert Mockinnon for RR	4/25/00
11. Responsible Manager	R. MacKinnon	Robert Mockinnon	4/25/00

12. Remarks:

This document is associated with AMR F0155

References include citations of documents that are currently in progress. Approval of this AMR is dependent upon approval of supporting documents.

OFFICE OF CIVILIAN RADIOACTIVE WASTE MANAGEMENT
ANALYSIS/MODEL REVISION RECORD
Complete Only Applicable Items

2. Model or Analysis Title:

Clad Degradation – Summary and Abstraction

3. Document Identifier (including Rev. No. and Change No., if applicable):

ANL-WIS-MD-000007 REV 00

4. Revision/Change No.	5. Description of Revision/Change
REV 00	Initial Issue

CONTENTS

FIGURES

Page

TABLES

Page

LIST OF ACRONYMS

AMR	Analysis and Model Report
ASTM	American Society for Testing and Materials
BWR	Boiling Water Reactor
CCDF	Complementary Cumulative Distribution Function
CDF	Cumulative Distribution Function
CFR	Code of Federal Register
CPU	Central Processing Unit
CRC	Chemical Rubber Company
CRWMS	Civilian Radioactive Waste Management System
CSNF	Commercial Spent Nuclear Fuel
DCCG	Diffusion Controlled Cavity Growth
DHC	Delayed Hydride Cracking
DIRS	Document Input Reference System
DOE	U.S. Department of Energy
DTN	Data Tracking Number
EPRI	Electric Power Research Institute
ESB	Engineered Barrier Systems
FEP	Features, Events & Processes
IRSR	Issue Resolution Status Report
I-SCC	Iodine Stress Corrosion Cracking
KTI	Key Technical Issues
ISG	Interim Staff Guidance
LWR	Light Water Reactor
M&O	Management and Operating Contractor
MGR	Monitored Geologic Repository
NRC	U.S. Nuclear Regulatory Commission
PA	Performance Assessment
PAO	Performance Assessment Operations Department
PCI	Pellet Clad Interaction
PWR	Pressurized Water Reactor
QA	Quality Assurance
QARD	Quality Assurance Requirements and Description
SCC	Stress Corrosion Cracking
SS	Stainless Steel
TBD	To Be Determined
TBV	To Be Verified
TSPA	Total System Performance Assessment
TSPAI	Total System Performance Assessment and Integration
US	United States
WP	Waste Package
YMP	Yucca Mountain Project

1. PURPOSE

The purpose of this analysis is to develop the summary cladding degradation abstraction that is consistent with and used in the Total System Performance Assessment - Site Recommendation (TSPA-SR). This analysis is to describe the postulated condition of commercial Zircaloy clad fuel after it is placed in the Yucca Mountain Project (YMP) site (post-closure) as a function of time. Most commercial nuclear fuel is encased in Zircaloy cladding. This analysis is developed to describe cladding degradation from the expected failure modes. These include failure before receipt at YMP (reactor operation impacts including incipient failures; during spent fuel storage in pool and dry storage; and impacts due to transportation) and degradation in the repository (cladding creep, seismic failures, localized corrosion and cladding unzipping). This AMR does not address potential damage to assemblies that might occur at the YMP surface facilities. In accordance with AP-2.13Q, *Technical Product Development Planning*, a work plan (CRWMS M&O 1999a) was developed, issued, and utilized in the preparation of this document.

There are constraints, caveats and limitations to this analysis. This cladding degradation analysis is based on commercial Pressurized Water Reactor (PWR) fuel with Zircaloy cladding but is applicable to Boiling Water Reactor (BWR) fuel. Fuel reliability from reactor operation is determined for both PWRs and BWRs. This analysis is also limited to fuel exposed to normal operation and anticipated operational occurrences (i.e. events which are anticipated to occur within a reactor lifetime), and is not applicable to fuel that has been exposed to severe accidents. Fuel burnup projections have been limited to the current commercial reactor licensing environment with restrictions on fuel enrichment, oxide coating thickness, and rod plenum pressures. Ranges and uncertainties have been defined. The information provided in this analysis will be used in evaluating the post-closure performance of the Monitored Geologic Repository (MGR) in relation to waste form degradation.

2. QUALITY ASSURANCE

The Quality Assurance program applies to the development of this analysis documentation. The Performance Assessment Operations responsible manager has evaluated the technical document development activity in accordance with QAP-2-0, *Conduct of Activities*. The QAP-2-0 activity evaluation, *Conduct of Performance Assessment* (CRWMS M&O 1999b), has determined that the preparation and review of this technical document is subject to *Quality Assurance Requirements and Description* DOE/RW-0333P (DOE 2000) requirements. Note that the activity evaluation (CRWMS M&O 1999b) remains in effect even though QAP-2-0 has been superseded by AP-2.16Q, *Activity Evaluation*. This AMR was prepared in accordance with AP-3.10Q, *Analyses and Models.* Preparation of this analysis did not require the classification of items in accordance with QAP-2-3, *Classification of Permanent Items.* This activity is not a field activity. Therefore, an evaluation in accordance with NLP-2-0, *Determination of Importance Evaluations* was not required.

3. COMPUTER SOFTWARE USAGE

Microsoft Excel for Windows Version 4.0 was used in the analysis to develop a software routine. Excel is a commercially available software, and one macro was used. The software routine was run on a Dell Pentium personal computer (CPU number 111920) with a Windows 95 operating system. The software routine, including the one macro, is documented in Attachments I and II of this AMR in accordance with AP-SI.1Q, *Software Management*, Section 5.1.1. The software routine is contained in file "AMR-F0155-V1.xls" and the version number is one (1) as implied in the file name. This file is contained in Data Tracking Number (DTN: MO00004SPACLD07.043).

There were no models used in support of this analysis activity.

This AMR was documented using only commercially available software (Microsoft Word 97-SR2) for word processing, which is exempt from qualification requirements in accordance with AP-SI.1Q, *Software Management*. There were no additional applications (routines or macros) developed for documentation using this commercial software.

SigmaPlot, Scientific Graphic Software, Version 2.0, Jandel Corporation is used to plot data from the analysis. No calculations are performed with this software.

4. INPUTS

4.1 DATA AND PARAMETERS

This AMR summarizes several other AMRs and generates the cladding degradation abstraction that is to be used in the TSPA-SR. Much of the data used in this AMR and the cited AMRs is from published literature for Pressurized Water Reactor (PWR) fuel performance and the respective reference is cited where the data is used. These data are appropriate for describing commercial nuclear fuel since they are published descriptions of commercial fuels. The following AMRs or calculations supply input (with Data Tracking Numbers (DTNs) noted) to this AMR:

a) *Initial Cladding Condition* (CRWMS M&O 2000a).
Contains discussion and analysis of cladding condition as received at YMP.

Data supplied in DTN: MO0001SPAICC48.037.

1) Complementary Cumulative Distribution Function (CCDF) for rods perforated before receipt at Yucca Mountain Project (YMP) (Table 14), used in Section 6.1.
2) Rod stress distribution (Output table represented by Figure 26) file = Rod-Initial-C.xls, Sheet = "Crack", Cells = K15 through M2014, used in Section 6.2.2.
3) Dry storage and shipping temperature history: file = Rod-Initial-C.xls, Sheet = "Creep", Cells B25 through C39, used in Section 6.2.1.

b) *CSNF Waste Form Degradation: Summary Abstraction* (CRWMS M&O 2000d).
Intrinsic dissolution rate equation for basic and acidic conditions (Equation 16, 18, page 82) and Figure 12 of this AMR showing the intrinsic dissolution equation. Gap inventories for cesium and iodine as a function of fission gas release fraction. Roughness factors are taken from this reference.

c) *Clad Degradation – Wet Unzipping* (CRWMS M&O 2000e).
Equations for cladding wet unzipping (Equation 29) as a function of intrinsic dissolution rate. Distribution of ratio of unzipping speeds to intrinsic dissolution speeds. Molar volumes of metaschoepite and UO_2.

d) *Thermal History of Cladding in a 21-PWR SNF WP Loaded with Average Fuel,* (CRWMS M&O 2000f).

Design information ACC: MOL.20000216.0105.
Radial temperature distribution across the waste package (WP) and change in temperature in WP as a function of time. Peak internal WP temperatures from Table 6-2 are used in Section 6.2.1 for establishing uncertainties.

e) *Thermal Evaluation of Breached 21-PWR Waste Packages (*CRWMS M&O 1999e).

Design information ACC: MOL.20000120.0447.
Peak internal WP temperature profile from Table 6-7 used for establishing uncertainties. Used in Section 6.2.1.

f) *In-Drift Thermodynamic Environment and Percolation Flux* (CRWMS M&O 2000h).

Data Used for this AMR: DTN: SN0001T0872799.006.
Bin 4 average temperatures used in Section 6.2.1.
Bin 4 peak temperatures used to define waste package surface temperature uncertainties in Section 6.2.1.

g) *Comparison of Creep Correlations*. Input Transmittal PA-WP-0048.Ta. (CRWMS M&O, 2000j).

Design information used in this AMR: ACC: MOL.20000223.0002.
Uncertainty range of 80% for creep strain from Attachment Item 1, on the 503 item data table. Used in Section 6.2.2.

h) *Stainless Steel in Waste Packages for TSPA-SR.*(CRWMS M&O 2000k).

Data used from this AMR: DTN: SN0001T0810599.008.
WP fraction with stainless steel cladding and fraction of stainless steel in them. Used in Section 6.7.

i) *Breakage of Commercial Spent Nuclear Fuel Cladding by Mechanical Loading,* (CRWMS M&O 1999d).

Design information used from ACC: MOL.19991213.0237.
Frequency of seismic event that damages all cladding determined to be 1.1×10^{-6} events/year. This frequency is used in Section 6.4.1.

Outside sources of data include:

j) "Fracture Behavior and Microstructural Characteristics of Irradiated Zircaloy Cladding." *Special Technical Publication,* (Chung et al. 1987, Table 1 and 2, p. 780, 781).

Data used: DTN: MO9912SPASFC01.032.
Reported failure strain measurements used to develop CCDF for creep failure criterion. Used in Section 6.2.3.

k) *Results from NNWSI Series 1 Spent Fuel Leach Tests.* (Wilson, C.N. 1985, Tables 3 and 12) TIC: 210347.

Data used in DTN: MO0003SPATCR30.039.
Measurements of releases of technetium reported in cited tables used in Section 6.5.2 to predict fast release fraction for fuel.

l) *Results from Cycles 1 and 2 of NNWSI Series 2 Spent Fuel Dissolution Tests.* (Wilson, C.N. 1987, Tables 13, A.3, A.4, A.7, and A.8). TIC: 202294

Data used in DTN: MO0003SPATCR22.038.
Measurements of releases of technetium reported in cited tables used in Section 6.5.2 to predict fast release fraction for fuel.

m) *Results From NNWSI Series 3: Spent Fuel Dissolution Tests.*(Wilson, C.N. 1990, Tables 3.8, A.5, and A.6). TIC: 200816. ACC: NNA.19900329.0142.

Data used in DTN: MO0003SPATCR70.040.
Measurements of releases of technetium reported in cited tables used in Section 6.5.2 to predict fast release fraction for fuel.

n) *Report of the Committee to Review the Use of J-13 Well Water in Nevada Nuclear Waste Storage Investigations* (Harrar et al. 1990). ACC: NNA.19910131.0274.

Data used in DTN: LL980711104242.054.
Content of fluorides in J-13 water used to calculate fluoride corrosion rate from flow through geometry in Section 6.3. Alkalinity is used to calculate UO_2 dissolution rate in Section 6.5.2.

o) *CRC Handbook of Chemistry and Physics* (Lide 1995).

Accepted data from handbook in TIC: 216194.

The molar masses of H (1.00794 g/mol), C (12.011 g/mol) and O (15.9994 g/mol) taken from the inside cover are used to calculate fluoride corrosion rates in Section 6.5.2. Density of UO2, fluorine, and zirconium, taken from page 4-94 through 4-98, used in 6.3 and 6.5.2.

p) *Modeling of Zirconium Stress-Corrosion Cracking: Texture Effects and Dry Storage Spent Fuel Behavior* (Tasooji et al. 1984, p. 600, their Figure 3) TIC: 223247.

Data used from DTN: MO0003SPASSC24.041.
Reference Figure 3 shows stress threshold of 180 MPa is needed to fail cladding from stress corrosion cracking. This is used in Section 6.2.3 as a failure threshold.

4.2 CRITERIA

The U.S. Nuclear Regulatory Commission's (NRC's) Total System Performance Assessment and Integration (TSPAI) Issue Resolution Status Report (IRSR) (NRC 1998) establishes generic technical acceptance criteria considered by the NRC staff to be essential to a defensible, transparent, and comprehensive assessment methodology for the repository system. These regulatory acceptance criteria address four fundamental elements of the DOE TSPA analysis for the Yucca Mountain site, namely:

Data and analysis shall address their justification (The AMR shall focus on sufficiency of data to support the conceptual basis of the process analysis and abstractions)

1. The AMR shall address the data uncertainty and verification (focusing on technical basis for bounding assumptions and statistical representations of uncertainties and parameter variabilities)

2. Analysis uncertainty shall be addressed (focusing on alternative conceptual analysis consistent with available site data)

3. Analysis verification shall be addressed (focusing on testing of analysis abstractions using detailed process-level analysis and empirical observations)

4. Integration shall be addressed (focusing on appropriate and consistent coupling of analysis abstractions).

Relevant to the topic of this AMR, elements (1) through (4) of the acceptance criteria are addressed herein. Element (5) of the acceptance criteria, which strictly applies to the completed synthesis of process-level analysis and abstractions, will be addressed separately in the Total System Performance Assessment-Site Recommendation (TSPA-SR).

In addition, a second NRC IRSR Key Technical Issue: Container Life and Source Term (NRC 1999) establishes generic technical acceptance criteria used by the NRC staff for the waste form, with the cladding degradation abstraction being part of this Key Technical Issue (KTI). Section 7 describes how this AMR addresses the IRSR issues.

4.3 CODES AND STANDARDS

American Society for Testing and Materials (ASTM) Standard C1174-97–*Standard Practice for the Long-Term Behavior of Materials, Including Waste Forms, Used in Engineered Barrier Systems (EBS) for Geologic Disposal of High-Level Radioactive Waste* (ASTM 1997) is used to support the degradation analysis development methodology, categorize the analysis developed with respect to its usage for long-term TSPA, and relate the information/data used to develop the analysis to the requirements of the standard.

This AMR was prepared to conform with the above NRC TSPAI acceptance criteria, as well as the DOE interim guidance (Dyer 1999) which requires the use of specified Subparts/Sections of the proposed NRC high-level waste rule, 10 Code of Federal Register (CFR) Part 63 (64 FR 8640). Subparts of this proposed rule that are particularly applicable to data include Subpart B, Section 15 (Site Characterization) and Subpart E, Section 114 (*Requirements for Performance Assessment*). Subparts applicable to analysis are outlined in Subpart E, Sections 114 (*Requirements for Performance Assessment*) and 115 (*Characteristics of the Reference Biosphere and Critical Group*).

5. ASSUMPTIONS

5.1 CLADDING CONDITION AS RECEIVED

The assumptions from CRWMS M&O 2000a apply and are summarized below.

5.1.1 The Waste Packages (WP) will be loaded with spent fuel in the order of discharge of the fuel from the various reactors as a function of calendar years. This generates some variability in the fraction of rods failed within a WP. This loading sequence tends to place fuel with higher cladding failure rates into the same WP or consecutively loaded WPs and produces larger variations in rod failure fractions than would be expected if thermal blending were employed. This is a credible and reasonable assumption based on the fuel that current owners would be expected to ship first. (Section 6.1)

5.1.2 Each failed Pressurized Water Reactor (PWR) fuel assembly has an average of 221 rods and has an average of 2.2 failed fuel rods. The basis for the average of 2.2 failed fuel rods per failed assembly is described in the Initial Cladding Condition AMR (CRWMS M&O 2000a**)**. This failure value applies for the early years of nuclear reactor power operations in the US (the 1960s and 1970s) and the number of failed rods per failed assembly has decreased to be closer to one (1) today. It is reasonably bounding to apply this failure rate for all time since it increases the fuel available for unzippping. (Section 6.1)

5.1.3 All rods are exposed to the conditions of dry storage at the design temperature of the Castor Mark V (CRWMS M&O 2000a) cask. Best estimate dry storage temperatures were not available at the time of this AMR, therefore the design temperature of the

Castor Mark V cask with 55 MWd/kgU burnup fuel was selected to be reasonably bounding since actual temperatures are lower than design temperatures. (Section 6.2.1)

5.1.4 All rods are exposed to the temperature conditions in a shipping cask for three weeks at 350°C. This is a reasonable upper limit as 350°C is the peak design basis temperature for all rods during shipment. Most rods will actually be exposed to lower temperatures for a shorter time frame during shipment. (Section 6.2.1)

5.1.5 The uncertainty value for the rod failure data is four (4). This is based on a square pitch array of fuel rods in the fuel assembly. The rods more likely to have damage are these rods near the damaged rod. There are four rods near the damaged rod in a square pitch. This is bounding when compared to operating experience which shows reliability improves with time in reactor (little incipient failures). (Section 6.1)

5.1.6 BWR cladding degrades in a similar manner as the base case PWR fuel. This is reasonably bounding since, in comparison to PWR fuel, the BWR cladding is thicker, the BWR fuel typically is discharged with lower burnups and stresses, and each BWR fuel assembly is enclosed in a flow channel for additional protection. (Section 6.1)

5.1.7 It is assumed that no further cladding degradation occurs at the YMP surface facilities. This is accomplished by appropriate operating and administrative procedures. Sufficient care will be exercised in these facilities such that damaging the cladding which would lead to radionuclide contamination, higher operating expenses, and greater radiation risk to employees, does not occur. (Section 7)

5.2 CREEP AND SCC FAILURE

5.2.1 Creep is analyzed using Murty's correlation. Both Murty's correlation and Matsuo's correlation (Matsuo 1987, p. 23) fit the available data almost equally well. Murty's correlation was selected because it explicitly considers Coble Creep, a type of creep that could be important at lower stresses and temperatures. The uncertainty in the creep correlation is 0.80, the maximum error range for Murty's correlation. The uncertainty is assumed to be uniformly distributed with the calculation of creep for all the rods and varies in the range of ±80%. (Section 6.2.2)

5.2.2 The creep failure distribution is determined by a series of tests by Chung et al. (1987). Chung et al. (1987) did a series of 20 burst tests with irradiated cladding and in 18 of these tests measured an average strain at failure of 3.3% with a range of 0.4% to 11.7%. They also did scanning electron microscope inspection of the failures. The inspection identified over half the failures as occurring at cracks. Four of the tests were on BWR fuel which showed a lower failure strain. The use of this failure criterion accounts for both crack damage and possibly weaker cladding types (i.e. BWR fuel). (Section 6.2.3)

5.2.3 Any rod with a stress greater than 180 MPa is assumed to fail from Stress Corrosion Cracking (SCC). This is based on both experiments and analysis presented by Tasooji et al. (1984, p. 600, their Figure 3). In this AMR, sufficient iodine is assumed to exist

such that SCC occurs at the stress threshold of 180 MPa. This is a bounding assumption. (Section 6.2.2)

5.3 LOCALIZED CORROSION

5.3.1 It is assumed that corrosion of the cladding is limited by the supply of fluoride. The rationale for this assumption is that little information is available on the rate of consumption of fluoride in a waste package. In the absence of information, a bounding approach is needed. Since the assumption is an upper limit, no confirmation is necessary. (Section 6.3)

5.3.2 Fluoride attack is assumed to completely degrade the cladding on a 10 mm length of one fuel rod before degradation begins on another rod. This length represents a reasonable drip width. The rationale for this assumption is that little information is available on how corrosion is distributed within a waste package. This assumption is reasonably bounding because each rod breaches as soon as enough fluoride is available; there is no delay in breaching one rod because fluoride is being diverted to start the degradation of another. Since the assumption is a reasonable bound, no confirmation is necessary. (Section 6.3)

5.3.3 It is assumed that all fuel rods are subject to fluoride corrosion. The rationale for this assumption is that little information is available on how water flows within a waste package. This assumption is a reasonable bound because each rod is exposed to water and therefore subject to fluoride corrosion. Under many exposure conditions, some of the fuel rods would be out of the flow path. In those cases, only the fuel rods in the flow path would be subject to fluoride corrosion. Since the assumption is an upper limit, no confirmation is necessary. (Section 6.3)

5.3.4 In determining the amount of fluoride that is necessary to breach a fuel rod, it is assumed that fluoride removes all the cladding from a 10-mm length of the fuel rod. The rationale for this assumption is that this width is comparable to the width of typical water drop splat sizes and water flow paths. However, the actual wetted width would be wider because the rough, porous products of corrosion on the surface of fuel rods would tend to wick water and promote wider flow paths. Since this assumption is a reasonable bound, it does not require verification. (Section 6.3)

5.4 OTHER FAILURE MECHANISMS

5.4.1 Seismic analysis showed that rods would fail from a very severe earthquake (a once per million years event) and that most of the rods would fail. Therefore, in the TSPA-SR, the seismic event is assumed to have a frequency of 1.1×10^{-6} /yr and it is assumed that all the cladding is failed at the rod center and available for clad unzipping when a seismic event occurs. Failing all the rods is an upper limit and failing the rods in the center minimizes the release time for unzipping. (Section 6.4.1)

5.5 FAST RELEASE OF RADIONUCLIDES

5.5.1 It is assumed that the absolute rate of fast release of radionuclides from a breached fuel rod is proportional to the length of the rod. Results for short rod segments are used to predict the performance of full-length rods, and the same fractional release rate is used for both. The rationale for this assumption is that, over the time necessary to plug the cracks in a fuel rod, the characteristic distance for aqueous diffusion is comparable to the active length of a fuel rod (Section 6.5.2). The assumption could be inaccurate if transport limitations result in smaller release rates, and in that case the assumption would be reasonably bounding. Since this assumption is both realistic and a reasonable bound, it does not require verification. (Section 6.5)

5.5.2 It is assumed that, during the fast release phase, the fuel reacts with water to form metaschoepite. This assumption is consistent with a similar assumption for the unzipping phase. Reaction products with a large volume increase would tend to produce small fast release fractions (because cracks would plug quickly) and fast unzipping, whereas reaction products with a small volume increase would tend to produce larger fast release fractions and slower unzipping. However, the fast release fraction is small, so it is reasonably bounding to favor fast unzipping. Since the assumption is reasonably bounding, no confirmation is necessary. (Section 6.5)

5.6 CLADDING UNZIPPING AND FUEL DISSOLUTION

5.6.1 It is assumed that, during the unzipping phase, the fuel reacts with water to form metaschoepite. Oxidation and hydration of uranium dioxide can result in a variety of mineral species. Of these, metaschoepite is the one that entails the largest change in volume, and larger volume increases correspond to faster degradation. Other uranium minerals (such as sodium boltwoodite) can also be formed from uranium dioxide, but these require a supply of a solute (such as sodium), so the rate of formation will be limited by the supply of solute. Therefore, the rationale for this assumption is that conversion to metaschoepite provides the largest plausible volume increase. Since the assumption is reasonably bounding, no confirmation is necessary. (Section 6.6)

5.6.2 It is assumed that the rate of reaction of the uranium dioxide with water is controlled by the intrinsic dissolution rate of UO_2. The rationale for this assumption is that this is the fastest rate at which reaction can advance into a uranium dioxide pellet surface. If the products of reaction of UO_2 limit the transport of water to the uranium dioxide surface, the reaction will necessarily be slower. Since this assumption is reasonably bounding, no confirmation is necessary. (Section 6.6)

5.6.3 It is assumed that all cladding breaches occur at the center of the active fuel length. The rationale for this assumption is that this location provides the fastest unzipping of a fuel rod. If the breach is at the center of the active fuel length, propagation of the breach by a distance of half the active fuel length (toward each end) will result in complete unzipping of the active fuel length of the rod. If the breach is at some other location, the required propagation distance will be larger for one end. Since this assumption is reasonably bounding, no confirmation is necessary. (Section 6.6)

5.7 STAINLESS STEEL CLADDING

5.7.1 The stainless steel (SS) clad fuel is loaded into WPs as it is received at the YMP facilities. This is used to define the number of WPs containing SS cladding and the fraction of SS cladding in these WPs. The basis of this assumption is that it simplifies surface facility operations. This assumption is not critical since the product of WPs containing SS cladding and fraction of SS in each WP is constant (i.e. there is a fixed amount of SS cladding). (Section 6.7)

6. ANALYSIS

Earlier studies (Ahn et al. 1999, Henningson 1998, Rothman 1984, Pescatore et al. 1990, Manaktala, 1993) have evaluated cladding degradation under repository conditions. Others (Cunningham et al. 1987, Peehs 1998, Einziger and Kohli 1984) evaluated fuel performance under dry storage conditions, which are similar to early repository conditions. As part of the Environmental Protection Agency's development of environmental standards, S. Cohen & Associates (1999) did a detailed study of cladding degradation, both before reception at a repository and in the repository. Sanders et al. (1992) reviewed the condition of cladding after reactor operation and reviewed the potential of damage from external mechanical loading. Experiments (Wilson 1985, 1987, 1990) also measured the releases from damaged cladding. The Yucca Mountain Project (YMP) 1998 Total System Performance Assessment Viability Assessment (TSPA-VA) included cladding degradation as part of the fuel degradation analysis. TSPA-1995, a previous analysis of repository performance, neglected the presence of cladding, as did most earlier performance assessments (PAs). In doing so, all the fuel in the Waste Package (WP) was considered available for dissolution at the speed of the intrinsic fuel dissolution rate. For some radionuclides, solubility limits were reached which controlled the rate of those radionuclides' leaving the WP. In the Total System Performance Assessment Site Recommendation (TSPA-SR), the cladding is considered an integral part of the waste form.

The cladding degradation abstraction summarizes numerous studies of cladding degradation and is incorporated into the TSPA-SR computer analysis as an abstraction. The abstraction consists of two phases, cladding perforation and cladding unzipping. Cladding perforation is the formation of small cracks or holes in the cladding from various sources ranging from failures during reactor operation to cladding creep rupture during repository storage. Perforation permits the fuel inside the cladding to begin to react with moisture or air and potentially leads to the cladding unzipping phase. In the unzipping phase, the cladding is torn open by the formation of secondary mineral phases on the UO_2 fuel, and the radionuclides are available for release. The various components of the abstraction are discussed below.

The numbers reported in this section are given to three (3) figures to assist in making the numbers more traceable. This analysis is considered accurate to only the first significant figure, that is, accurate to approximately 80% to 90%. The remaining figures are only reported for traceability.

6.1 CLADDING CONDITION AS RECEIVED

The Initial Cladding Condition AMR (CRWMS M&O 2000a) describes the condition of the commercial nuclear fuel as it is expected to be received at the YMP site. This analysis generates the initial boundary condition for the subsequent analysis of degradation of the cladding in the repository. It also evaluates the fraction of fuel rods that are perforated before emplacement in the repository and are immediately available for cladding unzipping when the WP fails.

A distribution for the fraction of cladding within a WP that failed as a result of reactor operation was developed from the fraction of rods failed as a function of calendar years by assuming that the fuel assemblies are loaded into WPs in their order of discharge from the reactors. This is the Complementary Cumulative Distribution Function (CCDF) shown in Table 1. This loading sequence tends to place fuel with high failure rates (BWR fuel in 1970 and also in 1973-1976, and PWR fuel in 1972, 1983, and 1989) into the same or consecutive WPs and produces larger variations in rod failure fractions than would be expected if thermal blending were employed. A factor of four uncertainty was applied to represent the uncertainty in rod failure data. Rod failure from dry storage (0.045% of rods failed per WP) and transportation (vibration and impact, at 0.01% of rods failed per WP) were also included (CRWMS M&O 2000a, Section 7). Failure from creep during dry storage and transportation is included with the creep analysis presented in Section 6.2 of this AMR. Table 1 gives the distribution of rods that have failed cladding at emplacement in the repository. This table is the same as Table 14 of CRWMS M&O 2000a and is given in the Excel file: fuel-rel.xls, cells G112 through J134 of DTN: MO0001SPAICC48.037. In the TSPA-SR, the WPs are grouped into 5 bins, each representing approximately 1500 CSNF WPs. Table 1 represents the distribution of individual WPs and cannot be applied to the individual bins because of the limited number of WPs represented by the distribution tail. For example, the very far point of the distribution is represented by the BWR fuel discharged in 1970 with 4.5% of the rods failed. That year, only 29 assemblies were discharged, about 70% of a single BWR WP containing 44 assemblies. In sampling for a bin or group of 1500 WPs, it would be incorrect to represent the whole group by an individual WP that exists in such small numbers. For the TSPA-SR abstraction of bins or groups, the bins are represented by the 98% to 5% range of the CCDF in Table 1 with the median representing the best estimate. A triangular distribution was assigned. In summary, the initial failure percentage for the rods in a WP in the TSPA-SR for the five bins or groups of WPs is represented by:

Minimum = 0.0155%
Best Estimate = 0.0948%
Maximum = 1.285%

and the probabilistic distribution is triangular. These percentages of fuel rods undergo cladding unzipping and fuel dissolution when the WP fails.

As received at YMP, the cladding of rods that are not perforated also has an internal pressure resulting from reactor operation and therefore will be stressed. The creep strain calculations in this AMR use the stress distribution developed in the Initial Cladding Condition AMR (CRWMS M&O 2000a, file = Rod-Initial-C.xls, Sheet = “Crack”, Cells = K15 through M2014). The cladding analysis is based on the Westinghouse 17 x 17 fuel design. This design represents over 30% of the PWR fuel discharged to date and is also the thinnest Zircaloy cladding design. The BWR cladding degrades in a similar manner. This is reasonably bounding since BWR cladding

is thicker, is discharged with lower burnups and stresses, and is enclosed in flow channels for additional protection. Starting with a distribution of PWR fuel burnups that are anticipated for storage at YMP, distributions for various cladding properties were developed, culminating with the room temperature stress distribution represented by Figure 1.

Table 1. CCDF of Rod Perforation for As-Received Fuel

CCDF	Lower Uncertainty.	Best Estimate % Failure	Upper Uncertainty
1.000	0.0138	0.0550	0.220
0.999	0.0146	0.0585	0.234
0.985	**0.0155**	0.0622	0.249
0.856	0.0179	0.0717	0.287
0.655	0.0212	0.0849	0.340
0.582	0.0224	0.0895	0.358
0.506	0.0237	**0.0948**	0.379
0.271	0.0284	0.1136	0.454
0.1966	0.0361	0.1445	0.578
0.1084	0.0507	0.2028	0.811
0.0970	0.0522	0.2089	0.836
0.0766	0.0741	0.2965	1.186
0.0640	0.0746	0.2983	1.193
0.0503	0.0803	0.3213	**1.285**
0.0373	0.1248	0.4990	1.996
0.0323	0.247	0.9875	3.95
0.0221	0.289	1.1568	4.63
0.0196	0.450	1.7985	7.19
0.0190	0.509	2.035	8.14
0.0115	0.694	2.776	11.10
0.0036	0.763	3.051	12.20
0.0002	1.321	5.286	21.14
0.0000	1.321	5.286	21.14
DTN: MO0001SPAICC48.037			

6.2 CREEP STRAIN AND SCC FAILURE

The current repository design utilizes backfill, which affects the temperatures. A statistical distribution of rod properties has been developed so that creep failure is included in the analysis. All the rods are assumed to be exposed to a temperature history that includes 20 years of dry storage, three weeks of transportation and then a temperature profile for storage in the repository. Rods at six zones across the WP are evaluated, and Murty's creep strain correlation is used. The failure strain criterion is a distribution based on eighteen tests of irradiated cladding. The peak surface temperature of the WP is varied and the fraction of rods failed is calculated. The following sections discuss the analysis in more detail.

6.2.1 Temperature History

The rods are exposed to a temperature history that includes 20 years of dry storage starting at 350°C and then decreasing during dry storage plus an additional three weeks of transportation at 350°C (CRWMS M&O 2000a, Section 6.10.1, cladding initial condition data, file = Rod-Initial-C.xls, Sheet = "Creep", Cells B25 through C39). Best estimate dry storage temperatures were not available at the time of this analysis and the peak (center rod) temperature history for the Castor V package with 55 MWd/kgU fuel (Peehs 1998, Figure 13a) was used in this analysis. These temperatures were given for the first ten years and have been extrapolated to 20 years. In addition, a three-week period of temperatures at 350°C has been added to represent design bases shipping temperatures. It is reasonably bounding to use the peak design bases temperatures for all rods since most will actually see lower temperatures.

For storage in the WP, the temperature distribution across the WP was obtained from CRWMS M&O 2000f. These temperatures are reproduced in AMR-F0155-V1.xls, Sheet "TempC2", Cells = D5 through U44. This temperature distribution varies both radially across the WP and with time. Figure 2 shows the location of the different temperature nodes. The WP internals were divided into 6 zones, which are also shown in Figure 2. An estimate of the fraction of each assembly in each zone is made by visual inspection of Figure 2. Table 2 gives the fraction of rods in each zone and the temperature nodes used to calculate the zone temperature. The temperature of the WP surface was obtained from CRWMS M&O 2000h. Temperatures for 5 bins, grouped by water ingression, were supplied in CRWMS M&O 2000h and are shown here as Figure 3. The bin numbers are assigned by increasing water ingression rate with Bin 4 representing 20 to 60 mm/year water ingression. This AMR uses Bin 4 with water ingression in the range of 20 to 60 mm/yr. Bin 4 has one of the widest temperature peaks and therefore could produce the most creep but, more importantly, it also represents over 53% of the WPs. Figure 4 shows the WP surface temperature, temperature increase across the WP, and center rod temperature. Figure 5 shows the total center rod temperature profile used for the creep analysis. This profile (reading from left to right) shows dry storage for 20 years starting at 350°C, three (3) weeks of shipping at 350°C, preclosure with forced ventilation for 50 years, and then the postclosure temperature profile. This profile extends for 1000 years although only 200 years are shown on the figure. All rods undergo identical dry storage and shipping conditions. The creep analysis of the different phases of the life cycle of the rods must be integrated so that the creep components from the various stages (dry storage, shipping) are added. Creep failures during dry storage are combined with the creep failures during shipping because the damage is cumulative.

Table 2. Fuel Rod Zones in a WP

Zone	Assemblies	Fraction of Rods	Temperature Nodes	Temperature (^{o}C) Scaling Factor
1	0.4	0.019	1	1.000
2	0.6	0.029	Avg, 1 & 2	0.933
3	2.4	0.114	Avg, 5 & 6	0.888
4	4.4	0.210	Avg, 6 & 7	0.820
5	7.0	0.333	Avg, 9 & 10	0.661
6	6.2	0.295	Avg,10 & 11	0.446
Sum	21	1.0	N/A	N/A

DTN: MO00004SPACLD07.043

Temperature uncertainties are also included in the creep strain analysis. The difference between the maximum WP surface temperature for Bin 4 and the average WP surface temperature is 22.1°C (CRWMS M&O 2000h) (see Figure 7 of this AMR). The uncertainty in WP internal temperature was 19.5°C (at peak times), which is the difference in peak temperature between a helium filled WP (CRWMS M&O 2000f, p. 29) and an air/water vapor filled WP (CRWMS M&O 1999e, p. 38). These differences sum to 41.6^{o}C and represent an uncertainty of 13.5% above the peak temperature for the average WP of 308°C. The uncertainty is uniformly distributed with a range of " 13.5%. The uncertainty in the WP internal power was neglected because of the small predicted uncertainty (CRWMS M&O 1999c, Item 1, p.1/1)

The creep analysis is performed for 12,000 fuel rods. The initial room temperature stress as received at YMP for each of 2000 rods is determined from the CCDF in Figure 1. A rod with each of these 2000 initial stresses is then placed into each of the six WP zones (totaling 2000 rods/zone x 6 zones = 12,000 rods) and is exposed during repository storage to the temperature profile predicted for that particular zone (with uncertainty included). The temperature scaling factors to calculate the temperature of a rod in each zone are given in Column 5 of Table 2. The temperature of the center rod is multiplied by this factor to calculate the rod temperature for each zone. The uncertainty is then applied for each rod in each zone. The temperature uncertainty is uniformly distributed over a range of " 13.5%.

The center rod in an average WP peaks at 308^{o}C at 53 years, three years after closure. At this time, the outer rods peak at 291^{o}C and the WP surface temperature is 277^{o}C. After an additional 50 years, the center rod has cooled to 226^{o}C and the outer rod is 215^{o}C. The hottest center rod will peak at 350^{o}C (13.5% above 308^{o}C) while the hottest outer rod will peak at 314^{o}C (see Attachment II, Table II-10a).

In generating the failure probability distribution for stress and SCC, the WP peak surface temperature is treated in this analysis as an independent variable and failures are predicted for various WP peak surface temperatures. In the TSPA-SR for each realization, the WP peak temperature will be established and then creep and SCC rod failure fractions will be looked up on a table.

6.2.2 Creep Strain and SCC Correlation

CRWMS M&O 2000j compares the creep predictions using six (6) different creep correlations to the results from five (5) different experiments (Tables 3 and 4). The tables give the relative error, that is the absolute value of the difference between the calculated and measured values divided by the measured values [Abs((Calculated-Measured)/Measured)]. Using relative error as a measurement, the smaller numbers represent the better fit. The five (5) different experiments were for unirradiated material, with the temperature range: 250°C < T°C < 385°C, and the stress range: 55 MPa < Stress < 120 MPa. There were a total of 503 reported strain measurements, many of which were obtained at intermediate times in the analysis and 95 of which were at end points (last measured strain). Table 3 compares the equations for all the data points, including the intermediate and end points. Both Murty's correlation and Matsuo's correlation fit the data approximately equally well. Murty's correlation was selected because it explicitly considers Coble creep, a type of creep that could be important at lower stresses and temperatures and that might not have been observed in the ranges of these experiments. Table 4 compares the fit at the end points (last measured strain) for each of the 95 analyses. This prediction is more important for this AMR because failure is predicted for the larger creep strains, for which the end points of the analyses should be more representative. It is important to note that the experimental ranges, 250°C < T°C < 385°C and 55 MPa < Stress (MPa) < 120 MPa are close to the upper end of repository conditions shortly after closure. Some of these tests also ran for 10,000 hours (1.1 years) (CRWMS M&O 2000j, p.II-1). Again, Murty's correlation gives one of the better fits and will be used for creep failure calculations. For Murty's correlation, the uncertainty in the creep correlation for all 503 data points ranges from 0.283 to 0.727 and with a weighted average of 0.557 (Table 3). The uncertainty used in the creep correlation is 0.80 (0.727 rounded upward) uniformly distributed with the calculated creep for each of the 12,000 rods and varies in the range of +/- 80% of the calculated value.

Table 3. Comparison of Relative Error of Creep Correlations for All Data Points *

		Creep Correlations					
Ref.[2]	**Total Data Points[1]**	**Matsuo**	**Murty**	**Mayuzumi**	**Limback**	**Spilker**	**Peehs**
Spilker, T2	192	0.758	0.727	0.648	0.560	0.344	0.726
Spilker, T3	240	0.340	0.482	0.901	1.779	2.256	0.546
Matsuo	21	0.135	0.392	0.640	0.557	1.994	0.521
Mayuzumi	31	0.282	0.283	0.121	0.477	1.291	0.579
Limback	19	0.334	0.417	0.142	0.145	1.354	0.596
Weighted Average	N/A	0.487	0.557	0.717	1.121	1.431	0.606

NOTE: *Values are: Absolute Value [(Calculated-Measured)/Measured]

[1]Total number of points : 503

[2]Tests: unirradiated material, over the range 250≤T (C) ≤385 and 55≤ Stress (Mpa) ≤ 120

(MOL.20000223.0002)

Table 4. Comparison of Relative Error of Creep Correlations for Experimental End Points *

		Creep Correlations					
Ref.[2]	Total Data Points[1]	Matsuo	Murty	Mayuzumi	Limback	Spilker	Peehs
Spilker, T2	32	0.780	0.669	0.603	0.581	0.166	0.773
Spilker, T3	40	0.294	0.339	0.834	2.533	1.871	0.674
Matsuo	15	0.092	0.823	2.886	0.931	3.042	0.296
Mayuzumi	4	0.338	0.133	0.148	0.993	1.099	0.624
Limback	4	0.411	0.340	0.134	0.147	0.980	0.680
Weighted Average	N/A	0.432	0.518	1.022	1.457	1.232	0.634

NOTE: *Values are: Absolute Value [(Calculated-Measured)/Measured]

[1]Total number of points : 95

[2]Tests: unirradiated material, over the range 250≤T (C) ≤385 and 55≤ Stress (Mpa) ≤ 120 (MOL.20000223.0002)

The Murty correlation is described in Henningson (1998, Section 4, pp. 51 to 61) and the recommended equations (Henningson 1998, p. 57) are reproduced below. Hoop creep characteristics of Zircaloy tubing were collected at temperatures between 316°C and 427°C and at stress levels in the range of 55 MPa to 235 MPa. Three different sets of experimental data were used by Murty in generating the equations. The equations combine a high-stress creep mechanism of glide creep with a low-stress creep mechanism of Coble creep:

$$\dot{e}_{Glide} = 4.97 x 10^{6} e^{-31200/T} \frac{E}{T} [\sinh(807 \frac{s}{E})]^{3} \quad \text{(Eq. 6.2-1)}$$

$$\dot{e}_{Coble} = 8.83 e^{-21000/T} \frac{s}{T} \quad \text{(Eq. 6.2-2)}$$

Glide creep strain:

$$e_{glide} = \dot{e}_{gli\ de} t + \frac{k e_T \dot{e}_{gli\ de} t}{e_T + k \dot{e}_{gli\ de} t} \quad \text{(Eq. 6.2-3)}$$

Coble creep strain:

$$e_{Coble} = \dot{e}_{Coble} t \quad \text{(Eq. 6.2-4)}$$

Total creep:

$$e = e_{glide} + e_{Coble} \quad \text{(Eq. 6.2-5)}$$

Various parameters and constants include:

$\varepsilon_T = 0.008$,

$\kappa = 10$

$E = (1.148 \times 10^5 - 59.9T) \times 10^6$, Young's Module, Pa (T in K) (Eq. 6.2-6)

T = temperature (K)

σ = stress (Pa)

t = time (hours)

The above equations calculate the creep for a specific time at a constant temperature. To calculate creep strain for a rod exposed to the temperature history shown in Figure 5, the temperature history is divided into finite intervals and a time hardened technique recommended by Murty (Henningson 1998, p. 57, equation 15) and given below is used:

$$\varepsilon(t_i) = \varepsilon(T_{i-1}, t_{i-1}) + [\varepsilon(T_{i,} t_i) - \varepsilon(T_i, t_{i-1})] \quad \text{(Eq. 6.2-7)}$$

Where the subscript i-1 represents the previous time step and the subscript i represents the current time step. This is necessary because the creep rate for a constant temperature starts out very fast (primary creep) and then decreases to a slower secondary creep rate. If Equations 6.2-2 through 6.2-6 were applied separately to each time step, the primary creep would never saturate and the total creep would be over-predicted and also would be dependent on the number of time steps (number of times that the primary creep calculation was started). The actual analytical method and the software routine are discussed in Attachment II.

This creep correlation is for unirradiated cladding. Its use for irradiated cladding is reasonably bounding. Peehs (1998, Figure 10) compares the creep for irradiated and unirradiated cladding and shows that the creep for irradiated cladding is about half (1/2) that of unirradiated cladding.

The analysis presented in this section is based on an empirical creep equation developed by Murty. Many of the alternative equations are discussed by Pescatore and Cowgill (1994, pp. 47-86). One equation discussed is the Diffusion Controlled Cavity Growth (DCCG). Pescatore and Cowgill (1994, p. 83-85) concludes that the DCCG has not been validated against cavity data and voids or cavities are very infrequently seen in irradiated Zircaloy. He recommends (p. 85) a methodology similar to the approach used here. Commercial power plant dry storage license applicants were once required by the NRC to use the DCCG method to evaluate dry storage designs. The current NRC Interim Staff Guidance (ISG) - 11 (NRC 2000) recognizes the controversy with this conceptual method and permits commercial power plant license applicants to use other creep equations and methods in their license application. The use of Murty's correlation is consistent with this ISG.

For SCC failures, no detailed analysis of iodine concentrations or crack velocities is used. The maximum rod stress is compared with a threshold SCC stress and failure is predicted if the rod stress exceeds the threshold stress.

6.2.3 Creep and SCC Failure Criterion

To estimate the percent of the rods that will fail from creep, a creep failure criterion must be established. For this, data from Chung et al. (1987, pp. 780-781) will be used. Chung et al. (1987) conducted a series of 20 slow pressure burst tests and mandrel tests with irradiated cladding. Four tests were on BWR Zircaloy 2 cladding with a burnup of 22 MWd/kgU and the remaining tests were on PWR Zircaloy 4 cladding with a burnup of 28 MWd/kgU. For 18 tests, they reported strains at failure which averaged 3.3% with a range of 0.4% to 11.7%. They also conducted scanning electron microscope inspection of the failures and found evidence that, in 11 of the tests, the failures occurred at cracks formed in the cladding. The use of these results for a failure criterion addresses the potential for lower failure strains from pre-existing internal cracks and the situation that failure might not be a pure material creep. Figure 6 gives the CCDF for the creep failure criterion. This CCDF is sampled for each of the 12,000 rods analyzed (2,000 rods/zone x 6 zones). The lower 4 creep failures in the CCDF are for BWR fuel and are applied in the PWR rod analysis. This failure criterion does not address potential changes in the failure strain criterion with strain rate. The strain rates in Chung's gas pressurization experiment are such that the tests extended for periods of 1 to 312 hours with an average of 152 hours. The mandrel test durations were in the range of 0.3 to 691.8 hours with an average of 236 hours. While these strain rates are faster than expected in repository conditions, they are not rapid burst tests. The creep tests summarized in CRWMS M&O 2000j (p. II-1) extend up to 10,000 hours (approximately 1.14 year) and show creep strains, without failure, in excess of the failure criterion being used in this AMR.

There is corroborating evidence for using this creep failure criterion which is summarized in Section 6.10.1 of CRWMS M&O 2000a (Initial Cladding Condition AMR).

For most rods, the stresses during dry storage are too low to produce Stress Corrosion Cracking (SCC). Tasooji et al. (1984, p. 600, their Figure 3) show that stresses need to be above 180 MPa for SCC to occur. In this analysis, sufficient iodine exists and a rod with a peak stress greater than or equal to 180 MPa fails from SCC.

6.2.4 Creep and SCC Failure Results

Figure 1 gives the CCDF for the hoop stress (at room temperature of 27EC) in the rods expected to be received at YMP. A sampling of 2000 rods with stresses that are defined by this distribution was used for the stress variation. A rod (total of 12,000 rods analyzed, 6 x 2000) with each of these 2000 stresses was placed in each of the six (6) zones shown in Figure 2 and described in Table 2. This rod represents the fraction of the total WP inventory in the zones as given in Table 2, Column 3. Each rod is exposed first to a temperature profile represented by Figure 5 (for dry storage and shipping) and then to the repository temperature history normalized by the WP radial scaling factor corresponding to the particular zone as given in Table 2, Column 5. A uniform temperature uncertainty of " 13.5% is included. The creep strain is then calculated for the rod using the equations in Section 6.2.2 (including a uniform uncertainty of " 80%). This strain is compared to a random sampling of the creep failure strain criteria CCDF in Figure 6. The peak stress is also compared to a SCC stress threshold of 180 MPa. If the rod creep strain exceeds the creep failure strain criterion, or the SCC stress threshold is met, the fraction of the rods in that radial zone of the WP has become perforated and that fraction of a rod

is available for cladding unzipping. This procedure is repeated for 12,000 rods in a software routine and the fraction of the WP inventory perforated is calculated. The details of this analysis are described in Attachment II and the software routine AMR-F0155-V1.xls has been submitted as DTN: MO00004SPACLD07.043.

The above analysis has not been directly incorporated into the TSPA-SR but an abstraction has been included. For this abstraction, the independent variable is the peak WP surface temperature. The above analysis was performed for peak WP surface temperatures that vary from 177°C to 412°C. The WP temperature history as shown in Figure 4 is linearly shifted upward or downward by the difference between the base case and new peak WP surface temperature. Figure 7 shows the WP temperature for the peak, average and minimum WP in group 4 (CRWMS M&O 2000h). The peak temperatures are approximately a constant shift above the average temperatures. The minimum temperature falls off more quickly than the average. Analyzing the minimum temperature WPs as a constant temperature difference below the average WP temperature is reasonably bounding because it increases the amount of time at an elevated temperature. The change in temperature radially across the WP is then added to the scaled WP surface temperature. The temperature uncertainty is established to cover the maximum temperatures.

Table 5 gives the fraction of rods failed in a WP (failed from creep) as a function of peak WP surface temperature. This table is imported into the TSPA-SR and the TSPA-SR interpolates the fraction of rods failed in a realization after establishing the peak WP surface temperature for that realization. Figure 8 is a graphical representation of this table. The plateau of the fraction of rods perforated from creep at the lower WP peak surface temperatures represents the rods that were failed in dry storage and shipping. These rods can only fail once and therefore cannot fail again in the repository. Rods that have not failed have undergone some creep during dry storage and shipping and start to accumulate additional creep from that point. Figure 8 shows that above a peak WP surface temperature of about 300°C, the best estimate fraction of rods perforated from creep increases dramatically. This is because the creep correlation has an Arrhenius temperature dependency and the activation energy is reached at that point. The upper limit curve represents the fraction of rods failed from creep if the failure criterion were 0.4% creep, the minimum value in the creep failure strain criterion CCDF. The lower limit curve represents the fraction of rods failed from creep if the maximum creep failure strain criterion of 11.7% were applied. The best estimate value represents a random sampling of the creep failure strain criterion CCDF. In the TSPA-SR, a triangular distribution is used between the upper limit, best estimate and lower limit to incorporate uncertainties.

SCC requires a susceptible material, an aggressive chemical environment, and high stress levels. Iodine induced SCC requires an iodine concentration in the fuel-cladding gap greater than 5×10^{-6} g/cm^2 (Cunningham et al. 1987, p. A.5). Below this threshold of free iodine concentration, Zircaloy cracking due to SCC has not been observed. In actual fuel rods, free iodine concentrations are expected to be negligible. For this analysis the amount of iodine was considered to be present in sufficient quantities for SCC. The times at high stress and the times of elevated temperatures were sufficiently long such that, once cracking started, there was sufficient time to propagate through the cladding (crack velocities were not considered). A rod with a stress above 180 MPa fails by SCC. This threshold was reported by Tasooji et al. (1984, p.600, their Figure 3). Few rods have such high stresses and the same rods that fail from SCC

are also prone to fail from creep. If the calculations were not combined, double counting of the failed rods would be possible. The inclusion of SCC increases the mean failure from creep alone from 2.0% to 2.4% for dry storage and transportation (left side of Figure 8). For higher repository temperatures, the difference disappears.

Table 5. Fraction of Rods Perforated From Creep as a Function of Peak WP Surface Temperature

WP Peak Temperature, °C	Upper Limit	Best Estimate	Lower Limit
#177	0.1942	0.0244	0.0105
227	0.1949	0.0244	0.0105
252	0.2057	0.0258	0.0105
262	0.2156	0.0267	0.0105
277	0.2479	0.0339	0.0106
292	0.3264	0.0604	0.0120
297	0.3628	0.0783	0.0133
302	0.4080	0.0987	0.0173
312	0.5052	0.1622	0.0370
327	0.6379	0.3019	0.1067
352	0.8227	0.5567	0.3424
377	0.9553	0.7789	0.5920
402	0.9970	0.9302	0.7986
$412	0.9985	0.9658	0.8720

(DTN: MO00004SPACLD07.043)

6.3 LOCALIZED CORROSION

Corrosion of zirconium has been observed in fluoride-containing environments. Since fluoride is present in Yucca Mountain groundwater, fluoride corrosion may occur in waste packages. Two scenarios for fluoride corrosion may be considered. In the first (water filled WP scenario), the waste package is full of water, and fluoride ions are transported to the cladding by aqueous diffusion. In the second (flow-through scenario), water enters the waste package through one or more breaches on the upper surface of the waste package and drips out through a breach on the bottom. These two scenarios represent extremes of the rate of drainage.

The flow-through scenario is the more severe of the two. In this scenario, fluoride can be rapidly transported through the waste package by advection, whereas in the water filled WP scenario it is transported by diffusion, which is a comparatively slow mechanism. In the flow-through scenario, advective flow is directed downward by gravity, so fluoride attack can be localized on a relatively small area of cladding (and even on a small area of an individual fuel rod). In contrast, diffusion does not have a preferred direction, so in the water filled WP scenario the fluoride can be transported to a large volume of the waste package. Spreading the fluoride over a larger area of cladding (i.e. a larger area on an individual rod or area on more than one fuel rod) means that more fluoride will be consumed in breaching each fuel rod. Since the flow-through scenario is more severe, the water filled WP scenario will not be considered further.

A bounding approach has been used to describe the flow-through scenario. At least three sources of conservatism have been identified. First, it might be expected that the corrosion of zirconium is sufficiently slow, and the flow of groundwater through the waste package is sufficiently fast, that some fluoride will simply flow through the waste package without reacting. Credit has not been taken for this loss of fluoride. Instead, corrosion of the cladding is limited by the supply of fluoride.

A second source of conservatism is that fluoride attack is assumed to degrade one fuel rod before degradation begins on another rod. This is reasonably bounding because each rod breaches as soon as enough fluoride is available to corrode a 10-mm length of cladding; there is no delay in breaching one rod because fluoride is being diverted to start degrading another. Credit has not been taken for simultaneous attack of more than one fuel rod. Instead, all the available fluoride goes to and reacts with a single fuel rod. When that patch on a fuel rod is completely degraded (corroded through), the fluoride starts to attack another fuel rod.

Finally, there is conservatism in that it is assumed that all fuel rods are subject to fluoride corrosion. Such an exposure might result if the water entered through numerous breaches or through a cracked circumferential weld over the top half of the waste package. In that case, drips could be distributed over all of the fuel rods. Under many other exposure conditions, however, some of the fuel rods would be out of the flow path. In those cases, only the fuel rods in the flow path would be subject to fluoride corrosion.

In determining the amount of fluoride that is necessary to breach a fuel rod, fluoride removes all the cladding from a 10-mm length of the fuel rod by reacting to form ZrF_4. The as-manufactured thickness of the cladding may be used because, although some of the zirconium may be oxidized, the zirconium atoms remain in the products of corrosion.

The volume of zirconium V_{Zr} that must react to breach all of the fuel rods may be calculated with the formula

$$V_{Zr} = mL\frac{p}{4}(d^2 - (d-2w)^2) = mLpw(d-w) \qquad \text{(Eq. 6.3-1)}$$

where m is the number of fuel rods, L is the length that is subject to corrosion, d is the outside diameter of the cladding, and w is the wall thickness of the cladding. For this calculation, the most common waste package type (21 PWR) and the most common fuel assembly type (W1717WL) are used. Since W1717WL is a 17×17 assembly and the waste package contains 21 assemblies, the number of positions is $m = 17^2 \times 21 = 6069$. Since the control rod guide tubes and instrument tubes are similar in geometry to fuel rod cladding, all rod positions are counted, rather than just the number of fuel rods.

In a volume of water V_w with a fluoride concentration of c_F, the number of moles of fluoride is $V_w c_F / m_F$, where m_F is the molar mass of fluorine. In forming ZrF_4, $n = 4$ moles of fluoride are required for each mole of zirconium. Therefore, the volume of zirconium V_{Zr} that can be reacted with this volume of water is

$$V_{Zr} = \frac{V_w c_F v_{Zr}}{m_F n} \qquad \text{(Eq. 6.3-2)}$$

where v_{Zr} is the molar volume of zirconium. By combining Equations 6.3-1 and 6.3-2 , one finds that

$$V_w = \frac{m_F n}{c_F v_{Zr}} mLpw(d - w) \qquad \text{(Eq. 6.3-3)}$$

In Equation 6.3-3, m_F = 19.0 g/mol (Lide 1995, inside front cover), c_F = 2.18 mg/L = 2.18 g/m^3 (Harrar et al. 1990, Table 4.1), n = 4, m = 6069, L = 10 mm, w = 0.5715 mm, and d = 9.50 mm (CRWMS M&O 2000a, Table 2). The molar volume of zirconium is $v_{Zr} = m_{Zr} / \rho_{Zr}$, where m_{Zr} = 91.2 g/mol (Lide 1995, inside front cover) is the molar mass of zirconium and ρ_{Zr} = 6520 kg/m^3 (Lide 1995, p. 4-98) is the density of zirconium. Evaluation of Equation 6.3-3 yields V_w = 2424 m^3. The result is that the fraction of fuel rods failed by fluoride corrosion starts at zero when the waste package is breached. After breach, the fraction failed is proportional to the volume of water that has entered the package, reaching one when 2424 m^3 of water has entered the waste package. An alternative description is that the fraction of fuel rods that fail in a given year is the volume of water that enters the waste package during that year divided by 2424 m^3. This volume (2424 m^3) is equivalent to filling and emptying the waste package hundreds of times. Upper and lower limits are 10 times and 1/10 the best estimate rate to represent the uncertainties in this model and a log uniform distribution is selected between the maximum and minimum values. This analysis makes the rod failure fraction linearly dependent on the water ingression rate (% failed = 0.0413 * m^3 water in WP). The water ingression into the WP increases with time as additional patches on the WP fail or open. Rod failure rate also depends on the location of the WP group because of different drip rates in different repository regions. Figure 9 is an example; with 50 liters/year of J13 water (2.2 ppm fluorides) entering the WP, 20% of the rods would fail by fluoride corrosion in 10,000 years.

6.4 OTHER FAILURE MECHANISMS

6.4.1 Mechanical Damage

Seismic analysis (CRWMS M&O 1999d) shows that most of the rods in the WPs would fail from a very severe earthquake (a once per million years event) but no rods would fail for less severe and moderate frequency seismic events. This is consistent with studies (Witte et al. 1989, p. 194) of rod damage during transportation accidents that concluded that 63 g accelerations are needed to fail the rods in the shipping container (or WP). This also indicates that rock drops onto an intact WP will not cause rod failure. Therefore, the seismic failures have been included in the analysis as a disruptive event.

The analysis of seismic events is included in the TSPA-SR. Based on the analysis (CRWMS M&O 1999d), seismic events with a frequency of 1.1x10^{-6} events/year would break most of the

fuel. Such events are sampled, and, when such an event occurs, all cladding is failed and to be available for unzipping.

CRWMS M&O 1999d (Section 6.2) also considered the effect of a rubble bed consisting of rocks from a drift collapse on bare fuel rods (no WP or possible drip shield protection). The analysis showed that the bare fuel assemblies would fail under the static loading of the rocks. This effect was not included in the cladding degradation abstraction because it does not occur until after the WP no longer affords any protection. The first patches (about 100 cm by 100 cm) penetrate the WP in 50,000 to 60,000 years, and a significant number of patches (about 100 patches) are open in about 350,000 years. With the potential for rubble bed damage not occuring until well after the 10,000 years considered for the TSPA-SR, rubble bed damage to the cladding was neglected.

6.4.2 DHC and FEP Issues

Delayed hydride cracking (DHC) of existing cracks is analyzed (CRWMS M&O 2000a, Section 6.10.2) using the distribution of stresses shown in Figure 1. Stress intensity factors are calculated to have a mean of 0.47 MPa-$m^{0.5}$ (range 0.002 to 2.7 MPa-$m^{0.5}$), which is below the threshold stress intensity factors that are in the range of 5 to 12 MPa-$m^{0.5}$. Therefore, crack propagation by DHC is not expected. These stress intensities are also below those needed to produce embrittlement failures ($K_I < K_{IC}$). Failure of the cladding by hydride reorientation is unlikely and has not been included in the abstraction for the TSPA-SR analysis. Stresses and temperatures are too low for reorientation to occur. Even if the material did reorient, it will maintain sufficient strength such that failure would not be expected.

Various AMRs have ruled out many cladding failure modes. CRWMS M&O 2000b outlines the Features, Events, and Processes (FEPs) that have been excluded from this analysis. CRWMS M&O 2000c describes the various corrosion mechanisms that are not expected to fail the cladding, considering the expected in-package chemistry predicted in CRWMS M&O 2000i. CRWMS M&O 2000l describes the various hydride mechanisms that are not expected to fail the cladding. This Summary and Abstraction AMR only addresses the cladding failure mechanisms that are expected to contribute to radionuclide release from CSNF.

6.5 FAST RELEASE OF RADIONUCLIDES

The release of radionuclides from the fuel rod occurs in three stages, (1) release of true gap inventory, (2) fast release from initial UO_2/water reaction and (3) wet unzipping (tearing of the cladding). Sections 6.1 through 6.4 discuss the potential of failing (perforating) the cladding. This section addresses the release of radionuclides through the initial cladding failure. Section 6.6 analyzes the tearing open (unzipping) of the cladding and the release of radionuclides from the bulk fuel matrix.

6.5.1 Fast Release Abstraction

The true gap inventory (iodine, cesium, and noble gasses) is released in proportion to the fission gas release fractions (CRWMS M&O 2000d, p. 82). The release of iodine is the same fraction as the noble fission gas release fraction of 4.2% (CRWMS M&O 2000a, Table 12). Cesium gap inventory is 1/3 of the fission gas release fraction or 1.4%.

The fast release refers to the radionuclides that are released with the initial fuel dissolution before the cladding starts to unzip. Wilson (1985, 1987, 1990) reports releases of various radionuclides from fuel rod samples. The samples included intact and defected fuel rod sections and bare fuel. Wilson exposed the samples to water and measured the amounts of various radionuclides that were released during the exposure period. The first measurements were made in about 200 days. The samples were again exposed, and the measurements were repeated after an additional exposure of similar length. The fast release from the uranium pellet through slits and holes in the cladding is estimated by calculating the release rate from Wilson's eight experiments and extrapolating this release rate until the larger gaps are closed by secondary phases (approximately 50 years). Figure 11 presents a uniform distribution of fast release fraction between 0 and 0.4% (mean and median value = 0.2%) which is used in the TSPA-SR abstraction. This linear fit is reasonably bounding, over-predicting the fast release fraction for the lower Cumulative Distribution Function (CDF, equivalent to 1-CCDF) samplings. The cesium and iodine true gap inventories are added to this fuel matrix fast release fraction.

6.5.2 Fast Release Analysis

The purpose of this section is to estimate the fast release inventory. The current conceptual analysis of release from a breached fuel rod considers that the radionuclide inventory may be divided into three parts: a true gap inventory, a fast release inventory, and a delayed release inventory.

The true gap inventory is the portion of the few elements (e.g., Cs, I and noble gasses) that segregate to the gap during reactor operation. In the TSPA-SR treatment, this inventory is immediately released upon cladding and WP failure.

The fast release inventory results from the process of plugging the cracks and gaps in the fuel rod. A substantial length of the fuel rod may be wetted, and uranium dioxide in the wetted length will be converted to a hydroxide (e.g., metaschoepite). As a result, the volume of solid material increases. When the cracks and gaps are fully plugged with reaction products, the conversion process slows to insignificant rates. However, alteration of uranium dioxide will make other radionuclides available for release. In the TSPA-SR treatment, the fast release inventory should be made available for release during the first time step. In total system performance assessment, the true gap and fast release inventories are made available for release during the first time step.

The delayed release inventory is the remainder of the inventory in the fuel rod. This is released during cladding unzipping.

CRWMS M&O 2000e (Section 7) predicts a fast release inventory of 2.8% to 5.5%. This value is reasonably bounding because it is based on complete plugging occurring over the entire active length of the fuel rod and that all radionuclides other than uranium are released. A less conservative treatment can be developed on the basis of data for ^{99}Tc release as measured by Wilson (1985, 1987, 1990). Wilson's experiments included intact and defected fuel rod sections and bare fuel. Only the results for defected fuel rods were considered. Results for bare fuel are not relevant because it has no protection by cladding; results for intact fuel rods are not relevant

because the fuel is not exposed. In Wilson's experiments, the cladding of the defected samples had either one slit or two holes.

To estimate the fast release fraction, Wilson's results were analyzed by an approach that is shown schematically in Figure 10. The period from time 0 to time t_1 corresponds to Wilson's first exposure cycle. During this period, ^{99}Tc is released at rate R_1, which is the measured release rate for this cycle. The period from time t_1 to time t_2 corresponds to the second exposure cycle, and during this period ^{99}Tc is released at rate R_2, which is the measured release rate for the second cycle. The rate of release during the second cycle of testing was often smaller than that during the first cycle. At later times, the release rate decreases linearly from a rate of R_2 at time t_2 to a rate of zero at time t_{pl}, which is the time for complete plugging of the cracks by metaschoepite. Narrow cracks will plug quickly because they can be filled with a small amount of metaschoepite, but wide cracks will take longer to plug because they require a larger amount of metaschoepite. The gradual decrease in release rate thus corresponds to progressive plugging of cracks of different widths. In all cases, the release rate is expressed as a fraction of the total inventory, so it has the units of reciprocal time (e.g, yr^{-1}) and is not expressed as an amount of material per unit time (e.g., mol/yr). The analysis described above was repeated for each of Wilson's fuel rod samples, and the fast release fraction F was calculated as

$$F = R_1 t_1 + R_2 (t_2 - t_1) + [R_2 (t_{pl} - t_2) / 2] \qquad \text{Eq. 6.5-1}$$

where the variables are as defined above. A cumulative distribution function is determined in the following paragraphs based on the values of F from the eight (8) tests by Wilson (1985, 1987, 1990).

The fast release fractions were calculated on the basis of measurements of ^{99}Tc. Of the releases tabulated by Wilson (1985, Tables 7 through 13, total measured release divided by 10^{-5} inventory for slit defect and holes defect), ^{99}Tc has the second-largest release as a fraction of inventory. The only radionuclide with a larger release fraction is ^{137}Cs. However, ^{137}Cs would be expected to have a substantial true gap inventory, so its measured releases would be larger than the fast release inventory.

Of the variables used in Equation 6.5-1, all but t_{pl} can be obtained from the data tabulated in Table 6. The value of t_{pl} may be estimated from photomicrographs of the fuel. Wilson (1990, p. 2.7, Figure 2.3) provided a photomicrograph of a cross section of one of his fuel samples. The widest crack of interest is the middle section of the nearly diametral crack. A few cracks appear even wider. However, their irregular shapes and variable widths indicate that these are not unusually wide cracks but rather cracks that appear wide because there is a small dihedral angle between the crack and the plane of the cross section. The middle section of the nearly diametral crack in the photomicrograph (Wilson 1990, p. 2.7, Figure 2.3) has a width of about 0.8 mm in the print provided in the document. Since the magnification in the print is 14.5×, the actual crack width w is about $w = 55$ μm.

CRWMS M&O (2000d, Equation 16) gives the following equation for the forward reaction rate of spent fuel in alkaline water:

$$\log_{10} Dr = 4.69 - \frac{1085}{T} - 0.12 \cdot pCO_3 - 0.32 \cdot pO_2 \qquad \text{Eq. 6.5-2}$$

where Dr is the reaction rate in mg/m^2·day, pCO_3 is the negative of the common logarithm of the total carbonate concentration in mol/L, and pO_2 is the negative of the common logarithm of the oxygen partial pressure.

For exposure of spent fuel in a repository, it is reasonable to approximate the environment by J-13 water in equilibrium with air at 25 °C. This is the same water chemistry as is used in calculating the unzipping speed. The bicarbonate concentration of J-13 water is 128.9 mg/L (Harrar et al. 1990, Table 4.1). Using the molar masses of H (1.00794 g/mol), C (12.011 g/mol) and O (15.9994 g/mol) (Lide 1995, inside front cover), one finds that the concentration of carbonate is 0.1289 g/L / (1.00794 g/mol + 12.011 g/mol + 3·15.9994 g/mol) = $2.11 \cdot 10^{-3}$ mol/L, and thus $pCO_3 = -\log_{10}(2.11 \cdot 10^{-3}) = 2.68$. In a standard atmosphere, the fraction of O_2 is 0.2095 (Weast and Astle 1980, p. F-208), so $pO_2 = -\log_{10}(0.2095) = 0.679$. By applying Equation 6.5-2, one obtains Dr = 3.26 mg/m^2·day. The density ρ of UO_2 is ρ = 10970 kg/m^3 (Lide 1995, p. 4-94). By dividing Dr by ρ, one finds that Dr / ρ = 0.297 nm/day.

Wet oxidation of the fuel produces metaschoepite. The molar volume of metaschoepite ($UO_3 \cdot 2H_2O$) is v_{ms} = 64.5 cm^3/mol; that of UO_2 is v_{UO2} = 24.6 cm^3/mol (CRWMS M&O 2000e, Table 4). Therefore, oxidation of a layer of UO_2 yields a layer of metaschoepite that is (v_{ms} / v_{UO2}) times as thick as the original layer. Since the original UO_2 is consumed, the surface moves by ((v_{ms} / v_{UO2}) − 1) times the thickness of the original layer.

The reaction rates predicted by Equation 6.5-2 are for a microscopically smooth surface. In contrast, the surfaces of cracks will be rough, so the exposed surface area will be larger, and the oxidation rate will be higher. The ratio R of the actual surface area to the apparent surface area is estimated as R = 3 (CRWMS M&O 2000d, p. 82).

By combining the results above, one obtains the plugging time t_{pl} as

$$t_{pl} = \frac{wr}{2(v_{ms} / v_{UO2} - 1)RDr} \qquad \text{Eq. 6.5-3}$$

The factor of 2 is present because oxidation occurs on both sides of the crack. Using the values above, one finds that $t_{pl} = 1.9 \cdot 10^4$ day (about 50 years).

The data from Table 6 are put into the notation of this section as follows. The values for first cycle ^{99}Tc release (10^{-5} of sample inventory) are $R_1 t_1$. The values for second cycle ^{99}Tc release (10^{-5} of sample inventory) are $R_2(t_2 - t_1)$. The first cycle time (days) and second cycle time (days) are t_1 and $t_2 - t_1$, respectively. From these values, R_2 and t_2 can be calculated. Using the data in Table 6, the results in Table 7 are obtained.

Using the approach described above, the fast release fraction was calculated for each of Wilson's eight samples. The results were plotted as an experimental Cumulative Distribution Function (CDF) in Figure 11.

The CDF for the fast release fraction is generally expected to overestimate the actual fast release fraction for two reasons. First, Wilson's tests are for short samples rather than full-length fuel rods. In full-length rods, transport limitations may reduce the fraction released. Transport limitations are discussed in more detail below. Second, some preferential release of ^{99}Tc is expected. Wilson (1985, p. 36) states, "It is likely that ^{99}Tc partitions to the grain boundaries in the hotter central portions of the fuel. As grain boundary attack (which is clearly visible in Figure 3 of Wilson 1985) progresses in these regions, enhanced ^{99}Tc release would then be observed." For these reasons, it is expected that the recommended CDF gives a reasonably bounding estimate of the fast release fraction.

In determining the fast release fraction, the CDF is determined from experiments on short rod sections. For total system performance assessment, the same CDF applies to full-length rods. This treatment is clearly reasonably bounding, but it may be thought to be overly conservative. To determine whether it is overly conservative, it is helpful to compare the fuel rod length to the characteristic diffusion distance, $2(Dt)^{1/2}$ where D is the diffusion coefficient and t is the time allowed for diffusion. For strong electrolytes dissolved in water at 25 °C, diffusion coefficients are typically on the order of 10^{-9} m^2/s (Weast and Astle 1980, p. F-62). The diffusion time may be approximated by the plugging time $t_{pl} = 1.9 \cdot 10^4$ day $= 1.65 \cdot 10^9$ s. The diffusion distance is then $2(Dt)^{1/2} = 2.6$ m. Since this distance is comparable to the active length of a fuel rod, it is reasonable to expect that, if the entire length of the fuel rod is saturated, the entire length will contribute to radionuclide releases. Additional conservatism will result if only part of the rod is saturated. However, information on rod saturation is not available, so credit cannot be taken for partial saturation.

Table 6. Inputs on 99Tc Releases

Sample	Source	First Cycle ^{99}Tc Release (nCi)	First Cycle ^{99}Tc Release (10^{-5} of Inv.)	Second Cycle ^{99}Tc Release (nCi)	Second Cycle ^{99}Tc Release (10^{-5} of Inv.)	Location[d]	First Cycle Time (days)	Second Cycle Time (days)	Location[d]
H-6-12	Wilson (1985)	28.2+5.4[b]	12.1×33.6/50.8[c]	15.8+1.4[b]	12.1×17.2/50.8[c]	Table 12	252	128	Table 3
J-8-24	Wilson (1985)	4.5+1.4[b]	6.7×5.9/27.7[c]	18.0+3.8[b]	6.7×21.8/27.7[c]	Table 12	244	128	Table 3
C5C-E	Wilson (1987)	25	2.8	18.5	2.1	Table 13	223	202	Table A.3
I9-19	Wilson (1987)	73	15.3	32	6.6	Table 13	181	195	Table A.7
C5C-C	Wilson (1987)	--	0.5[a]	--	0.5[a]	Table 13	223	202	Table A.4
I9-12	Wilson (1987)	--	0.5[a]	--	0.5[a]	Table 13	181	195	Table A.8
C5B-D	Wilson (1990)	12.7	1.4	--	0.5[a]	Table 3.8	174	181	Table A.5
C5B-B	Wilson (1990)	18.9	2.2	--	0.5[a]	Table 3.8	174	181	Table A.6

Sample	Defect Type	Location[d]
H-6-12	Slit	Table 3
J-8-24	Holes	Table 3
C5C-E	Slit	Table 1
I9-19	Slit	Table 1
C5C-C	Holes	Table 1
I9-12	Holes	Table 1
C5B-D	Slit	Table 2.1
C5B-B	Holes	Table 2.1

NOTES: Inv. = Sample inventory.
-- = Not reported.
[a] Release was below detection limit. The value used here ($5 \cdot 10^{-6}$) is half of the detection limit (10^{-5}) (Wilson (1985, p. 35).
[b] Total was not reported.
[c] Expression is (release for both cycles divided by 10^{-5} of inventory)×(release for cycle 1 in nCi)/(release for both cycles in nCi)
[d] Location refers to the Table in the Reference Source identified in the second column of this Table 6.
DTN: MO0003SPATCR30.039, MO0003SPATCR22.038, MO0003SPATCR70.040.

Table 7. Fast Release Fractions for Defected Samples

Sample	Fast Release Fraction
H-6-12	0.00311
J-8-24	0.00392
C5C-E	0.00102
I9-19	0.00338
C5C-C	0.00024
I9-12	0.00025
C5B-D	0.00028
C5B-B	0.00029

DTN: MO00004SPACLD07.043

6.6 CLADDING UNZIPPING AND FUEL DISSOLUTION

Under wet conditions, the fuel matrix reacts with moisture at the intrinsic fuel matrix dissolution rate and precipitates locally as metaschoepite. This secondary phase isolates most of the fuel from the moisture but the fuel in the split cladding region continues to react with moisture, thus increasing in volume and forcing the split further along the cladding. Such alteration results in significant volume expansion, and the cladding breach will eventually propagate from its original location to the ends of the fueled length. Propagation of a cladding breach is termed “unzipping” which is used interchangeably with “splitting”.

As discussed in CRWMS M&O 2000e (Section 6.8), the reaction front is cone shaped and propagates along the rod at a rate that is related to the intrinsic fuel matrix dissolution rate (see Section 6.6.1 of this AMR). However, since fuel rods are long and thin, the conical reaction front can be approximated by a planar front that propagates at some multiple of the intrinsic fuel matrix dissolution rate.

To determine the inventory of radionuclides that is available for release from the entire repository, it is necessary to have a means for predicting the fraction of breached waste packages, the fraction of fuel rods with cladding breaches, and the speed of propagation of a cladding split. This section provides a mathematical framework for describing these processes in a way that is computationally efficient. The approach is intended for use in total system performance assessments.

The various subsections have different emphases. Section 6.6.1 summarizes the abstraction for fuel rod unzipping. That abstraction uses the intrinsic dissolution rate, so Section 6.6.2 restates the equations for dissolution rate that were developed in CRWMS M&O 2000d. The general formalism for unzipping described in Section 6.6.3 is intentionally abstract and general. It is applicable to essentially any combination of waste package and waste form analysis. In Section 6.6.4, the treatment is made more specific. It is applied to a particular analysis of fuel rod unzipping, and simplifications to the general formalism are discussed. In Section 6.6.5, the specific treatment of Section 6.6.4 is summarized for many waste packages. Finally, in

Section 6.6.6, the results of Section 6.6.5 are simplified for a system with only one waste package. This form is useful in implementing a performance assessment.

6.6.1 Wet Unzipping Abstraction

Fuel rods with perforated cladding are expected to remain intact until the WP breaches and permits air and moisture to enter. While the humidity is low, dry unzipping could occur. Since the WP is expected to remain intact for at least 200 years, the fuel temperatures will be too low for dry unzipping (fuel conversion to U_3O_8) to occur. Wet unzipping of failed rods is analyzed to start when the WP breaches. Rods that fail after WP breach immediately start to unzip. The fuel matrix is dissolved at the intrinsic dissolution rate that is evaluated for the current temperature and in-package chemistry. The dissolved UO_2 precipitates locally as metaschoepite. This secondary phase isolates most of the fuel from the moisture and increases in volume compared to UO_2. In time, the cladding in the reaction region is torn as the reaction continues. This reaction region is cone shaped and the cone angle is based on experimental observations in dry unzipping and theoretical analyses.

The unzipping propagates along the rod at a rate that is proportional to the intrinsic dissolution rate. The ratio of unzipping speed to intrinsic dissolution rate is given by a triangular distribution. The distribution has a minimum of 1, a mode of 40, and a maximum of 240 (CRWMS M&O 2000e, Section 7). It is assumed that the perforation is at the middle of the fueled length of the rod. This maximizes the release rate. The unzipping time or velocity is also a function of local chemistry and pH. In TSPA-SR, the unzipping velocity and fraction of fuel exposed are evaluated at each time step because of the evolution of in-package chemistry and temperature. Section 6.6.6 gives equations for determining the rate at which fuel is exposed as a result of unzipping. These equations take into account the effect of having fuel rods fail at different times.

6.6.2 Intrinsic Dissolution Abstraction

The intrinsic dissolution rate is used in the unzipping calculations to determine the reaction rate velocity. The intrinsic dissolution equation is to be applied at each TSPA-SR simulation time step and is to be based on the local chemical conditions. At some times the pH could be basic and at other times it could be acidic (CRWMS M&O 2000i). The abstraction is therefore divided into regions of pH greater than and less than a neutral pH (pH = 7). CRWMS M&O 2000d (p. 82) develops the intrinsic dissolution equations that are recommended for TSPA-SR.

For basic conditions (pH > 7),

$$\mathrm{Log}_{10}\, Dr = a_0 + a_1 / \mathrm{Tk} + a_2 \cdot \mathrm{PCO}_3 + a_3 \cdot \mathrm{PO}_2 \qquad \text{(Eq. 6.6-1)}$$

where $a_0 = 4.69$, $a_1 = -1085$, $a_2 = -0.12$, and $a_3 = -0.32$.

For acid conditions (pH < 7),

$$\mathrm{Log}_{10}\, Dr = a_0 + a_1 / \mathrm{Tk} + a_3 \cdot \mathrm{PO}_2 + a_4 \cdot \mathrm{pH} \qquad \text{(Eq. 6.6-2)}$$

where $a_0 = 7.13$, $a_1 = -1085$, $a_3 = -0.32$, and $a_4 = -0.41$.

Equations 6.6-1 and 6.6-2 may be combined in the following form:

$$\text{Log10}(Dr) = a_0 + a_1/Tk + a_2 \cdot PCO_3 + a_3 \cdot PO_2 + a_4 \cdot pH \qquad \text{(Eq. 6.6-3)}$$

where Tk = absolute temperature (K)
PCO_3 = –Log10 (molar concentration of CO_3--)
PO_2 = –Log10 (partial pressure in atmospheres of O_2)
Dr = intrinsic dissolution rate = mg /m^2·d.

The coefficients for these equations are summarized in Table 8. This function is used in the TSPA-SR. The uncertainty in the intrinsic dissolution rate is applied to the coefficient a0. The value of a_0 is uniformly distributed by + or – 1.0. This is equivalent to a log uniform distribution of the intrinsic dissolution rate by a multiple of ten (10). CRWMS M&O 2000d recommended an uncertainty of 1.5 orders of magnitude. An inspection of the test results shown in CRWMS M&O 2000d (Table 1) suggests a much smaller range. Three tests under identical conditions (Runs 1,2 3) varied by only 18% from the mean. There is also an independent uncertainty of a factor of six (6) associated with the unzipping velocity in the use of the intrinsic dissolution rate. Figure 12 (CRWMS M&O 2000d, p. 55) shows the dependency of the intrinsic dissolution on temperature and pH for a constant O_2 and CO_3^{--} content. In the TSPA-SR, each of the variables could vary with time.

Table 8. Intrinsic Dissolution Equation and Terms

	a_0	a_1	a_2	a_3	a_4
pH>7	4.69	-1085	-0.12	-0.32	0
pH<7	7.13	-1085	0	-0.32	-0.41

CRWMS M&O 2000d, p. 55

Both the intrinsic dissolution tests and the equations given above are based on tests for individual grains of UO_2. The unzipping analyzed in TSPA-SR occurs on the pellet surface and the rate in mg/m^2·d is converted to a reaction rate velocity of cm/yr. A grain boundary penetration factor of six (6) from CRWMS M&O 2000e (Section 7) is applied to the intrinsic dissolution rate to account for water penetration into grain boundaries. Figure 13 is an example of unzipping times as a function of temperature for a constant chemistry of approximate J-13 water, and Figure 14 shows the dependency on pH at a fixed temperature of 35 °C. In the TSPA-SR, both in-package chemistry and temperature are changing with time and the unzipping velocity is evaluated within the TSPA-SR analysis itself.

6.6.3 General Formalism for Wet Unzipping

Each fuel rod can be classified as either intact, unzipping, or exhausted. “Intact” is used broadly to denote those rods whose fuel is protected from alteration, thus the intact fraction includes all rods in intact waste packages and all rods with intact cladding in breached waste packages. “Unzipping” denotes rods that are in the process of alteration, that is those rods that are in breached waste packages and have breached cladding but are not yet fully unzipped.

"Exhausted" refers to those rods that were breached so long ago that they are fully unzipped, that is the split has propagated all the way to the ends of the fueled region of the rod.

For convenience, the "time of emplacement" will be taken as "time = zero" and "time since emplacement" will simply be called "time." The waste package and waste form analysis must provide the following three functions. Let $W(t)$ be the fraction of waste packages breached at some time t. For a particular waste package that breached at time t_w, let $f_b(t, t_w)$ be the fraction of fuel rods that are breached at time t. "Breached" fuel rods are those that are either unzipping or exhausted, so $f_b(t, t_w) = 0$ for $t < t_w$. Let $v(t)$ be the unzipping speed for a breached fuel rod in a breached waste package at time t. The method described here applies only for $t \geq 0$.

To describe the instantaneous state of unzipping for the entire group of waste packages, define $f_i(t)$, $f_u(t)$, and $f_e(t)$ which are the fractions of the fuel rods that are intact, unzipping, and exhausted, respectively, at time t. These functions are not applied to individual waste packages; rather, they describe all the rods in the entire group of waste packages. Note that the unzipping fraction includes rods with a variety of split lengths, from very short to nearly the entire fueled length. No distinction among these rods is made on the basis of split length. None of the functions $f_i(t)$, $f_u(t)$, and $f_e(t)$ is specified in advance; they are all derived from $W(t)$, $f_b(t, t_w)$, and $v(t)$. Note, however, that $f_i(t) + f_u(t) + f_e(t) = 1$ for any time t, so only two of $f_i(t)$, $f_u(t)$, and $f_e(t)$ are independent.

The first of these functions to be derived is $f_i(t)$. Initially:

$$f_i(0) = 1 - W(0)\, f_b(0,0) \qquad \text{(Eq. 6.6-4)}$$

Equation 6.6-4 follows because, out of the entire set of rods, the fraction that is breached rods in breached waste packages at the time of emplacement is $W(0)f_b(0, 0)$; all other rods are "intact" in the sense defined above. At later times, there may be additional breached waste packages and breached rods. The fraction that remains intact at time t will be:

$$f_i(t) = 1 - W(0)\, f_b(t,0) - \int_0^t \frac{dW(t)}{dt}\, f_b(t,t)\, dt \qquad \text{(Eq. 6.6-5)}$$

Equation 6.6-5 is justified as follows. The first term (1) corresponds to the entire set of rods. The second term corresponds to those rods that are in defective waste packages (i.e., the WPs have failed at the time of emplacement) and the rods either are breached at emplacement or breach after emplacement but before time t. The third term corresponds to rods in the waste packages that breach after emplacement. During a given infinitesimal time interval from τ to $\tau + d\tau$, the fraction of waste packages that breach is $(dW(\tau) / d\tau)\, d\tau$. At some later time t, the fraction of breached rods in these packages is $f_b(t, \tau)$. The integral takes into account all waste package failure times up to time t.

The amount of fuel altered could be determined by solving a partial differential equation for the distribution of split lengths as a function of time, but this approach is computationally costly. A more efficient approach is derived here. Figure 15 is a schematic plot of the alteration rate as a function of time for two individual fuel rods in a breached waste package. For the time scales of interest in performance assessment, the radionuclide inventory can be divided into two parts: the

gap inventory and the fuel matrix inventory. The alteration of both parts is shown schematically in Figure 15. The cladding of rod A breaches at time t_{0A}. There is a pulse of alteration at this time; the pulse corresponds to the gap inventory. The fuel matrix inventory takes much longer to alter; fuel matrix alteration begins at time t_{0A} and continues until time t_{1A}, when the fuel rod is fully unzipped (exhausted) and the fuel matrix is fully altered. The fuel matrix alteration rate is time-dependent because the conditions (e.g., temperature and water chemistry) inside the waste package are time-dependent. The alteration of the fuel in rod B is similar, but the cladding of rod B breaches later, at time t_{0B}. Since the fuel matrix alteration rate is decreasing with increasing time, alteration of the entire inventory in rod B takes longer, and the rod is not exhausted until time t_{1B}. The alteration rate for an entire waste package will be a superposition of the alteration rates for each rod.

Let $F_g(t)$ be the fraction of the total gap inventory (for the entire group of waste packages) that has been altered at time t. The gap inventory is altered immediately if the waste package and fuel cladding are both breached, and thus the altered fraction can be written as follows

$$F_g(t) = 1 - f_i(t) \qquad \text{(Eq. 6.6-6)}$$

The following approach can be used to determine the fraction of the fuel matrix inventory that has been altered. Before significant numbers of waste packages begin to breach, the heat output of the packages will have become fairly small, so the temperatures and in-package chemical environment will be fairly uniform. Therefore, it is a reasonable approximation to use a single unzipping speed for all the fuel rods in the entire group of WPs. In light of that approximation, define the function $h(t)$ as:

$$h(t) = \int_0^t v(t)dt \qquad \text{(Eq. 6.6-7)}$$

where $v(\tau)$ is the speed of unzipping at time τ. Note that $h(0) = 0$ because the interval of integration will have zero length. The function h is referred to as the "propagation distance". As an alternative to Equation 6.6-7, changes in $h(t)$ may be expressed in differential form:

$$\frac{d}{dt}h(t) = v(t) \qquad \text{(Eq. 6.6-8)}$$

For simplicity, the initial cladding damage always occurs at the center of the fueled region. The split will then propagate to both ends of the fueled length. This gives the fastest alteration rate: If the split starts at the center, the rod is exhausted when each end of the split has propagated by a distance of $L / 2$, where L is the length of the fueled region. In contrast, if the split starts somewhere besides the center, the split must propagate farther in one direction, and thus for a longer time, before the rod is exhausted.

The time for unzipping of fuel rods A and B is shown schematically in Figure 16, where the propagation distance h is plotted as a function of time. For the purposes of this illustration, it is assumed that rod A is failed at the time of emplacement and is in a waste package that is breached at emplacement. (This will presumably be an extremely rare occurrence.) In this case $t_{0A} = 0$. As can be seen from Figure 16, rod A starts unzipping at time t_{0A}, when $h = 0$, and is

exhausted at time t_{1A}, when $h = L / 2$. This is readily understandable in light of the definition of $h(t)$ in Equation 6.6-7. The situation for rod B is slightly more complicated. The fuel in rod B is not exposed for alteration until time t_{0B}; this is the time when both the waste package and cladding are breached. At this time, rod A is already partially unzipped. As is shown in Figure 16 for rod A, $h(t_{0B}) = c$. Both rods then unzip at the same rate, since there is a single unzipping speed for all rods. At time t, the distance that the split has propagated from the center of rod A is $h(t)$ (for $t_{0A} \le t \le t_{1A}$), but the distance that the split has propagated from the center of rod B is $h(t) - c$ (for $t_{0B} \le t \le t_{1B}$). Thus, rod B is exhausted when h reaches $L / 2 + c$.

The discussion above also sheds additional light on the nature of h. In an actual rod, splitting initiates at some time, the split propagates until it reaches the ends of the fueled region, and splitting stops. In contrast, $h(t)$ increases without limit. Thus, $h(t)$ is the propagation distance for an infinitely long rod that starts splitting at the time of emplacement.

The invariance of the unzipping speed has an important implication: It is not necessary to track the propagation of splits in individual rods or even the state of individual waste packages. The fraction of matrix alteration can be deduced from $f_i(t)$ and $v(t)$ alone, as is shown below.

The first step in determining the fraction of matrix alteration is to define a function h^{-1}, which is the inverse function of h, that is:

$$h^{-1}(h(t)) = t \text{ for } t \ge 0 \qquad \text{(Eq. 6.6-9)}$$

The physical meaning of h^{-1} is straightforward. Given a time $t \ge 0$, $h(t)$ is the distance that the split has propagated at that time. Given a propagation distance $x \ge 0$, $h^{-1}(x)$ is the time at which that propagation distance is reached.

Consider a time t that is sufficiently large that some rods are exhausted. The exhausted rods became exhausted by breaching at some earlier time and having the split propagate by a distance of $L / 2$ to the ends of the fueled region. At the time t in question, the propagation distance is $h(t)$. The rods that are exhausted at time t are therefore exactly those that were breached (either exhausted or unzipping at the earlier time) when the propagation distance was $h(t) - L / 2$. But a propagation distance of $h(t) - L / 2$ corresponds to a time of $h^{-1}(h(t) - L / 2)$. Therefore:

$$\begin{aligned} f_e(t) &= 1 - f_i(h^{-1}(h(t) - L/2)) \text{ for } t \ge h^{-1}(L/2) \\ &= 0 \text{ for } t < h^{-1}(L/2) \end{aligned} \qquad \text{(Eq. 6.6-10)}$$

because $1 - f_i$ is the fraction of breached rods. For times earlier than $h^{-1}(L / 2)$, there are no exhausted rods because there has not been enough time for any split to propagate by a distance of $L / 2$.

Given the fraction of intact rods and the fraction of exhausted rods, the fraction of unzipping rods follows:

$$f_u(t) = 1 - f_i(t) - f_e(t) \qquad \text{(Eq. 6.6-11)}$$

Let $F_m(t)$ be the fraction of the total fuel matrix inventory that has been altered at time t. At the time of emplacement ($t = 0$), $F_m(0) = 0$. At later times, some of the fuel may be altered. Let n be the total number of fuel rods in all the waste packages and let A be the cross-sectional area of one fuel rod. The total volume of fuel is ALn. In each unzipping rod, the rate at which fuel is being altered is $2Av(t)$. But there are $nf_u(t)$ unzipping rods, so:

$$\frac{dF_m(t)}{dt} = \frac{2Av(t)nf_u(t)}{ALn} = \frac{2}{L}v(t)\,f_u(t) \qquad \text{(Eq. 6.6-12)}$$

Since $F_m(0) = 0$, integration of Equation 6.6-12 yields:

$$F_m(t) = \frac{2}{L}\int_0^t v(t)\,f_u(t)\,dt \qquad \text{(Eq. 6.6-13)}$$

6.6.4 Application to a Specific Analysis of Unzipping

The general formalism presented in Equations 6.6-4 through 6.6-13 is quite general, but it is still computationally costly to implement. In particular, Equation 6.6-5 requires evaluation of an integral whenever a value of $f_i(t)$ is needed. To simplify the implementation, this section applies the general formalism to a particular analysis for unzipping.

In place of the general function $f_b(t, t_w)$ for the fraction of fuel rods that are breached, define a new function $f_b(t - t_w)$ where t is the time since emplacement and t_w is the time of waste package breach. This function can be used in the general formalism above by replacing Equations 6.6-4 and 6.6-5 above with the following equations:

$$f_i(0) = 1 - W(0)\,f_b(0) \qquad \text{(Eq. 6.6-14)}$$

$$f_i(t) = 1 - W(0)\,f_b(t) - \int_0^t \frac{dW(t)}{dt}\,f_b(t-t)\,dt \quad \text{for } t \geq 0 \qquad \text{(Eq. 6.6-15)}$$

Even with this simplification, Equation 6.6-15 includes a convolution integral, and a complete evaluation of the integral is necessary whenever $f_i(t)$ is needed. However, the form of f_b that has been proposed for performance assessment is particularly simple:

$$\begin{aligned} f_b(z) &= 0 \text{ for } z < 0 \\ &= a_0 + a_1 z \text{ for } 0 \leq z \leq \frac{1-a_0}{a_1} \\ &= 1 \text{ for } z > \frac{1-a_0}{a_1} \end{aligned} \qquad \text{(Eq. 6.6-16)}$$

As in the general formulation, fuel rods in an intact waste package are not considered to be "breached," regardless of the condition of the cladding. In Equation 6.6-16, a_0 and a_1 are positive constants; a_0 is the fraction of fuel rods that are breached when the waste package breaches. Rods that breach by short-term processes (such as creep rupture) may be included in

this set because these processes will be essentially complete before significant numbers of waste packages breach. The constant a_1 gives the rate of change of the fraction of breached rods after the waste package is breached. This constant describes processes such as localized corrosion of the cladding. The fraction of breached rods cannot exceed 1. In general, the values of a_0 and a_1 will reflect the abstraction of the cladding degradation analysis, and their values will vary from one realization to the next. Note that $f_b(z)$ is continuous at $z = (1 - a_0)/a_1$, but it is discontinuous at $z = 0$ because all the rods that were perforated earlier are suddenly considered as "breached". However, $f_b(z)$ is generally not of interest for $z < 0$, so the discontinuity will not cause difficulty.

The form of Equation 6.6-16 allows for further simplification of Equation 6.6-15, but it requires separate consideration of the different time intervals listed in Equation 6.6-16. For $0 \le t \le (1 - a_0)/a_1$:

$$\begin{aligned} f_i(t) &= 1 - W(0) f_b(t) - \int_0^t \frac{dW(t)}{dt}[a_0 + a_1(t - t)]dt \\ &= 1 - W(0) f_b(t) - (a_0 + a_1 t)\int_0^t \frac{dW(t)}{dt}dt + a_1 \int_0^t \frac{dW(t)}{dt} t dt \\ &= 1 - W(0) f_b(t) - (a_0 + a_1 t)[W(t) - W(0)] + a_1 \int_0^t \frac{dW(t)}{dt} t dt \\ &= 1 - W(0) f_b(t) - f_b(t)[W(t) - W(0)] + a_1 \int_0^t \frac{dW(t)}{dt} t dt \\ &= 1 - f_b(t) W(t) + a_1 \int_0^t \frac{dW(t)}{dt} t dt \end{aligned}$$

(Eq. 6.6-17)

Equation 6.6-17 can then be differentiated with respect to time:

$$\begin{aligned} \frac{df_i(t)}{dt} &= -f_b(t)\frac{dW(t)}{dt} - \frac{df_b(t)}{dt}W(t) + a_1 \frac{dW(t)}{dt} t \\ &= -a_0 \frac{dW(t)}{dt} - a_1 t \frac{dW(t)}{dt} - a_1 W(t) + a_1 t \frac{dW(t)}{dt} \\ &= -a_0 \frac{dW(t)}{dt} - a_1 W(t) \end{aligned}$$

(Eq. 6.6-18)

Equation 6.6-18 applies for all t such that for $0 \le t \le (1 - a_0)/a_1$.

For convenience, define:

$$t_c = \frac{1 - a_0}{a_1} \qquad \text{(Eq. 6.6-19)}$$

From Equations 6.6-15 and 6.6-16 it follows that, for $t = {}^{99}\text{Tc} + t_x$, where $t_x > 0$:

$$
\begin{aligned}
f_i(t) &= 1 - W(0)\, f_b(t) - \int_0^{t_x} \frac{dW(t)}{dt}\, f_b(t-t)\,dt \;\; - \int_{t_x}^{t} \frac{dW(t)}{dt}\, f_b(t-t)\,dt \\
&= 1 - W(0) - \int_0^{t_x} \frac{dW(t)}{dt}\,dt \;\; - \int_{t_x}^{t} \frac{dW(t)}{dt}\,(a_0 + a_1(t-t))\,dt \\
&= 1 - W(0) - [W(t_x) - W(0)] - (a_0 + a_1 t)\int_{t_x}^{t} \frac{dW(t)}{dt}\,dt \;\; + a_1 \int_{t_x}^{t} \frac{dW(t)}{dt}\,t\,dt \\
&= 1 - W(t_x) - (a_0 + a_1 t)[W(t) - W(t_x)] + a_1 \int_{t_x}^{t} \frac{dW(t)}{dt}\,t\,dt
\end{aligned}
$$

(Eq. 6.6-20)

In writing Equation 6.6-20, the interval of integration from Equation 6.6-15 has been divided in two. These intervals reflect the differing forms of f_b in different regions.

By differentiating Equation 6.6-20, one obtains:

$$
\begin{aligned}
\frac{df_i(t)}{dt} &= -\frac{dW(t_x)}{dt} - (a_0 + a_1 t)\frac{dW(t)}{dt} + (a_0 + a_1 t)\frac{dW(t_x)}{dt} - a_1 W(t) + a_1 W(t_x) \\
&\quad + a_1 t \frac{dW(t)}{dt} - a_1 t_x \frac{dW(t_x)}{dt} \\
&= -a_0 \frac{dW(t)}{dt} + (a_0 + a_1 t - 1 - a_1 t_x)\frac{dW(t_x)}{dt} - a_1 W(t) + a_1 W(t_x) \\
&= -a_0 \frac{dW(t)}{dt} - a_1 W(t) + a_1 W(t_x)
\end{aligned}
$$

(Eq. 6.6-21)

In carrying out the differentiation, it is important to recognize that t_x is a function of t; $t_x = t - t_c$. To obtain the last line of Equation 6.6-21, note that $a_1 t_x = a_1(t - t_c) = a_1 t - (1 - a_0)$, so $a_0 + a_1 t - 1 - a_1 t_x = 0$. Equation 6.6-21 applies for $t > t_c$.

6.6.5 Unzipping Abstraction Summary for Many Waste Packages

This section summarizes the results of Sections 6.6.3 and 6.6.4 in a concise form for guidance in implementing a performance assessment. First, the inputs and outputs are defined. Next, the initial state of degradation is expressed in terms of the inputs. Finally, the method for determining changes in state of degradation is given.

Definition of Inputs and Outputs–The following inputs are required:

t	Time since emplacement.
L	Fueled length of rod.

$W(t)$ Fraction of waste packages breached at time t. $W(t)$ will be provided by a analysis of waste package degradation and will vary from one realization to the next.

$v(t)$ Unzipping speed at time t. $v(t)$ will be provided by a analysis of fuel rod unzipping and will vary from one realization to the next.

$f_b(t-t_w)$ Fraction of breached fuel rods at time t for a particular waste package that breached at time t_w. The function is defined by the following equation:

$$f_b(z) = 0 \text{ for } z < 0$$
$$= a_0 + a_1 z \text{ for } 0 \le z \le \frac{1-a_0}{a_1}$$
$$= 1 \text{ for } z > \frac{1-a_0}{a_1}$$

(Eq. 6.6-22)

The constant a_0 is the fraction of fuel rods that are breached when the waste package breaches. Rods that breach by short-term processes (such as creep rupture) may be included in this set because these processes will be essentially complete before significant numbers of waste packages breach. The constant a_1 gives the rate of change of the fraction of breached rods after the waste package is breached. This constant describes processes such as localized corrosion of the cladding. The values of a_0 and a_1 will reflect the cladding degradation analysis, and their values will vary from one realization to the next.

The following outputs are produced:

$h(t)$ Split propagation distance at time t.

$f_i(t)$ Fraction of "intact" fuel rods at time t. $f_i(t)$ is an average over all the rods in the entire group of waste packages. "Intact" means rods whose fuel is protected from alteration, thus the intact fraction includes all rods in intact waste packages and all rods with intact cladding in breached waste packages.

$f_u(t)$ Fraction of unzipping fuel rods at time t. $f_u(t)$ is an average over all the rods in the entire group of waste packages. No distinction among these rods is made on the basis of split length.

$f_e(t)$ Fraction of exhausted (fully unzipped) fuel rods at time t. $f_e(t)$ is an average over all the rods in the entire group of waste packages.

$F_g(t)$ Fraction of fuel gap inventory altered at time t.

$F_m(t)$ Fraction of fuel matrix inventory altered at time t.

Initial State of Degradation–The initial state of degradation (t = 0) is given by the following equations:

$$h(0) = 0 \quad \text{(Eq. 6.6-23)}$$

$$f_i(0) = 1 - W(0)\, f_b(0) \quad \text{(Eq. 6.6-24)}$$

$$f_u(0) = W(0)\, f_b(0) \quad \text{(Eq. 6.6-25)}$$

$$f_e(0) = 0 \quad \text{(Eq. 6.6-26)}$$

$$F_g(0) = W(0)\, f_b(0) \quad \text{(Eq. 6.6-27)}$$

$$F_m(0) = 0 \quad \text{(Eq. 6.6-28)}$$

Changes in State of Degradation–Changes in the state of degradation are calculated by the following method. First, values of h and f_i are calculated at a new value of time by integrating the following rates of change:

$$\frac{d}{dt} h(t) = v(t) \quad \text{(Eq. 6.6-29)}$$

$$\begin{aligned} \frac{d}{dt} f_i(t) &= -a_0 \frac{dW(t)}{dt} - a_1 W(t) \text{ for } 0 \le t \le \frac{1-a_0}{a_1} \\ &= -a_0 \frac{dW(t)}{dt} - a_1 W(t) + a_1 W\left(t - \frac{1-a_0}{a_1}\right) \text{for } t > \frac{1-a_0}{a_1} \end{aligned} \quad \text{(Eq. 6.6-30)}$$

Values of h and f_i must be accumulated so that previous values can be looked up later. After h and f_i have been calculated for a new value of time, f_e, f_u, and F_g are calculated at that time:

$$\begin{aligned} f_e(t) &= 1 - f_i(h^{-1}(h(t) - L/2)) \text{ for } t \ge h^{-1}(L/2) \\ &= 0 \text{ for } t < h^{-1}(L/2) \end{aligned} \quad \text{(Eq. 6.6-31)}$$

$$f_u(t) = 1 - f_i(t) - f_e(t) \quad \text{(Eq. 6.6-32)}$$

$$F_g(t) = 1 - f_i(t) \quad \text{(Eq. 6.6-33)}$$

In applying Equation 6.6-31, h^{-1} is the inverse function of h, that is:

$$h^{-1}(h(t)) = t \text{ for } t \ge 0 \quad \text{(Eq. 6.6-34)}$$

The last step is to calculate changes in F_m by integrating the following rate of change:

$$\frac{dF_m(t)}{dt} = \frac{2}{L} v(t) f_u(t) \quad \text{(Eq. 6.6-35)}$$

6.6.6 Unzipping Abstraction Summary for One Waste Package

The definitions and equations in Section 6.6.5 apply with the following exceptions:

Definition of Inputs and Outputs–The following input is changed:

t_w Time of waste package breach.

$W(t)$ This function is replaced by a Heaviside step function at $t = t_w$, i.e., $\Phi(t-t_w)$. For simplicity, $W(t)$ does not appear in the equations. Instead, its value (1 for times of interest) is used directly.

Initial State of Degradation–Since fuel alteration does not occur in an intact waste package, the initial state of degradation is defined at $t = t_w$ rather than $t = 0$:

$$h(t_w) = 0 \quad \text{(Eq. 6.6-36)}$$

$$f_i(t_w) = 1 - f_b(0) \quad \text{(Eq. 6.6-37)}$$

$$f_u(t_w) = f_b(0) \quad \text{(Eq. 6.6-38)}$$

$$f_e(t_w) = 0 \quad \text{(Eq. 6.6-39)}$$

$$F_g(t_w) = f_b(0) \quad \text{(Eq. 6.6-40)}$$

$$F_m(t_w) = 0 \quad \text{(Eq. 6.6-41)}$$

Changes in State of Degradation–Equations 6.6-30 and 6.6-34 are replaced by the following equations:

$$f_i(t) = 1 - f_b(t - t_w) \quad \text{(Eq. 6.6-42)}$$

$$h^{-1}(h(t)) = t \text{ for } t \geq t_w \quad \text{(Eq. 6.6-43)}$$

6.7 STAINLESS STEEL CLADDING

As discussed in CRWMS M&O 2000a, about 1.1% of the commercial fuel was clad with Stainless Steel (SS) cladding material. This material was used in the early core designs and is no longer used. CRWMS M&O 2000k analyzed the expected inventory of SS clad fuel and concluded that 3.49% of the CSNF WPs would contain SS clad fuel and the average percent of fuel in these WPs with SS cladding is 29.9%. This analysis is based on loading the fuel at the

repository as it is expected to be delivered. In TSPA-SR, the SS cladding will be assumed to be perforated when the WP fails and to be immediately available for unzipping. It was also discussed in Section 6.1 of CRWMS M&O 2000a that failed rods from reconstituted assemblies were loaded into assembly size cans for pool storage and later disposal. These cans will be analyzed as SS clad and will be available for unzipping as soon as the WP fails (no credit for the can itself). This group was analyzed to be 10% of the SS assemblies or about 200 cans. This raised the fraction of stainless steel assemblies from 29.9% to 32.9%. This is summarized in Attachment I, Rows 109 and 110.

7. CONCLUSIONS

The purpose of this AMR is to develop the summary cladding degradation abstraction that is consistent with and used in the TSPA-SR. This summary is also submitted to the Waste Form PMR. The methodology developed for this AMR is consistent with ASTM Standard C1174-97 (ASTM 1997). Earlier TSPAs analyzed the waste form as bare UO_2 which was available for dissolution at the intrinsic dissolution rate. Water in the WP quickly became saturated with many of the radionuclides, limiting their release rate. In TSPA-VA cladding was analyzed as part of the waste form and limited the amount of fuel available at any time to dissolve. The major components of cladding failure were failure in reactor operation, mechanical failure from rocks and general corrosion of patches. The current analysis considers rod perforations from failure from reactor operation, creep and stress corrosion cracking (SCC) failures, localized corrosion from fluorides, and seismic events as mechanisms for perforating the cladding. All stainless steel cladding is assumed perforated. The second phase of the analysis is the release of radionuclides through the fast release and unzipping of the cladding from the reaction of water and UO_2. The unzipping starts in the middle of the cladding and progress toward each end. This unzipping is driven by the intrinsic dissolution rate, which is dependent on the local temperature and chemistry. The following is a summary of the components used in TSPA-SR. Attachment I is a table of the numerical values. This information is also given in DTN: MO00004SPACLD07.043.

Cladding Condition as Received

The groups of WPs represented in the TSPA-SR have an initial percent of rods failed defined by:

Lower limit	=	0.0155 %
Median	=	0.0948 %
Upper limit	=	1.285 %

This failure rate is based on historical data on reactor operation and includes an uncertainty factor of 4. It also includes failure from dry storage, handling, and transportation. This percentage of rods is available for radionuclide release through fast release and unzipping when the WP fails. This information is summarized in Attachment I, Rows 6 and 7.

Creep Strain and SCC Failure

Creep is analyzed using Murty's creep correlation. Also, a rod with a maximum stress exceeding 180 MPa is assume to fail by Stress Corrosion Cracking (SCC). The resulting rod failure distribution is displayed in Figure 8 and given in Rows 40 through 55 of Attachment I. In TSPA-SR, for each realization, the peak WP surface temperature is established and a triangular distribution of the rod fraction is interpolated from the table given in Attachment I, Rows 40 through 55. As an example, for the average WP, the peak WP surface temperature is 277°C. The center rod peak temperature is 308°C and the rod failure distribution is:

Lower limit	=	1.06 %
Mean	=	3.39 %
Upper limit	=	24.8 %

Almost all of these failures were calculated to occur in the highest stressed rods during dry storage and shipping during which time temperatures of 350°C were calculated. When WP peak surface temperatures reach 300°C which is not expected in the repository, rod failures in the repository start to become more significant.

The percent of failed rods from creep strain and SCC is summed with the failures from "as received" and is available to release radionuclides through fast release and unzipping when the WP fails.

Localized Corrosion

In the localized corrosion analysis, all the J13 water is concentrated on a 10 mm length of a single rod. All of the fluoride reacts with the 10 mm length of cladding of this single rod until the cladding fails from fluoride corrosion. Corrosion then starts on another rod. This analysis makes the rod failure fraction linearly dependent on the water ingression rate (% failed = 0.0413 * m^3 water in WP). The water ingression into the WP increases with time as additional patches on the WP fail or open. Rod failure rate also depends on the location of the WP group because of different drip rates in different repository regions. As an example, with 50 liters/year of J13 water entering the WP (2.2 ppm fluoride), 20% of the rods would fail by fluoride corrosion in 10,000 years. This information is summarized in Attachment I, Rows 57 through 59.

Mechanical (Seismic) Failures

A very severe seismic event which occurs with a frequency of 1.1×10^{-6} events/year fails all of the cladding and all the rods are available for fast release and unzipping when the WP fails. This is included in the TSPA-SR base case and sampled every time step. This information is summarized in Attachment I, Rows 115 through 117.

Stainless Steel Cladding

The abstraction places the Stainless Steel (SS) cladding into WPs as it arrives at YMP. This results in 3.49% of the WPs contain SS cladding. These WPs contain 32.9% SS cladding which is failed and available for fast release and unzipping when the WP fails. In the TSPA-SR, WPs containing SS cladding are considered a different fuel type group with a high initial cladding

failure percent (32.9%). This information is summarized in Attachment I, Rows 109 through 111.

Fast Release Fraction

When the WP fails or when the rod fails after WP failure, some of the radionuclides are immediately released. This includes the inventory of radionuclides in the gap between the fuel pellet and cladding, including that which is initially released from the early UO_2 interaction with the water. The gap release of iodine equals the fission gas release of 4.2% and cesium is one third this value or 1.4%. The fast release fraction for other radionuclides including additional cesium and iodine is an average of 0.2% (range 0 to 0.4%, uniformly distributed) from the UO_2 dissolution. This information is summarized in Attachment I, Rows 62 through 65.

Cladding Unzipping and Fuel Dissolution

The initial cladding damage occurs at the center of the fuel rod and the split (unzipping) will then propagate to both ends of the active fuel length. The unzipping velocity is 40 (range 1 to 240, triangle distribution) times the intrinsic dissolution velocity. The intrinsic dissolution velocity is a function of the temperature and chemistry inside the WP. This relationship is given in Rows 69 to 92 of Attachment I and is included in the TSPA-SR. An example calculation with a WP with J13 type water chemistry at $40^{o}C$, predicts 20% unzipping of failed rods in 10,000 years.

In summary, the cladding degradation is analyzed in TSPA-SR in two stages: Cladding failure and cladding fast release and unzipping. The cladding degradation abstraction depends on the WP temperature, internal chemistry, WP surface perforation rate, and location (amount of water dripping on the WP). Uncertainties have been established for the important parameters and the results vary for each TSPA-SR realization. Typically, 2.54% of the cladding is failed from previous reactor operations and creep or SCC failures. Little additional creep or SCC failures occur under design repository conditions but creep failures could become important for a high temperature repository design. Localized corrosion depends on the water ingression rate which depends on the number of patches open or failed on the WP surface and the location of the WP in the repository. For a water ingression rate of 50 liters/year of J13 water into a WP, 20% of the rods in that WP fail from localized corrosion in 10,000 years. Most WPs are located in regions of little or no water ingression and do not undergo localized failure. When the WP fails, there is a fast release of radionuclides from the failed cladding gap. Then an average additional 20% is released from cladding unzipping in the next 10,000 years after WP failure from cladding unzipping, depending on local chemistry. With the ranges and uncertainties included in the abstraction, this analysis is valid for its intended use, analyzing cladding degradation in the TSPA-SR . This analysis and the TSPA-SR abstraction do not address the potential for damaging the cladding at the surface facilities at YMP. The cladding degradation analysis considers the WP peak surface temperature as an independent variable, and the results are usable for a repository design with or without backfill. The models are sensitive to thermal loading and would have to be modified if the WP thermal loading were significantly changed.

Alternative Conceptual Analysis: The analysis by S. Cohen & Associates (1999, p. 7-1 to 7-4) is considered an alternative conceptual analysis and qualitatively agrees with this AMR. The earlier YMP TSPA's performed in 1993 and 1995 did not consider cladding, and as such are an

alternative conceptual analysis that is extremely conservative because it permits all fuel to dissolve at the intrinsic dissolution rate. A solubility limit (an indirect way of considering secondary phases) is used to limit the release rate of the fuel. European site TSPAs also did not consider cladding. The European sites were both saturated and reducing environments where the UO_2 dissolution rates were so slow that cladding degradation was not considered.

The following table contains a listing of specific technical issues addressed in Revision 2 of the NRC IRSR, for Container Life and Source Term (IRSR-CLST) (NRC 1999, pp. 56-59) and the status of their resolution.

Table 9. Resolution of IRSR-CLST Issues

Technical Issue	Resolution Status
Evaluate the processes of pitting corrosion and Stress Corrosion Cracking in the presence of oxidizing chloride solutions. Evaluate the effects on cladding integrity within the WC.	Pitting is addressed in CRWMS M&O 2000c SCC is addressed in this AMR Localized corrosion by Fluoride is addressed in this AMR
Evaluate and assess creep rupture models and the validity of extrapolation to lower temperatures. Resolve issues relating to the DCCG model of creep.	Creep Rupture addressed in CRWMS M&O 2000a and this AMR
Further qualify the DHC analysis with the use of a crack-size distribution in the cladding. Assess hydrogen embrittlement in the cladding as a function of cladding temperature and assess the possibility of hydride reorientation.	DHC is quantified in CRWMS M&O 2000a, and CRWMS M&O 2000l Hydride embrittlement is addressed in CRWMS M&O 2000b Hydride reorientation is addressed in CRWMS M&O 2000l
Develop models for clad splitting for repository storage temperatures in dry air and aqueous environments.	Clad dry splitting is addressed in CRWMS M&O 2000b Wet splitting is addressed in CRWMS M&O 2000e and this AMR
Assess the possibility of cladding mechanical failure during rock fall and seismic events using a fracture mechanics model.	Addressed in CRWMS M&O 1999d and this AMR
Evaluate the damage introduced during reactor operation and deterioration during transportation and dry storage that may affect the behavior under disposal conditions.	Addressed in CRWMS M&O 2000a and this AMR

DTN: MO00004SPACLD07.043

Some of the input data listed in Section 4 have been labeled “to be verified” (TBV) in the DIRS database. These reactor fuel parameters from the open literature have been submitted to the DOE for approval as accepted data. When acceptance is received, the TBV’s will be removed from these parameters.

This document may be affected by technical product input information that requires confirmation. Any changes to the document that may occur as a result of completing the confirmation activities will be reflected in subsequent revisions. The status of the input information quality may be confirmed by review of the Document Input Reference System database.

8. SOURCES OF INPUT

8.1 REFERENCES CITED

Ahn, T.M.; Cragnolino, G.A.; Chan, K.S.; and Sridhar, N. 1999. "Scientific Bases for Cladding Credit as a Barrier to Radionuclide Release at the Proposed Yucca Mountain Repository." *Scientific Basis for Nuclear Waste Management XXII, Symposium held November 30-December 4, 1998, Boston, Massachusetts, U.S.A.* Wronkiewicz, D.J. and Lee, J.H., eds. *556,* 525-533. Warrendale, Pennsylvania: Materials Research Society. TIC: 246426.

Chung, H.M.; Yaggee, F.L.; and Kassner, T.F. 1987. "Fracture Behavior and Microstructural Characteristics of Irradiated Zircaloy Cladding." *Zirconium in the Nuclear Industry, Seventh International Symposium Sponsored by ASTM Committee B-10 on Reactive and Refractory Metals, Strasbourg, France, 24-27 June 1985.* Adamson, R.B. and Van Swam, L.F.P., eds. Pages 775-801. Philadelphia, Pennsylvania: American Society for Testing and Materials. TIC: 238255.

CRWMS M&O 1999a. *Cladding Degradation - Abstraction and Summary Analysis Results for Input to TSPA Analyses.* TDP-WIS-MD-000005 REV 00. Las Vegas, Nevada: CRWMS M&O. ACC: MOL.19990902.0471.

CRWMS M&O 1999b. *Conduct of Performance Assessment.* Activity Evaluation, September 30, 1999. Las Vegas, Nevada: CRWMS M&O. ACC: MOL.19991028.0092.

CRWMS M&O 1999c. *Thermal Loading Histogram for 21-PWR (Pressurized Water Reactor) Absorber Plate Waste Packages.* Input Transmittal PA-WP-99366.T. Las Vegas, Nevada: CRWMS M&O. ACC: MOL.19991115.0138.

CRWMS M&O 1999d. *Breakage of Commercial Spent Fuel Cladding by Mechanical Loading.* CAL-EBS-MD-000001 REV 00. Las Vegas, Nevada: CRWMS M&O. ACC: MOL.19991213.0237.

CRWMS M&O 1999e. *Thermal Evaluation of Breached 21-PWR Waste Packages.* CAL-UDC-ME-000002 REV 00. Las Vegas, Nevada: CRWMS M&O. ACC: MOL.20000120.0447.

CRWMS M&O 2000a. *Initial Cladding Condition.* ANL-EBS-MD-000048 REV 00. Las Vegas, Nevada: CRWMS M&O. Submit to RPC. URN-0246.

CRWMS M&O 2000b. *Clad Degradation - FEPs Screening Arguments.* Input Transmittal 00138.T. Las Vegas, Nevada: CRWMS M&O. ACC: MOL.20000317.0475.

CRWMS M&O 2000c. *Clad Degradation - Local Corrosion of Zirconium and Its Alloys Under Repository Conditions.* ANL-EBS-MD-000012 REV 00. Las Vegas, Nevada: CRWMS M&O. ACC: MOL.2000405.0479.

CRWMS M&O 2000d. *CSNF Waste Form Degradation: Summary Abstraction.* ANL-EBS-MD-000015 REV 00. Las Vegas, Nevada: CRWMS M&O. ACC: MOL.20000121.0161.

CRWMS M&O 2000e. *Clad Degradation - Wet Unzipping: Release Rates from Breached Cladding and Potential Unzipping Velocity.* ANL-EBS-MD-000014 REV 00. Las Vegas, Nevada: CRWMS M&O. Submit to RPC. URN-0247.

CRWMS M&O 2000f. *Thermal History of Cladding in a 21 PWR SNF WP Loaded with Average Fuel.* CAL-UDC-ME-000001 REV 00. Las Vegas, Nevada: CRWMS M&O. ACC: MOL.20000216.0105.

CRWMS M&O 2000g. Reference Deleted.

CRWMS M&O 2000h. *Abstraction of Near Field Environment Drift Thermodynamic Environment and Percolation Flux.* ANL-EBS-HS-000003 REV 00. Las Vegas, Nevada: CRWMS M&O. Submit to RPC. URN-0039.

CRWMS M&O 2000i. *In-Package Chemistry Abstraction.* ANL-EBS-MD-000037 REV 00. Las Vegas, Nevada: CRWMS M&O. Submit to RPC. URN-0245.

CRWMS M&O 2000j. *Comparison of Creep Correlations.* Input Transmittal PA-WP-00048.Ta. Las Vegas, Nevada: CRWMS M&O. ACC: MOL.20000223.0002.

CRWMS M&O 2000k. *Stainless Steel in Waste Packages for TSPA-SR.* CAL-WAS-MD-000010. Las Vegas, Nevada: CRWMS M&O. Submit to RPC. URN-0252.

CRWMS M&O 2000l. *Hydride-Related Degradation of SNF Cladding Under Repository Conditions.* ANL-EBS-MD-000011 REV 00. Las Vegas, Nevada: CRWMS M&O. ACC: MOL.20000319.0048.

Cunningham, M.E.; Simonen, E.P.; Allemann, R.T.; Levy, I.S.; Gilbert, E.R.; and Hazelton, R.F. 1987. *Control of Degradation of Spent LWR Fuel During Dry Storage in an Inert Atmosphere.* PNL-6364. Richland, Washington: Pacific Northwest Laboratory. TIC: 210249.

Dyer, J.R. 1999. "Revised Interim Guidance Pending Issuance of New U.S. Nuclear Regulatory Commission (NRC) Regulations (Revision 01, July 22, 1999), for Yucca Mountain, Nevada." Letter from Dr. J.R. Dyer (DOE/YMSCO) to Dr. D.R. Wilkins (CRWMS M&O), September 3, 1999, OL&RC:SB-1714, with enclosure, "Interim Guidance Pending Issuance of New NRC Regulations for Yucca Mountain (Revision 01)." ACC: MOL.19990910.0079.

Einziger, R.E. and Kohli, R. 1984. "Low-Temperature Rupture Behavior of Zircaloy-Clad Pressurized Water Reactor Spent Fuel Rods Under Dry Storage Conditions." *Nuclear Technology, 67,* (1), 107-123. Hinsdale, Illinois: American Nuclear Society. TIC: 216868.

Harrar, J.E.; Carley, J.F.; Isherwood, W.F.; and Raber, E. 1990. *Report of the Committee to Review the Use of J-13 Well Water in Nevada Nuclear Waste Storage Investigations.* UCID-21867. Livermore, California: Lawrence Livermore National Laboratory. ACC: NNA.19910131.0274.

Henningson, P.J. 1998. *Cladding Integrity Under Long Term Disposal.* 51-1267509-00. Lynchburg, Virginia: Framatome Technologies. ACC: MOL.19990310.0103.

Lide, D.R., ed. 1995. *CRC Handbook of Chemistry and Physics.* 76th Edition. Boca Raton, Florida: CRC Press. TIC: 216194.

Manaktala, H.K. 1993. *Characteristics of Spent Nuclear Fuel and Cladding Relevant to High-Level Waste Source Term.* CNWRA 93-006. NRC-02-88-005. San Antonio, Texas: Center for Nuclear Waste Regulatory Analyses. TIC: 208034.

Matsuo, Y. 1987. "Thermal Creep of Zircaloy-4 Cladding Under Internal Pressure." *Journal of Nuclear Science and Technology, 24,* (2), 111-119. Tokyo, Japan: Atomic Energy Society of Japan. TIC: 237137.

NRC (U.S. Nuclear Regulatory Commission) 2000. *Interim Staff Guidance-11 — Storage of High Burnup Spent Fuel.* Washington, D.C.: U.S. Nuclear Regulatory Commission. TIC: 247227.

Peehs, M. 1998. *Assessment of Dry Storage Performance of Spent LWR Fuel Assemblies with Increasing Burn-Up.* Erlangen, Germany: Bereich Energieerzeugung. TIC: 245171.

Pescatore, C. and Cowgill, M. 1994. *Temperature Limit Determination for the Inert Dry Storage of Spent Nuclear Fuel.* EPRI TR-103949. Palo Alto, California: Electric Power Research Institute. TIC: 102933.

Pescatore, C.; Cowgill, M.G.; and Sullivan, T.M. 1990. *Zircaloy Cladding Performance under Spent Fuel Disposal Conditions Progress Report May 1 - October 31, 1989.* BNL 52235. Upton, New York: Brookhaven National Laboratory. ACC: NNA.19900710.0055.

Rothman, A.J. 1984. *Potential Corrosion and Degradation Mechanisms of Zircaloy Cladding on Spent Nuclear Fuel in a Tuff Repository.* UCID-20172. Livermore, California: Lawrence Livermore National Laboratory. ACC: NNA.19870903.0039.

S. Cohen & Associates 1999. *Effectiveness of Fuel Rod Cladding as an Engineered Barrier in the Yucca Mountain Repository.* McLean, Virginia: S. Cohen & Associates. TIC: 246541.

Sanders, T.L.; Seager, K.D.; Rashid, Y.R.; Barrett, P.R.; Malinauskas, A.P.; Einziger, R.E.; Jordan, H.; Duffey, T.A.; Sutherland, S.H.; and Reardon, P.C. 1992. *A Method for Determining the Spent-Fuel Contribution to Transport Cask Containment Requirements.* SAND90-2406. Albuquerque, New Mexico: Sandia National Laboratories. TIC: 232162.

Tasooji, A.; Einziger, R.E.; and Miller, A.K. 1984. "Modeling of Zircaloy Stress-Corrosion Cracking: Texture Effects and Dry Storage Spent Fuel Behavior." *Zirconium in the Nuclear Industry, Sixth International Symposium, Vancouver, British Columbia, June 28- July 1, 1982.* Franklin, D.G. and Adamson, R.B., eds. *ASTM STP 824,* 595-626. Philadelphia, Pennsylvania: American Society for Testing and Materials. TIC: 241417.

Weast, R.C. and Astle, M.J., eds. 1980. *CRC Handbook of Chemistry and Physics.* 61st Edition. Boca Raton, Florida: CRC Press. TIC: 242182.

Wilson, C.N. 1985. *Results from NNWSI Series 1 Spent Fuel Leach Tests.* HEDL-TME-84-30. Richland, Washington: Hanford Engineering Development Laboratory. TIC: 210347.

Wilson, C.N. 1987. *Results from Cycles 1 and 2 of NNWSI Series 2 Spent Fuel Dissolution Tests.* HEDL-TME-85-22. Richland, Washington: Hanford Engineering Development Laboratory. TIC: 202294.

Wilson, C.N. 1990. *Results from NNWSI Series 3 Spent Fuel Dissolution Tests.* PNL-7170. Richland, Washington: Pacific Northwest Laboratory. ACC: NNA.19900329.0142.

Witte, M.C.; Chun, R.C.; and Schwartz, M.W. 1989. "Dynamic Impact Effects on Spent Fuel Assemblies." *9th International Symposium on the Packaging and Transportation of Radioactive Materials, Washington, D.C., June 11-16, 1989. 1,* 186-194. Oak Ridge, Tennessee: Oak Ridge National Laboratory. TIC: 240741.

8.2 CODES, STANDARDS, REGULATIONS AND PROCEDURES

64 FR 8640. Disposal of High-Level Radioactive Wastes in a Proposed Geologic Repository at Yucca Mountain, Nevada. Proposed rule 10 CFR 63. Readily Available.

AP-2.13Q, Rev. 0, ICN 0. *Technical Product Development Planning.* Washington, D.C.: U.S. Department of Energy, Office of Civilian Radioactive Waste Management. ACC: MOL.19990701.0617.

AP-2.16Q, Rev. 0, ICN 0. *Activity Evaluation*. Washington, D.C.: U.S. Department of Energy, Office of Civilian Radioactive Waste Management. ACC: MOL.20000207.0716.

AP-3.10Q, Rev. 2, ICN 0. *Analyses and Models.* Washington, D.C.: U.S. Department of Energy, Office of Civilian Radioactive Waste Management. ACC: MOL.20000217.0246.

AP-SI.1Q, Rev. 2 ICN 4. *Software Management.* Washington, DC: U.S. Department of Energy, Office of Civilian Radioactive Waste Management. ACC: MOL.20000223.0508

ASTM C 1174-97. 1997. *Standard Practice for Prediction of the Long-Term Behavior of Materials, Including Waste Forms, Used in Engineered Barrier Systems (EBS) for Geological Disposal of High-Level Radioactive Waste.* West Conshohocken, Pennsylvania: American Society for Testing and Materials. TIC: 246015.

DOE (U.S. Department of Energy) 2000. *Quality Assurance Requirements and Description.* DOE/RW-0333P, Rev. 9. Washington, D.C.: U.S. Department of Energy, Office of Civilian Radioactive Waste Management. ACC: MOL.19991028.0012.

NLP-2-0, Rev. 5. *Determination of Importance Evaluations.* Las Vegas, Nevada: CRWMS M&O. ACC: MOL.19981116.0120.

NRC (U.S. Nuclear Regulatory Commission) 1998. *Issue Resolution Status Report Key Technical Issue: Total System Performance Assessment and Integration.* Rev. 1. Washington, D.C.: U.S. Nuclear Regulatory Commission. ACC: MOL.19990105.0083.

NRC (U.S. Nuclear Regulatory Commission) 1999. *Issue Resolution Status Report Key Technical Issue: Container Life and Source Term.* Rev. 2. Washington, D.C.: U.S. Nuclear Regulatory Commission. TIC: 245538.

QAP-2-0, Rev. 5. *Conduct of Activities.* Las Vegas, Nevada: CRWMS M&O. ACC: MOL.19980826.0209.

QAP-2-3, Rev. 10. *Classification of Permanent Items.* Las Vegas, Nevada: CRWMS M&O. ACC: MOL.19990316.0006.

8.3 SOURCE DATA

LL980711104242.054. Report of the Committee to Review the Use of J-13 Well Water in Nevada Nuclear Waste Storage Investigations. Submittal date: 08/05/1998.

MO0001SPAICC48.037. Initial Cladding Condition for CSNF. Submittal date: 01/27/2000. Submit to RPC. URN-0248.

MO0003SPASSC24.041. SCC Stress Threshold. Submittal date: 03/09/2000. Submit to RPC. URN-0251.

MO0003SPATCR22.038. Release from Wilson Series 2 Tests. Submittal date: 03/09/2000.

MO0003SPATCR30.039. TC Release From Wilson Series 1 Tests. Submittal date: 03/09/2000. Submit to RPC. URN-0249.

MO0003SPATCR70.040. TC Release From Wilson Series 3 Tests. Submittal date: 03/09/2000. Submit to RPC. URN-0250.

MO9912SPASFC01.032. Strain Failure Criteria. Submittal date: 12/15/99.

SN0001T0810599.008. Stainless Steel in Waste Packages for TSPA-SR (Total System Performance Assessment-Site Recommendation). Submittal date: 01/18/2000.

SN0001T0872799.006. In-Drift Thermodynamic Environment and Percolation Flux. Submittal date: 01/27/2000.

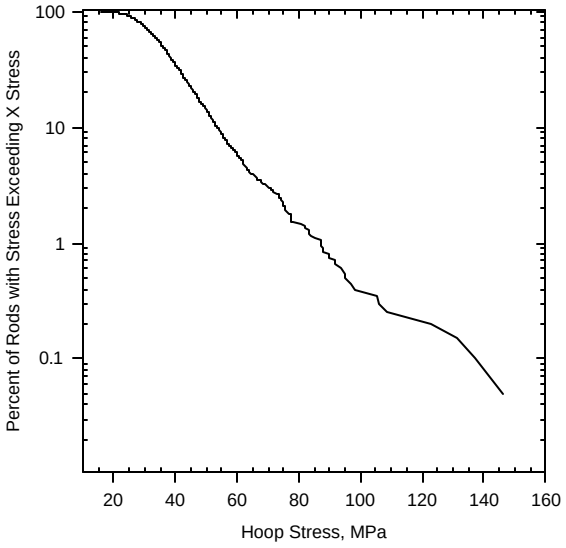

Figure 1. CCDF for Rod Stress as Received (Room Temperature)

(DTN: MO00001SPAIC48.037)

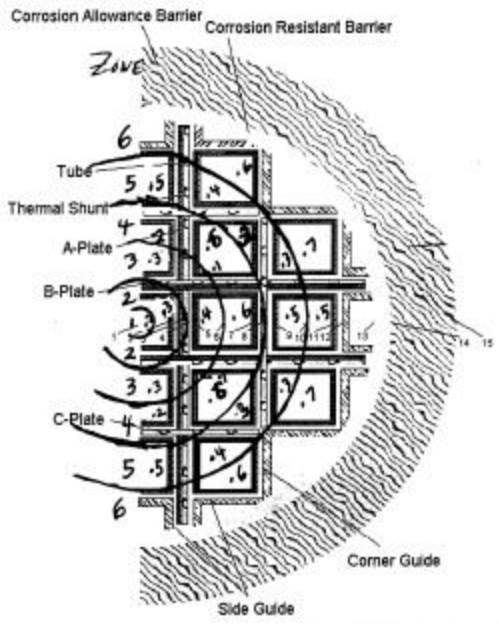

1	Mid-fuel Assembly (c01i000)	9	Inside Tube (s07i000)
2	Inside Tube (s01o000)	10	Mid-fuel Assembly (c07o000)
3	Inside A – Plate (b01o000)	11	Inside Tube (s07o000)
4	Outside A – Plate (a01o000)	12	Inside Side Guide (g07i000)
5	Inside Tube (s04i000)	13	Inside Alloy 22 Inner Barrier (i07i000)
6	Mid-fuel Assembly (c04o000)	14	Outside Alloy 22 Inner Barrier (i07o000)
7	Inside Tube (s04o000)	15	Outside A516 Outer Barrier (o07o000)
8	Mid-plate (b04i000)		

Figure 2. Nodal Locations and Zones for the 21 Assembly PWR Waste Package

(DTN: MO00004SPACLD07.043)

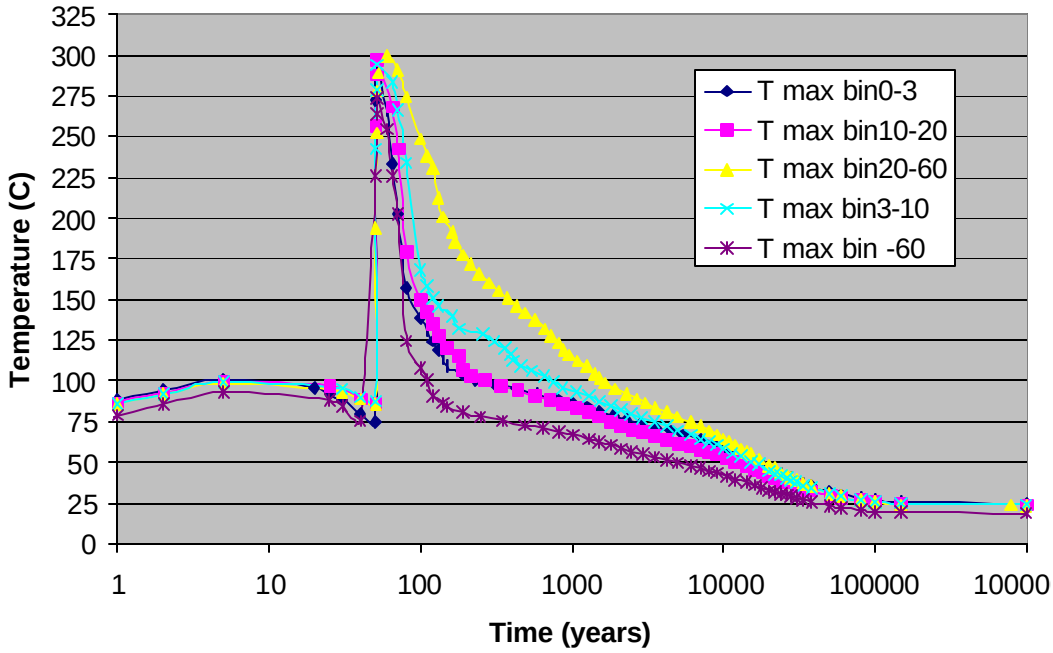

Figure 3. Maximum Temperature Distribution of the 5 Bins of WPs

(DTN: SN0001T0872799.006)

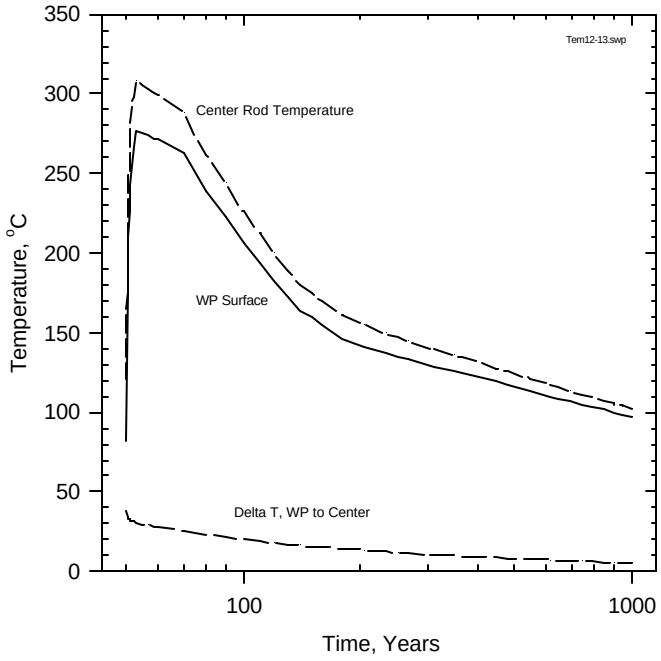

Figure 4. Temperature Histories for WP Surface and Center Rod

(DTN: MO00004SPACLD07.043)

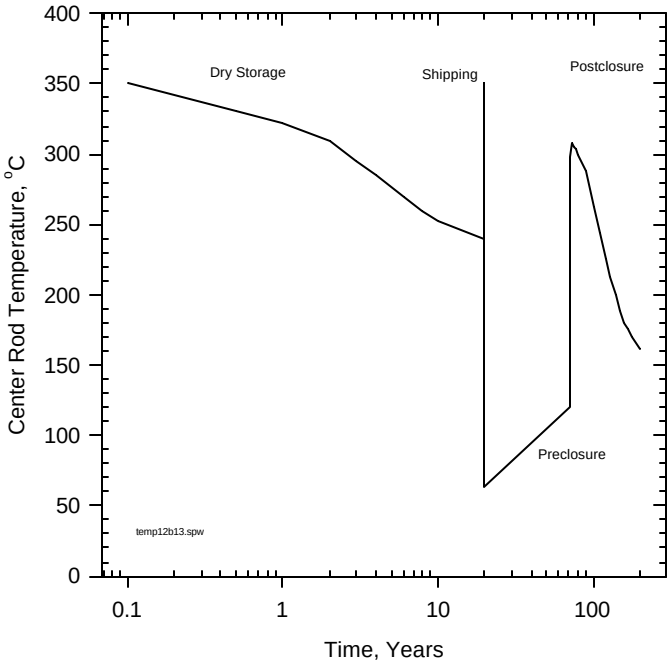

Figure 5. Center Rod Temperature History for Creep and SCC Analysis

(DTN: MO00004SPACLD07.043)

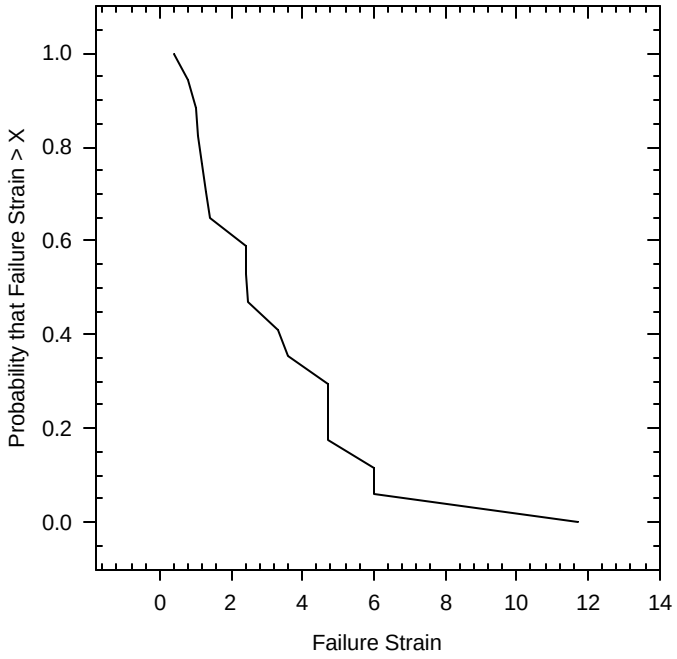

Figure 6. CCDF for Creep Strain Failure Criterion

(DTN: MO00004SPACLD07.043)

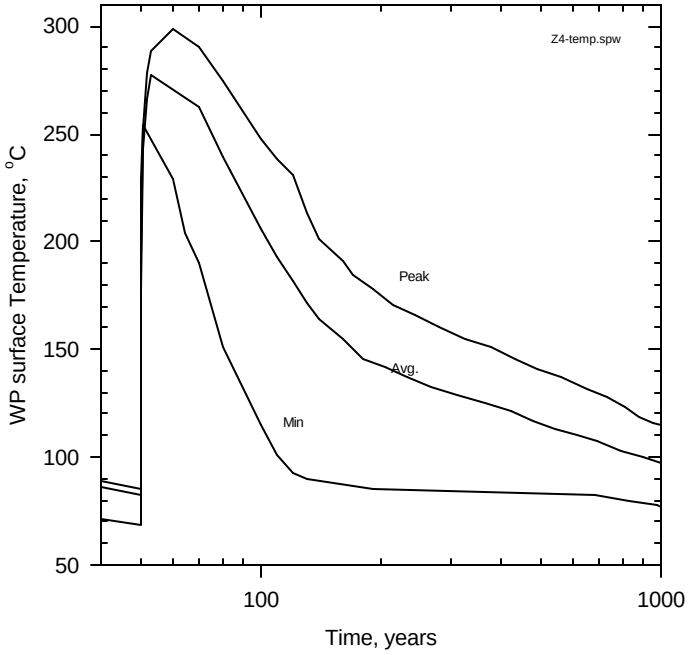

Figure 7. Minimum, Maximum, and Average Temperatures for Bin 4

(DTN: SN0001T0872799.006)

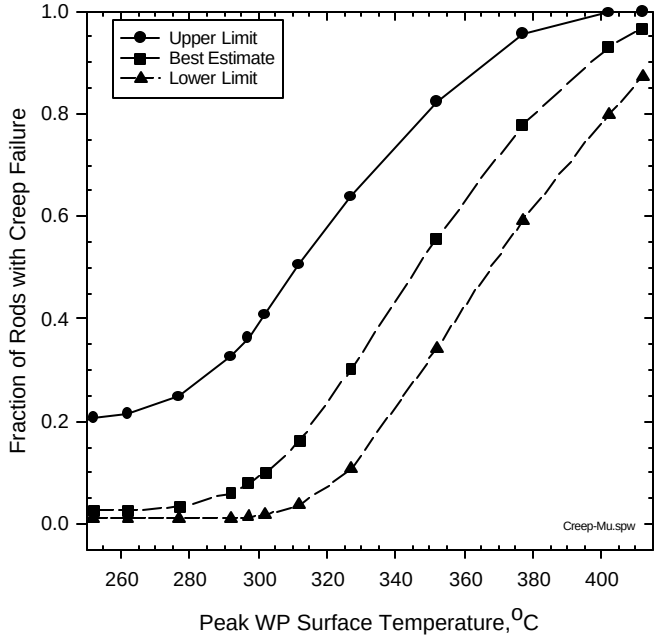

Figure 8. Creep Failure Fraction as a Function of Peak WP Surface Temperature

(DTN: MO00004SPACLD07.043)

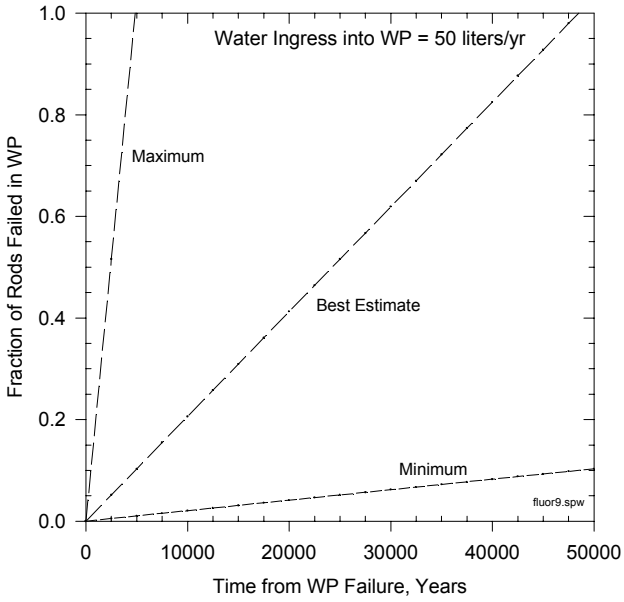

Figure 9. Example of Localized Corrosion with a Constant Water Ingression into WP

(DTN: MO00004SPACLD07.043)

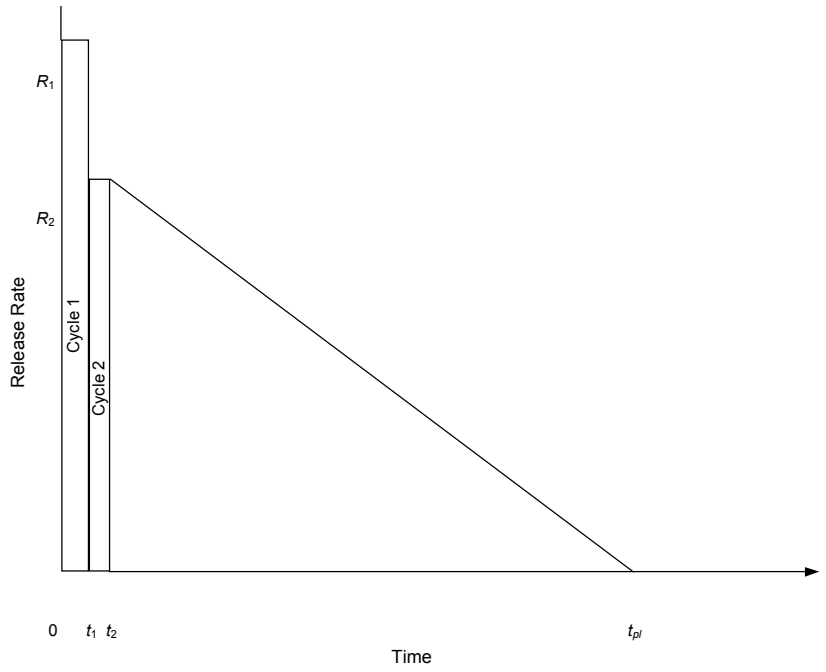

Figure 10. Radionuclide Release Rate Over Time for Fast Release

(DTN: MO00004SPACLD07.043)

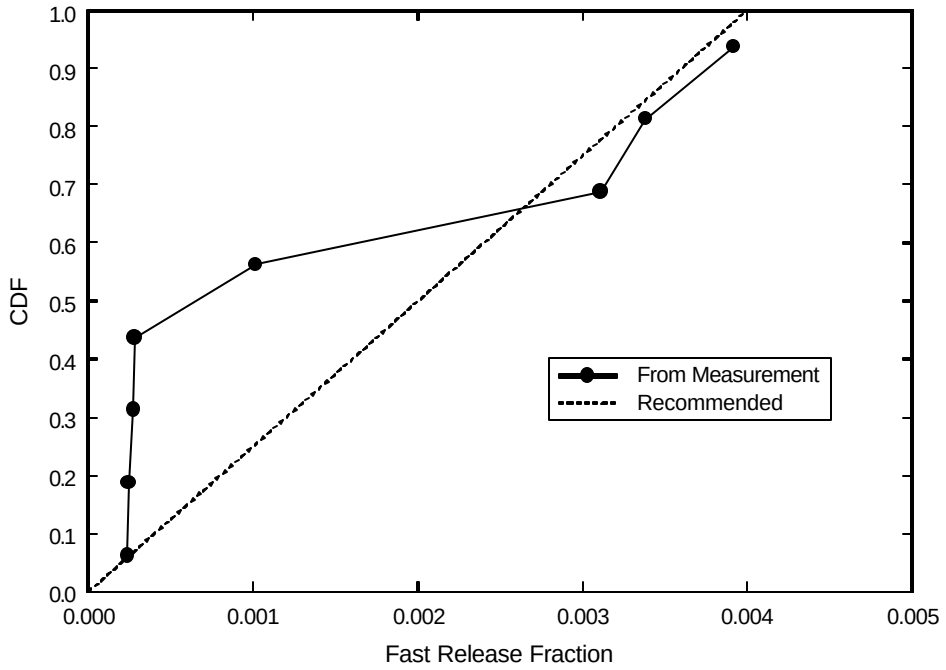

Figure 11. CDF for Fast Radionuclide Release Fraction from Fuel Matrix

(DTN: MO00004SPACLD07.043)

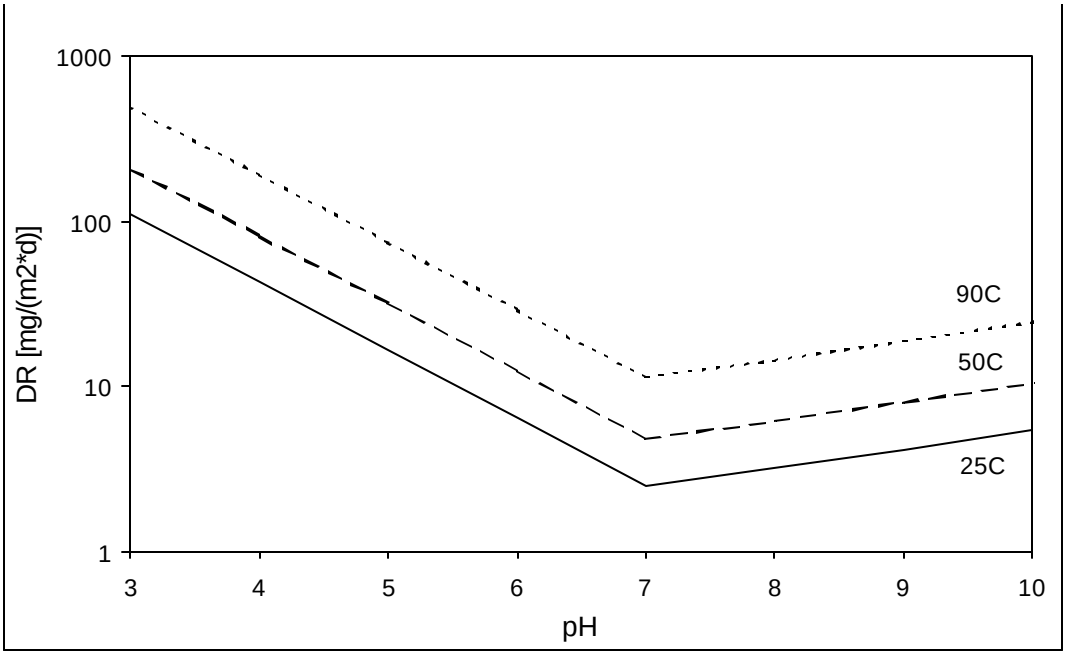

NOTE: Abstracted analysis evaluated at 10^{-3} atm. CO_2 and 0.2 atm. O_2

Figure 12. Abstracted Intrinsic Dissolution Analysis

(DTN: MOL.20000121.0161)

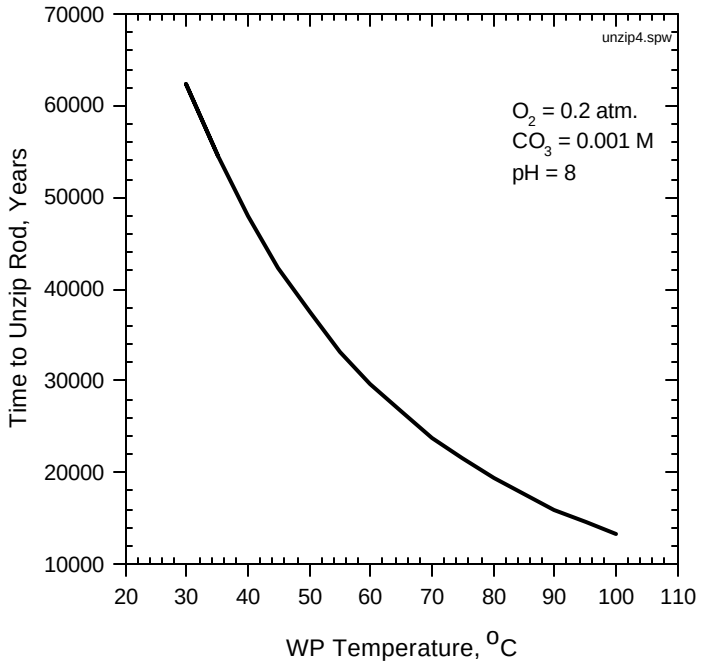

Figure 13. Unzipping Times vs. Temperature in WP

(DTN: MO00004SPACLD07.043)

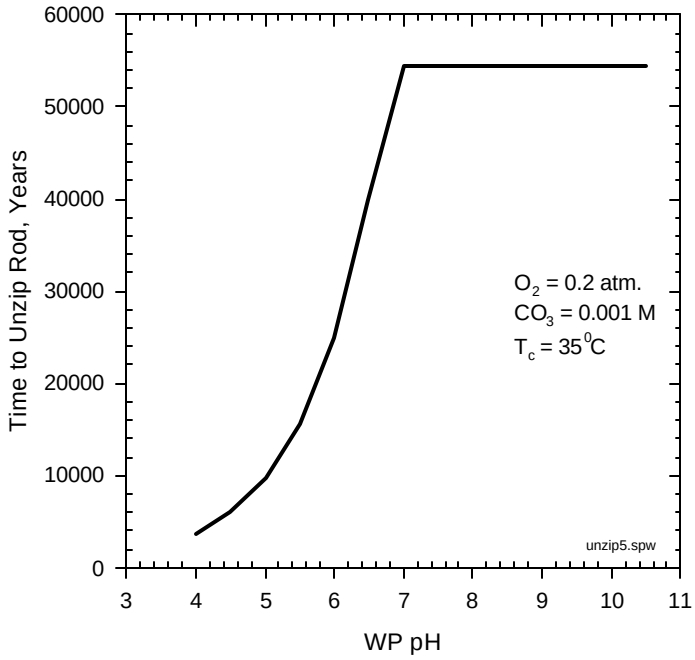

Figure 14. Unzipping Times vs. pH in Waste Package

(DTN: MO00004SPACLD07.043)

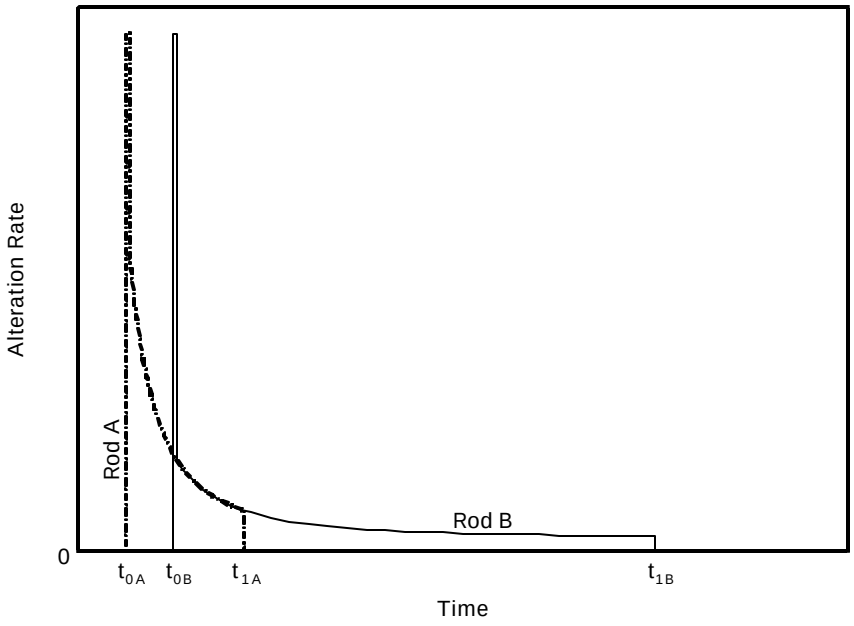

Figure 15. UO_2 Alteration Rate as a Function of Time for Two Fuel Rods (Schematic)

(DTN: MO00004SPACLD07.043)

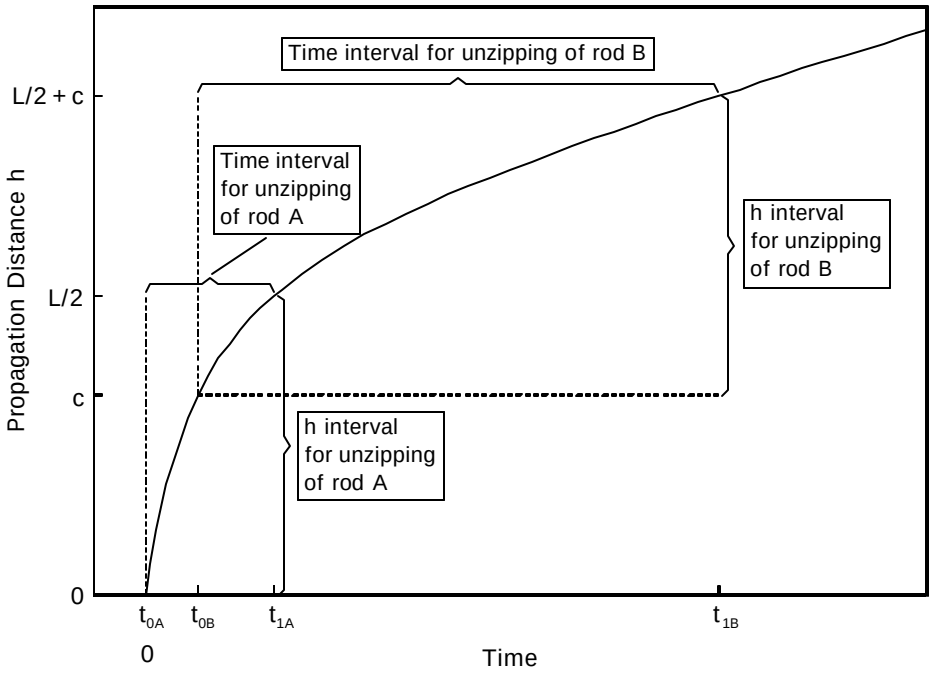

Figure 16. Propagation Distance and Unzipping of Two Fuel Rods (Schematic)

(DTN: MO00004SPACLD07.043)

9. ATTACHMENTS

The attachments are listed as follows:

Attachment	Title	Pages
I	Summary of Cladding Degradation Abstraction used in TSPA	2
II	Description of Software Routine: AMR-F0155 V1.xls	21

Attachment I

Summary of Cladding Degradation Abstraction Used in TSPA

	A	B	C	D	E	F	G	H
1	file = AMR-F0155-V1.xls							
2	**Sheet = Summary, p. 1**		**Total Cladding Abstraction**					
3								
4	**6.1) Cladding Condition as Received (to be added to creep failures)**							
5	For the 5 groups of WPs (approx. 1500 WPs / group)							
6	**Lower Limit=**	**0.0155**	%					
7	**Median=**	**0.0948**	%					
8	**Uppper lim=**	**1.2853**	%					
9	Distribution is triangular							
10	error factor =	4						
11	**CCDF**	**Lower Unc.**	**% failure, best estimate**	**Upper Unc**				
12	1.0000	0.0138	0.0550	0.2200	%			
13	0.9987	0.0146	0.0585	0.2341	%			
14	**0.9849**	**0.0155**	0.0622	0.2486	%			
15	0.8561	0.0179	0.0717	0.2869	%			
16	0.6555	0.0212	0.0849	0.3397	%			
17	0.5819	0.0224	0.0895	0.3582	%			
18	0.5058	0.0237	**0.0948**	0.3793	%			
19	0.2709	0.0284	0.1136	0.4545	%			
20	0.1966	0.0361	0.1445	0.5780	%			
21	0.1084	0.0507	0.2028	0.8111	%			
22	0.0970	0.0522	0.2089	0.8357	%			
23	0.0766	0.0741	0.2965	1.1859	%			
24	0.0640	0.0746	0.2983	1.1930	%			
25	**0.0503**	0.0803	0.3213	**1.2853**	%			
26	0.0373	0.1248	0.4990	1.9962	%			
27	0.0323	0.2469	0.9875	3.9499	%			
28	0.0221	0.2892	1.1568	4.6274	%			
29	0.0196	0.4496	1.7985	7.1941	%			
30	0.0190	0.5088	2.0352	8.1408	%			
31	0.0115	0.6939	2.7757	11.1029	%			
32	0.0036	0.7626	3.0505	12.2022	%			
33	0.0002	1.3214	5.2856	21.1424	%			
34	0.0000	1.3214	5.2856	21.1424	%			
35								
36								
37	**6.2) Creep&SCC Model, % Perforated rods at time=0**							
38	Table gives percents of pins considered perforated at time t=0							
39	use triangular distribution between low, best, high							
40	**WP Peak TC**	**Upper Limit**	**Best Estimate**	**Lower limit**				
41	<=177	19.4157	2.4400	1.0500	%			
42	177	19.4157	2.4400	1.0500	%			
43	227	19.4862	2.4414	1.0500	%			
44	252	20.5719	2.5762	1.0500	%			
45	262	21.5552	2.6686	1.0500	%			
46	277	24.7919	3.3914	1.0605	%, temp is nominal avg. WP temperature.			
47	292	32.6414	6.0357	1.2024	%			
48	297	36.2786	7.8276	1.3286	%			
49	302	40.7986	9.8676	1.7319	%			
50	312	50.5172	16.2162	3.6976	%			
51	327	63.7876	30.1857	10.6743	%			
52	352	82.2672	55.6748	34.2400	%			
53	377	95.5310	77.8867	59.1972	%			
54	402	99.6990	93.0167	79.8619	%			
55	>=412	99.8519	96.5757	87.1962	%			
56	**6.3) Localized Corrosion**		Uncertainty distribution log uniform between max and min					
57	**equation : fraction = M^3 water / 2.42E3M^3, max=10*fraction, min = fract/10**							
58	test case, 50 l/yr, 10,000 yrs, 1 L = 1E-3 m^3							
59	Fraction failed=	0.20661157						

	A	B	C	D	E	F	G	H
60					file = AMR-F0155-V1.xls			
61	**6.5 Fast Release Fraction, %**				**Sheet = Summary. P.2**			
62	Gap release	Iodine (I)	4.20%					
63	Gap release	Cesium (Cs)	1.40%					
64	Fast release	all radionuclides=	0 - 0.4%	uniform distribution				
65				Includes additional I, Cs				
66								
67	**6.6.1) Unzipping Velocity**							
68								
69	Perf =rods available for unzipping,sum(localized corrosion (2), creep (3), Initial failures(4))							
70	Vz = rod unzip velocity							
71	Vz = A * Vin			Active fuel length = 366 cm				
72	A = Unzip model parameter, triangle fit from lower, best estimate, upper							
73		**Possible range, Amin =1, Abest =40, Amax=240**						
74	Vin = Intrinsic dissolution Velocity							
75	**Vin = Dis rate (item 1) ***		**2.190E-05**	cm/yr / (mg/m2-d)				
76	Fuel exposed and disolved= Vz* Perf, check perf <=1.0							
77								
78	density, uo2			10	gm/cc	(includes 10% porosity)		
79	grain area/macro area=			6	area-micro/area-macro			
80	intrinsic, macro			0.000219	gm/cm2-yr			
81	cm/yr / (mg/m^2-d), conversion of dissolution			0.0000219	cm/yr / (mg/m2-d)			
82		to velocity						
83								
84								
85								
86								
87	**6.6.2) Abstraction of Intrinsic Dissolution Rate**							
88								
89	**log10(rate) = a0 + a1/Tk + a2* PCO3 + a3* PO2 + a4 * pH**							
90	**Term=**			**a0**	**a1**	**a2**	**a3**	**a4**
91	**pH>7**			**4.69**	**-1085**	**-0.12**	**-0.32**	**0**
92	**pH< =7**			**7.13**	**-1085**	**0**	**-0.32**	**-0.41**
93	**Example calc.**				**Tc**	**PCo3**	**PO2**	**pH**
94	**dis Rate**	**log10(dis rt)**	**Acidic solution**	**Basic solution**	**Tc**	**PCo3**	**PO2**	**pH**
95	6.066	0.783	0.6769	0.7829	50	2.7	0.7	7
96	14.224	1.153	1.0470	1.1530	90	2.7	0.7	7
97	73.624	1.867	1.8670	1.1530	90	2.7	0.7	5
98	325.638	2.513	2.5127	0.9787	70	2.7	0.7	3
99	units:	dis rate= mg/m2-d, m2 is microscopic (grains)						
100		Tc = temperature, centigrade, WP wall				Tk = Temp, Kelvin		
101		PCO3 = CO3 activity = -log10(molar CO3)						
102		PO2 = O2 activity = -log10(partial pressure O2)						
103		pH = standard,						
104	**Uncertainty in dissolution a0 +- 1.0, uniformly distributed**							
105	This equation is used in the unzipping abstraction							
106								
107	**6.7 Stainless Steel Clad Commercial Reactor Fuel**							
108								
109	**% of WPs containing SS cladding =**				**3.49**			
110	**% of fuel in these WPs with SS cladding =**				**32.89**			
111	Assumption, all SS cladding is perforated, available for unzipping							
112								
113	**6.4.1 Seismic Failures**							
114								
115	Frequency = 1.1E-6/yr							
116	All cladding failed (perforated)							
117	All cladding available for unzipping							

Attachment II

Description of Software Routine: AMR-F0155-V1.xls

The statistical analysis of the rod creep is performed in the software routine "AMR-F0155-V1.xls" (V1 represents Version 1) which is included in the DTN file: d$$. Microsoft Excel for Windows Version 4.0 was used for the analysis and the analysis is documented in this AMR as a software routine. The analysis was performed on a Dell Pentium personal computer (CPU number 111920) with a WINDOWS 95 operating system. One macro is used and is listed, tested and documented in this attachment. This attachment describes the various sheets that compose this software routine, including a listing of the top rows of each sheet of the file, and correlates the various equations presented in the text of this report to the software routine.

The software routine contains 9 sheets and one macro, many of which are linked. Each sheet addresses a specific aspect of cladding condition. Table II-1 summarizes the different sheets.

Table II-1. Description of Sheets in AMR-F0155-V1.xls

Sheet Title	Subject	Supports Sheet	Uses Sheet
Creep-Lim	Creep Failure Limit Samples	Fail-Calc	Rand #
Creep-Rod	Creep strain for single rod	Creep-WP	Temp-C
Creep-WP	Calculates creep across WP	Fail-Calc	Macro: Creep1, Creep-Rod
Fail-Calc	Collects statistics on creep failure	Final Creep Results	Creep-WP, Creep-Lim
Macro: Creep1	Calls Creep-Rod from Creep-WP	Creep-WP	Creep-Rod
Rand #	Table of random numbers	All distributions	None
Summary	Summary of output passed to TSPA	Listed as Attachment I	All
Temp-C	Temperature across WP	Creep-Rod	Temp-C2
Temp-C2	Initial rod and WP temperature histories	Temp-C	None
Unzip	Time to unzip rod	Figures 13,14	None

The Sheet "Summary" is listed as Attachment I and is not repeated in this attachment. The first 30 to 40 rows of the other sheets are included (in alphabetical order) in this attachment (Table II-5 to II-12). Many of the sheets have 2000 statistical samples and only the first few rows are included. A brief description of each sheet follows including the testing and test results.

This analysis is based on observed fuel performance for PWR fuel with Zircaloy cladding and therefore there are constraints, caveats and limitations to this analysis. This analysis is only applicable to U.S. commercial PWR and BWR fuel with Zircaloy cladding. It is also limited to fuel exposed to normal operation and anticipated operational occurrences (AOOs) and not for fuel that has been exposed to severe accidents. Fuel burnup projections have been limited to the current commercial power licensing environment

with restrictions on fuel enrichment, oxide coating thickness and rod plenum pressures. The ranges of applicability are:

1. Temperature: $27^{o}C$ to $420^{o}C$. The upper temperature limit is the highest temperatures of Matsuo's experiments. This is also the approximate temperature of the inside surface of the cladding during normal operation in a PWR ($340^{o}C$ to $370^{o}C$, (Pescatore et al. 1990, Table 3, p. 7)). The lower limit is not important since the cladding degradation rates become negligible at these temperatures.

2. Stress: 0 to 314 MPa. The lower limit is not important because low stress does not cause damage. The upper limit is the upper limit of Murty's test data for which the creep equation was derived.

3. Burnup: 2 to 80 MWd/kgU, the approximate range of experiments reported in this AMR.

The analysis itself addresses the uncertainties of the various parameters. Uncertainty ranges are defined for each parameter based on experimental observations reported in the literature. These uncertainties are statistically combined in the sampling routine. The range for each parameter is defined and justified in the body of this AMR.

The following sections describe how the analysis is performed and the analytical sequence used.

Sheet "Fail-Calc"

The Sheet "Fail-Calc" (for failure calculation) is the main driver for the calculation of creep failures in the WP (see Table II-8 for the first 2 of 6 zones). The user inputs the shift in the WP surface temperature into Cell D22 and starts the macro: Creep1. The creep calculations are then calculated for the specific WP temperature history. The user must copy the results for this WP temperature (Cells E22 through H22) into the table of results shown in Cells E3 through H18. This table is used to generate Figure 8 and is reproduced in the "Summary" Sheet, Rows 37 to 55.

The user also specifies the strain uncertainty (Cell B22, usually 0.8). Calculated strain is uniformly distributed by a multiplication factor of 0.2 to 1.8. This factor was developed in CRWMS M&O 2000m. The upper and lower creep failure criteria are also specified in Cells B23 and B24. These are the maximum and minimum creep failures measured by Chung et al. (1987, pp. 780,781).

The rod stress (room temperature) is given in Cells C29 through C2028. These are generated in CRWMS M&O 2000a and have been ordered by decreasing stress so that trends can be observed. Column B gives the sample or case number so that specific characteristics of a sample can be determined. One rod, at the stress specified in Column C, is placed in each of the 6 zones of the WP and the creep is calculated in the Sheet "Creep-WP". Table II-2 identifies the columns used for calculating the various failure indices for the six zones. Row 26 identifies the zones. For each zone, the resulting creep

strain is calculated in the Sheet: "Creep-WP" and is given in the first column of "Fail-Calc" for the specific zone. A creep strain (in percent) greater than 100 means that creep failure is expected for that rod. Creep strain of 99 means that the rod was identified as having a peak stress over 180 MPa and failure is expected for that rod by SCC. As the stresses decrease (i.e. at the higher row numbers in "Fail-Calc"), the strains decrease. The random sampled failure criterion is given in the second column for each zone of "Fail-Calc". This criterion is generated in the Sheet: "Creep-Lim" and will be discussed later.

The next three columns contain a rod failure index, either zero (0, i.e. the rod did not fail) or one (1, i.e. the rod failed). The creep strain uncertainty is calculated in these cells. The first column is the resulting comparison for the upper limit, using 0.4% creep as the failure criterion. The next column uses the full CCDF for the failure criterion and compares the creep (Column D for Zone 1) to the failure criterion (Column E for Zone 1). The third column is the resulting comparison for the lower failure limit, using 11.7% creep as the failure criterion.

Table II-2. Column Assignments in Sheet "Fail-Calc" for Rod Creep Failure Calculations

Zone	Creep Strain Column	Creep Failure Criteria Column	Upper Limit Failure Index	CCDF Failure Index	Lower Limit Failure Index
1	D	E	F	G	H
2	I	J	K	L	M
3	N	O	P	Q	R
4	S	T	U	V	W
5	X	Y	Z	AA	AB
6	AC	AD	AE	AF	AG

The final statistics for rod failure from creep are performed in rows 22 to 25. The fraction of the 2000 samplings failed in each zone using the three failure criteria is calculated in Row 25 and is the sum of the index column divided by 2000. Row 24 is the fraction of rods in the WP that are located in each zone. This is calculated in Table 2 and shown in Figure 2. Row 23 is the product of Rows 24 and 25 and represents the fraction of rods in the WP that are located in a zone and have failed. Row 22 (Cells F22, G22, H22) sums the zones in Row 23 for the three failure criteria and gives the fraction of rods in the WP that have failed using the three failure criteria. These results are copied into the table in Cells E3 through H18 and are used to generate Figure 8.

Tests: The stress and case number (Columns C and B, starting in Row 29) are imported from CRWMS M&O 2000a and are tested by visual inspection using the case number. For Zone 1, the resultant creep values are listed in Column D. This can be tracked back to "Creep-WP". Failure criteria are given in Column E and can be tracked back to "Creep-Lim", Col. C. Col. F compares the creep, multiplied by an uncertainty, to the upper limit failure criteria (Cell B23). The creep uncertainty factor is 0.8 (Cell B22) and a uniform distribution of uncertainty is used as shown below:

$$\text{Creep} = \text{Creep(Col. D)}*[(1-\text{uncertainty}) + 2 * \text{uncertainty}* \text{rand}()] \quad \text{(Eq. II-1)}$$

Creep = Creep(Col. D)*[0.2 + 1.6* rand()] (Eq. II-2)

Where rand() = a random number from Sheet "Rand #", Col. J

This calculation can be tested by hand calculations (at lower stresses where creep is near the failure criterion). Column F assigns a zero or one, depending on whether the creep exceeds the creep limit. This is tested by inspecting down the 2000 samples of decreasing stress (all 2000 samples are not actually shown in Table II-8). This calculation is repeated in Columns G, H (Zone 1), K, L, M (Zone 2), P, Q, R (Zone 3), U, V, W (Zone 4), Z, AA, AB (Zone 5), AE, AF, AG (Zone 6). The summing of the statistics is tested with visual inspection.

Sheet "Fail-Calc" used Sheets "Creep-Lim" and "Creep–WP". A description of these sheets follows.

Sheet "Creep-Lim"

This sheet contains 6000 samplings of creep failure criteria. Rows 3 through 20 give the 18 creep strains reported by Chung et al. (1987, pages 780, 781). These are repeated in Rows 20 and 21 where the linear interpolation on the CCDF is performed. The samples are given in Rows 25 through 6024. Column D is a random number taken from Sheet: "Rand #". The random number is interpolated in Columns E through U and the resulting strain failure criterion is presented in Column C. Table II-3 shows the assignment of random failure criteria to zones. Table II-5 shows the top rows of this sheet.

Table II-3. Assignment of Creep Failure Criteria to Zones

Zone	Starting Location	Ending Location
1	C25	C2024
2	C1025	C3024
3	C2025	C4024
4	C2500	C4499
5	C30250	C5024
6	C4025	C6024

Test: Only part of the interpolation table is shown in Table II-5. Using Row 27 as a test, the random number 0.602 is taken from "Rand #", Cell C7. The interpolation is done with Cells K20 through L21 and can be tested:

Creep Lim (C27) = 1.4 + (2.4-1.4)*(0.647-0.602) / (0.647-0.588)
= 1.4 + 0.762 = 2.16

Sheet "Creep-WP"

In this sheet, the rod temperature coefficients are calculated for the 12,000 rods sampled across the WP (2000 stress samples, located in each of 6 zones). The temperature uncertainty (13.5%) is specified in Cell E3 and represents an uncertainty of 41.6^{o}C from the combined WP surface temperature uncertainty (22.1^{o}C) and the uncertainty in temperature across the WP (19.5^{o}C). The temperature uncertainty is calculated in Sheet "TempC2" Cell N55. The 2000 stress samples are repeated in Column C. The zone numbers are given in Row 5. For each zone, the first column is the temperature shaping coefficient and the second column is the resulting creep from the Sheet "Creep-Rod". The macro "Creep1" is used to couple Sheets "Creep-WP" to "Creep-Rod" and will be described below. The temperature shaping coefficient represents the product of the uniformly distributed temperature uncertainty (Cell E3) and the WP radial temperature shaping term. The WP radial temperature shaping term is calculated in Sheet "TempC", Cells F7 to K7 and will be described in that sheet description. The radial temperature shaping term adjusts the WP center rod temperature downward for the outer zones. The rod stress (Column C) and temperature shaping coefficient (example: Column D for Zone 1) are input for the rod creep calculation (Sheet "Creep-Rod") and the resulting creep (example: Column E for Zone 1) is stored in this sheet. The macro "Creep1" couples the "Creep-WP" Sheet and the "Creep-Rod" Sheet. Table II-7 shows the top rows (Zone 1 and 2) of Sheet "Creep-WP".

Test: This sheet imports the stress (Column C) from "Fail-Calc" Column C. The only calculation done here is the calculation of the temperature shaping coefficient (Column D for Zone 1). Using Cell D7 as a test calculation, the temperature uncertainty (Cell E3) is uniformly distributed using an equation similar to Equation II-1 and "Rand #" Cell A5 (0.232 value). The shaping coefficient for Zone 1 is in "TempC", Cell F7 and is one (1, i.e. center zone). The test calculation for Cell D7 is:

$$\begin{aligned} \text{Temp. Adj} &= \text{Shape coef} * \text{Uncertainty} \\ &= 1.0 * [\,(1.0 - 0.135) + 2 * 0.135 * 0.232] \\ &= 0.928 \text{ (Cell D7)} \end{aligned}$$

This calculation is repeated for each stress sample and each zone (Cols. D, F, H, J, L, N).

Macro: "Creep1"

A macro is used to couple the "Creep-WP" Sheet and the "Creep-Rod" Sheet. As described above, "Creep-WP" generates the temperature shaping term and contains the stress for 12,000 rods located across the WP. The Sheet "Creep-Rod" calculates the amount of creep for a single rod using these two inputs: Stress and temperature shaping factor. "Creep-Rod" produces a single output number of creep strain for the one rod analyzed. The details of "Creep-Rod" are described below. The macro "Creep1" copies the two inputs from "Creep-WP" to "Creep-Rod" and then writes the resulting answer (creep strain) from "Creep-Rod" to "Creep-WP" for the 12,000 rods being analyzed. The actual listing of the macro is given below in numbered lines printed in italics.

First line is the Macro title:

1) *Sub Creep1()*

This next line steps down the 2000 lines of stress samples

2) For i = 0 To 1999

Zone 1

This next line copies the temperature shaping term from Sheet “Creep-WP”, Row I+7, Column 4 (Column D) to Sheet “Creep-Rod”, Location B3.

3) Sheets("Creep-Rod").Range("B3").Value = Sheets("Creep-WP").Cells(i + 7, 4).Value

This next line copies the stress value from “Creep-WP”, Row i+7 Column 3 (Column C) to Sheet “Creep-Rod”, Cell B4.

4) Sheets("Creep-Rod").Range("B4").Value = Sheets("Creep-WP").Cells(i + 7, 3).Value

The next line shifts the resulting calculated strain from “Creep-Rod” Cell B5 to “Creep-WP”, row i+7, Column 5 (Column E).

5) Sheets("Creep-WP").Cells(i + 7, 5).Value = Sheets("Creep-Rod").Range("B5").Value

For the next 5 WP radial zones the temperature shaping index is copied to “Creep-Rod” and the resulting creep strain is written into “Creep-WP”. The same value of stress is used in all zones as was used for Zone 1 above.

Zone 2

6) Sheets("Creep-Rod").Range("B3").Value = Sheets("Creep-WP").Cells(i + 7, 6).Value

7) Sheets("Creep-WP").Cells(i + 7, 7).Value = Sheets("Creep-Rod").Range("B5").Value

Zone 3

8) Sheets("Creep-Rod").Range("B3").Value = Sheets("creep-WP").Cells(i + 7, 8).Value

9) Sheets("Creep-WP").Cells(i + 7, 9).Value = Sheets("Creep-Rod").Range("B5").Value

Zone 4

10) Sheets("Creep-Rod").Range("B3").Value = Sheets("Creep-WP").Cells(i + 7, 10).Value

11) Sheets("Creep-WP").Cells(i + 7, 11).Value = Sheets("Creep-Rod").Range("B5").Value

Zone 5

12) Sheets("Creep-Rod").Range("B3").Value = Sheets("Creep-WP").Cells(i + 7, 12).Value

13) Sheets("Creep-WP").Cells(i + 7, 13).Value = Sheets("Creep-Rod").Range("B5").Value

Zone 6

14) Sheets("Creep-Rod").Range("B3").Value = Sheets("Creep-WP").Cells(i + 7, 14).Value

15) Sheets("Creep-WP").Cells(i + 7, 15).Value = Sheets("Creep-Rod").Range("B5").Value

Bottom of the i “Do Loop”.

16) Next i

Alarm to announce problem is complete

17) Beep

18) Beep

19) Beep

20) Beep

21) End Sub

Test: The macro can be tested the following ways:

A) After running the macro, “Creep-Rod” contains the last rod analyzed, 2000 stress sample, zone 6. This can be visually compared with the value stored in “Creep-WP”. The cells to compare are given in Table II-4.

Table II-4. Comparison of Cells after Macro Run

Value	Creep-Rod	Creep-WP
Temperature Index	B3	N2006
Stress	B4	C2006
Strain	B5	O2006

B) The value of temperature index and stress for any rod in "Creep-WP" can manually be copied into Cells B3 and B4 of "Creep-Rod" and the resulting strain can be compared with that in "Creep-WP".

C) While having the top of the Sheet "Creep-Rod" on the computer screen, the macro can be run. The macro may be confirmed to step down the rod sample stresses since they are ordered by decreasing stress.

D) First run the macro with very high WP temperatures ("Fail-Calc" Cell D22 = 135^{o}C). This will fail most rods and the failure indices in "Fail-Calc" will be 1. While showing the indices for the middle of the stress samples (about Row 1000) on the computer monitor, the macro can be run again with "Fail-Calc" Cell D22 = -100^{o}C (very cold WP). This will produce very few rod failures and the macro may be confirmed to sweep down Sheet "Fail-Calc" changing the failure indices.

Sheet "Creep–Rod"

This sheet calculates the creep strain for a single rod given the initial room temperature stress and temperature index. As described above, this sheet is used 12,000 times to calculate the creep for all the rods listed in " Creep-WP". Table II-6a and b list this sheet.

The actual calculations are performed in Rows 10 through 67. The room temperature stress is specified as an input in Cell B4 and the temperature index is specified in Cell B3. The resulting strain is shown in Cell B5. The details of the creep analysis are as follows:

For Rows 8 through 64

Column	Description
A	Time in years, at YMP
B	Time, years, starting with dry storage
C	Gives the cladding temperatures, ^{o}C, at that time. The temperature history of the rod being analyzed is of the center rod, multiplied by the scaling factor to reduce the temperature for other zones and multiplied by the uncertainty factor.
D	Gives the cladding temperatures, Kelvin, at that time.
E	Stress, adjusted for the temperature at time using ideal gas law for the fission gas in the gas plenum, MPa
F	Time in hours
G	Total running sum of creep strain (Eq. 6.2-7, below)
H	Total (Glide +Coble) creep for temperature i and time i(Eq. 6.2-5, below)
I	Glide creep for temperature and time i (Eq. 6.2-3, below)

J Coble creep for temperature i and time i (Eq. 6.2-4, below)
K Total (Glide +Coble) creep for temperature i but time i-1 (Eq. 6.2-5, below)
L Glide creep for temperature i but time i-1 (Eq. 6.2-3, below)
M Coble creep for temperature i but time i-1 (Eq. 6.2-4, below)
N Youngs module, E (Eq. 6.2-6, below)
O Temperature coefficient for Arrhenius term (Temperature term Eq. 6.2-1, below)
P Coble creep rate (fraction/yr) for temperature at time i (Eq. 6.2-2, below)
P Glide creep rate (fraction/yr) for temperature at time i (Eq. 6.2-1, below)

The creep correlation developed by Murty (Henningson, 1998, p. 57, eqs. 9b, 11, 12, and 15) was used and is repeated below from Section 6.2:

$$\dot{e}_{Glide} = 4.97x10^{6} e^{-31200/T} \frac{E}{T}[\sinh(807\frac{s}{E})]^{3} \quad \text{(Eq. 6.2-1)}$$

$$\dot{e}_{Coble} = 8.83e^{-21000/T} \frac{s}{T} \quad \text{(Eq. 6.2-2)}$$

Glide creep strain: $$e_{glide} = \dot{e}_{glide}t + \frac{ke_T\dot{e}_{glide}t}{e_T + k\dot{e}_{glide}t} \quad \text{(Eq. 6.2-3)}$$

Coble creep strain: $e_{Coble} = \dot{e}_{Coble}t$ (Eq. 6.2-4)

Total creep: $e = e_{glide} + e_{Coble}$ (Eq. 6.2-5)

Various parameters and constants include:

$\varepsilon_T = 0.008$,
$\kappa = 10$
$E = (1.148x10^5 - 59.9T)\ x10^6$, Pa (T in K) (Eq. 6.2-6)
T= temperature (K)
σ= stress (Pa)
t= time (hours)

Integration over thermal transient: $\varepsilon(t_i) = \varepsilon(T_{i-1}, t_{i-1}) + [\varepsilon(T_{i,}\ t_i) - \varepsilon(T_i, t_{i-1})]$ (Eq. 6.2-7)

The Sheet "Creep-Rod" uses a rod temperature history in Cells C10 through C64 that is developed in two different places for two different time intervals. The rod temperatures for dry storage and transportation are developed in CRWMS M&O 2000a. The temperatures in the repository are developed in Sheets "TempC" and "TempC2", which are discussed next.

Test: In Row 71 of the Sheet "Creep-Rod" is a test case. This case is presented in CRWMS M&O 2000m and is an analysis of three experiments reported by Matsuo. The test conditions are: time duration = 960 hours, temperature = 360C, stress = 118 MPa (at

360°C). The measured strains (three tests) were 0.33, 0.40, and 0.44%. The reference, CRWMS M&O 2000m, reports a calculated creep of 0.517%, the same result as shown in Cell G71. This demonstrated that the equations were programmed correctly. Visual inspection and hand calculations were also performed. The summing of the creep strains (Column G) is tested with a hand calculation of the first few points.

Sheet "TempC2"

Cells A5 through B39 (Table II-11a) contain the WP surface temperature history from CRWMS M&O 2000h. Cells D5 through T44 give the WP internal temperatures from CRWMS M&O 2000f, Table 6-2, p. 29. Cells U5 to U44 give the temperature difference between the WP surface and center rod. Rows 46 through 91 interpolate in time the WP surface temperatures and internal temperature difference so that temperatures are available at the same times and can be added. The results of the interpolation are listed in Cells G46 through I90. These are copied to Sheet "TempC", Cells A8 through F51.

The temperature uncertainty is also calculated in Cells L46 through N55. The difference between the WP surface maximum temperature and average temperature (at the time of maximum temperature) for the WP is 22.1°C (CRWMS M&O 2000h). The uncertainty in temperature across the WP is the difference in peak center rod temperatures for a WP with helium fill (325.8°C, CRWMS M&O 2000f, Table 6-2, page 29) and the peak temperature with air and water in the WP (345.3°C, CRWMS M&O 2000g, Table 6-2, p.29) or 19.5°C. These two uncertainties are added and the total uncertainty is calculated to be 13.5% in Cell N55.

Tests: Rows 7 through 44 are a repeat of input temperatures and times and are tested by inspection. Column U (not shown in Table II-11a) is the difference between Columns F and T and is verified by hand calculation. The interpolation of WP temperatures is in Cells C46 through C91 and the interpolation of temperature difference across the WP is in Cells F7 through F90. Both are tested by visual inspection and hand calculations.

Sheet "TempC"

Sheet "TempC2" calculated the WP surface temperature history and the WP internal temperature difference history. These are imported into Cells A8 through F51 of Sheet "TempC". Sheet "TempC" (see Table II-10a, b) develops the temperature history for the rods that are located in the five non-center zones. The ratio of the temperature in any zone divided by the center rod temperature is the temperature shaping factor.

The temperature in the various zones is calculated in Cells A57 through F72. Column A gives the location for the temperatures as shown in Figure 2 and supplied by CRWMS M&O 2000f, Table 6-2, p. 29). Column B gives the temperature at the time that the temperatures peak for the 15 locations across the WP (Row 19 of Sheet "TempC2"). The time for the peak temperature is used because the greatest cladding creep occurs at the peak temperature. Column C gives the points that are averaged to give the rod temperatures in the various zones (see Table 2 and Figure 2). The results are in Column

D and temperature differences between locations 1-6 and the surface (i.e. location 15) are in Column E. The reduction factor (temperature difference in each zone/temperature difference for center zone) is given in Column F and copied to Cells F6 to K6.

The temperature distribution, both in time and radial location, is given in Cells F8 through K51. These are calculated by adding the product of the zone temperature index (Cells F6 through K6) and center rod temperature difference (Column E) to the WP surface temperature (Column B + Cell B55 for WP temperature shift). The gross temperature index is then calculated and given in Cells F7 through K7. This is used in "Fail-Calc" to calculate the temperature for each rod. Cells F5 through K5 give the fraction of rods from the WP in each zone. This is the fraction that is given in Table 2 and also used in "Fail-Calc".

Test: This sheet averages the temperatures for the 6 zones. Testing is by visual inspection and hand calculations.

Sheet "Rand #" (Random Number Sheet)

This sheet contains 2000 rows of random numbers that were fixed after they were generated (see Table II-9). This has the same effect as using a fixed seed in a random number generator and is needed if the user is to get the same answer each time he accesses the spreadsheet. Row 4 identifies which calculation uses each column. Column P contains the sample number, which is available for tracking the results for any specific sample.

Test: This sheet is tested by inspection. As a test, the calculated mean and median for Cells A5 through O2004 are:

Test mean = 0.4992
Test median = 0.4989

These values are very close to the theoretical value of 0.5.

Sheet "Unzip"

This sheet calculated the time to unzip the cladding as a function of temperature (Rows 9 to 25) used for Figure 13 and pH (Rows 27 to 40) used for Figure 14. The intrinsic dissolution equation is given in Rows 4 to 7. For the temperature and chemical conditions given in Columns E through J, the dissolution rate is calculated in Column A. The unzipping velocity is calculated in Column K and the time to unzip a rod is calculated in Column L.

Test: This is tested by hand calculations. In addition, the calculations can be compared with the dissolution test calculation in Sheet "Summary," by applying the same chemical and temperature conditions.

Table II-5. Listing of Top Rows of Sheet: “Creep-Lim”

	A	B	C	D	E	F	G	H	I	J	K	L	M	N	O	P	Q	R
1	creep limit								file = AMR-F0155-V1.xls									
2	ccdf	strain %							**Sheet = Creep-Lim**									
3	1	0.4																
4	0.941177	0.8																
5	0.882354	1	This CCDF used for Fig. 6															
6	0.823531	1.1																
7	0.764708	1.2																
8	0.705885	1.3																
9	0.647062	1.4																
10	0.588239	2.4																
11	0.529416	2.4																
12	0.470593	2.5																
13	0.41177	3.3																
14	0.352947	3.6																
15	0.294124	4.7																
16	0.235301	4.7																
17	0.176478	4.7																
18	0.117655	6																
19	0.058832	6																
20	0	11.7		**CCDF**	1	0.941177	0.882354	0.823531	0.764708	0.705885	0.647062	0.588239	0.529416	0.470593	0.41177	0.352947	0.294124	0.235301
21	Mean	3.288889		**F. Strain**	0.40	0.80	1	1.1	1.2	1.3	1.4	2.40	2.40	2.50	3.30	3.60	4.70	4.7
22	Median	2.45																
23																		
24			Fail Strain	rand, f.Strain														
25			0.95	0.898514	0.00	0.95	0.00	0.00	0.00	0.00	0.00	0.00	0.00	0.00	0.00	0.00	0.00	0.00
26			4.70	0.202301	0.00	0.00	0.00	0.00	0.00	0.00	0.00	0.00	0.00	0.00	0.00	0.00	0.00	4.70
27			2.16	0.60249	0.00	0.00	0.00	0.00	0.00	0.00	2.16	0.00	0.00	0.00	0.00	0.00	0.00	0.00
28			0.65	0.962604	0.65	0.00	0.00	0.00	0.00	0.00	0.00	0.00	0.00	0.00	0.00	0.00	0.00	0.00
29			2.58	0.464965	0.00	0.00	0.00	0.00	0.00	0.00	0.00	0.00	0.00	2.58	0.00	0.00	0.00	0.00
30			1.04	0.860576	0.00	0.00	1.04	0.00	0.00	0.00	0.00	0.00	0.00	0.00	0.00	0.00	0.00	0.00
31			2.40	0.562003	0.00	0.00	0.00	0.00	0.00	0.00	0.00	2.40	0.00	0.00	0.00	0.00	0.00	0.00
32			0.79	0.942233	0.79	0.00	0.00	0.00	0.00	0.00	0.00	0.00	0.00	0.00	0.00	0.00	0.00	0.00
33			4.70	0.204424	0.00	0.00	0.00	0.00	0.00	0.00	0.00	0.00	0.00	0.00	0.00	0.00	0.00	4.70
34			0.83	0.931116	0.00	0.83	0.00	0.00	0.00	0.00	0.00	0.00	0.00	0.00	0.00	0.00	0.00	0.00

Table II-6a. Listing of Top Rows of Sheet: "Creep-Rod" (Col. A-J)

	A	B	C	D	E	F	G	H	I	J
1	Calculation of creep for a given stress and temperature profile							file = AMR-F0155-V1.xls		
2	Checks for SCC							**Sheet = Creep-Rd**		
3	**TC Unc**	0.9101584	**Input**							
4	**Room TC stress**	15.601665	**Input**							
5	**Resultant strain**	1.45E-02	**Output**							
6										
7		Columns B,C (with WP temperature shift = 0) used for Figure 5								
8	YMP time	total Time	T,C	Temperature	Stress	Time, hrs	Total strain	%	%	%
9		Yrs	C	K	Mpa	hrs	run sum	e(Ti,ti)	e-glide	e-coble
10		0	350							
11		0.50	330	613.2	31.89	4.38E+03	9.36E-03	9.36E-03	9.09E-03	2.69E-04
12		1.0	322	595.2	30.95	8.76E+03	1.12E-02	3.77E-03	3.58E-03	1.91E-04
13		2.0	310	583.2	30.33	1.75E+04	1.25E-02	2.48E-03	2.29E-03	1.85E-04
14		3.0	295	568.2	29.55	2.63E+04	1.28E-02	8.83E-04	7.76E-04	1.07E-04
15		4.0	285	558.2	29.03	3.50E+04	1.29E-02	4.41E-04	3.67E-04	7.35E-05
16		6.0	270	543.2	28.25	5.26E+04	1.29E-02	1.48E-04	1.09E-04	3.90E-05
17		8.0	260	533.2	27.73	7.01E+04	1.29E-02	7.20E-05	4.68E-05	2.52E-05
18		10.0	252	525.2	27.31	8.76E+04	1.30E-02	4.02E-05	2.30E-05	1.73E-05
19		20.000	240	513.2	26.69	1.75E+05	1.30E-02	2.43E-05	1.07E-05	1.36E-05
20		20.010	350	623.2	32.41	1.75E+05	1.31E-02	4.97E-01	4.78E-01	1.86E-02
21		20.068	350	623.2	32.41	1.76E+05	1.40E-02	4.98E-01	4.79E-01	1.87E-02
22	0	20.07	57	330.3	17.18	1.76E+05	1.40E-02	1.98E-15	8.26E-21	1.98E-15
23	50	70.07	110	382.8	19.91	6.14E+05	1.40E-02	4.21E-11	1.75E-14	4.21E-11
24	50.2	70.27	192	464.7	24.17	6.16E+05	1.40E-02	7.18E-07	5.04E-08	6.68E-07
25	50.4	70.47	206	479.1	24.91	6.17E+05	1.40E-02	3.02E-06	4.13E-07	2.60E-06
26	50.6	70.67	221	493.9	25.69	6.19E+05	1.40E-02	1.30E-05	3.20E-06	9.76E-06
27	50.8	70.87	236	508.8	26.46	6.21E+05	1.40E-02	5.59E-05	2.20E-05	3.39E-05
28	51	71.07	251	523.7	27.23	6.23E+05	1.40E-02	2.46E-04	1.37E-04	1.10E-04
29	52	72.07	271	544.2	28.30	6.31E+05	1.40E-02	1.98E-03	1.47E-03	5.07E-04
30	53	73.07	280	553.6	28.79	6.40E+05	1.41E-02	5.11E-03	4.12E-03	9.86E-04
31	55	75.07	278	551.0	28.66	6.58E+05	1.42E-02	4.06E-03	3.21E-03	8.49E-04
32	57	77.07	276	548.7	28.54	6.75E+05	1.43E-02	3.31E-03	2.57E-03	7.43E-04
33	59	79.07	273	546.5	28.42	6.93E+05	1.43E-02	2.73E-03	2.07E-03	6.53E-04
34	60	80.07	272	545.5	28.37	7.01E+05	1.44E-02	2.48E-03	1.87E-03	6.13E-04
35	70	90.07	262	535.0	27.83	7.89E+05	1.45E-02	9.81E-04	6.54E-04	3.26E-04
36	80	100.07	238	511.3	26.59	8.77E+05	1.45E-02	1.01E-04	4.25E-05	5.85E-05
37	90	110.07	222	495.1	25.75	9.64E+05	1.45E-02	2.26E-05	5.82E-06	1.68E-05
38	100	120.07	206	479.0	24.91	1.05E+06	1.45E-02	5.10E-06	6.97E-07	4.41E-06
39	110	130.07	193	466.2	24.24	1.14E+06	1.45E-02	1.55E-06	1.17E-07	1.43E-06
40	120	140.07	182	455.1	23.67	1.23E+06	1.45E-02	5.37E-07	2.31E-08	5.14E-07
41	130	150.07	172	445.3	23.16	1.31E+06	1.45E-02	2.05E-07	5.18E-09	2.00E-07
42	140	160.07	164	437.3	22.74	1.40E+06	1.45E-02	9.08E-08	1.45E-09	8.94E-08
43	150	170.07	159	432.3	22.48	1.49E+06	1.45E-02	5.52E-08	6.56E-10	5.46E-08
44	160	180.07	155	427.8	22.25	1.58E+06	1.45E-02	3.50E-08	3.16E-10	3.47E-08
45	180	200.07	146	419.4	21.81	1.75E+06	1.45E-02	1.46E-08	7.79E-11	1.45E-08
46	205	225.07	141	414.2	21.54	1.97E+06	1.45E-02	8.67E-09	3.30E-11	8.63E-09
47	232	252.07	136	409.3	21.29	2.21E+06	1.45E-02	5.33E-09	1.48E-11	5.32E-09
48	250	270.07	134	406.7	21.15	2.37E+06	1.45E-02	4.07E-09	9.42E-12	4.07E-09
49	265	285.07	132	404.7	21.05	2.50E+06	1.45E-02	3.34E-09	6.76E-12	3.34E-09
50	310	330.07	127	400.0	20.80	2.89E+06	1.45E-02	2.11E-09	3.09E-12	2.11E-09
51	350	370.07	123	396.6	20.63	3.24E+06	1.45E-02	1.50E-09	1.72E-12	1.50E-09
52	365	385.07	122	395.4	20.56	3.37E+06	1.45E-02	1.33E-09	1.40E-12	1.33E-09
53	450	470.07	116	389.3	20.25	4.12E+06	1.45E-02	7.10E-10	4.81E-13	7.10E-10
54	480	500.07	114	387.3	20.14	4.38E+06	1.45E-02	5.68E-10	3.30E-13	5.67E-10
55	550	570.07	110	383.3	19.93	4.99E+06	1.45E-02	3.68E-10	1.58E-13	3.67E-10
56	615	635.07	107	379.7	19.75	5.56E+06	1.45E-02	2.46E-10	8.08E-14	2.46E-10
57	650	670.07	105	378.2	19.67	5.87E+06	1.45E-02	2.06E-10	6.00E-14	2.06E-10
58	695	715.07	103	376.2	19.56	6.26E+06	1.45E-02	1.63E-10	4.05E-14	1.63E-10
59	750	770.07	101	374.1	19.45	6.75E+06	1.45E-02	1.29E-10	2.71E-14	1.29E-10
60	790	810.07	99	372.6	19.38	7.10E+06	1.45E-02	1.08E-10	2.02E-14	1.08E-10
61	850	870.07	97	370.6	19.27	7.62E+06	1.45E-02	8.58E-11	1.36E-14	8.58E-11
62	900	920.07	96	369.0	19.19	8.06E+06	1.45E-02	7.12E-11	9.96E-15	7.12E-11
63	950	970.07	95	367.7	19.12	8.50E+06	1.45E-02	6.17E-11	7.77E-15	6.16E-11
64	1000	1020.07	93	366.5	19.06	8.94E+06	**1.45E-02**	5.32E-11	6.03E-15	5.32E-11
65	SCC flag	0		%	32.41	Limited Strain=	1.45E-02			
66	Test Problem								eq. 11	eq.12
67	YMP time	total Time	T,C	Temperature	Stress	Time, hrs	Total strain	%	%	%
68		Yrs	C	K	Mpa	hrs	run sum	e(Ti,ti)	e-glide	e-coble
69		0.11	360	633.2	118.00	9.60E+02	0.517	5.17E-01	5.16E-01	6.23E-04
70					Test problem answer =		0.517			

Table II-6b. Listing of Top Rows of Sheet: "Creep-Rod" (Col. J-Q)

	J	K	L	M	N	O	P	Q
1					file = AMR-F0155-V1.xls			
2					**Sheet = Creep-Rd**			
3								
4								
5								
6								
7		**%**	fraction	fraction				
8	%	Creep tot,t(i-1)	t(i-1)	t(i-1)			fraction	fraction
9	e-coble	e(Ti,ti-1)	e-glide	e-coble	E	Tp Coe	Ec	Es-gl
10								
11	2.69E-04	na	na	na	7.81E+10	7.96E-23	6.13E-10	1.90E-09
12	1.91E-04	1.89E-03	1.79E-05	9.53E-07	7.92E+10	1.71E-23	2.18E-10	3.73E-10
13	1.85E-04	1.24E-03	1.15E-05	9.23E-07	7.99E+10	5.81E-24	1.05E-10	1.19E-10
14	1.07E-04	5.89E-04	5.17E-06	7.13E-07	8.08E+10	1.41E-24	4.07E-11	2.69E-11
15	7.35E-05	3.31E-04	2.75E-06	5.52E-07	8.14E+10	5.29E-25	2.10E-11	9.53E-12
16	3.90E-05	9.85E-05	7.25E-07	2.60E-07	8.23E+10	1.13E-25	7.43E-12	1.88E-12
17	2.52E-05	5.40E-05	3.51E-07	1.89E-07	8.29E+10	3.85E-26	3.60E-12	6.07E-13
18	1.73E-05	3.22E-05	1.84E-07	1.38E-07	8.33E+10	1.58E-26	1.97E-12	2.38E-13
19	1.36E-05	1.21E-05	5.36E-08	6.79E-08	8.41E+10	3.93E-27	7.75E-13	5.56E-14
20	1.86E-02	4.97E-01	4.78E-03	1.86E-04	7.75E+10	1.80E-22	1.06E-09	4.53E-09
21	1.87E-02	4.97E-01	4.78E-03	1.86E-04	7.75E+10	1.80E-22	1.06E-09	4.53E-09
22	1.98E-15	1.98E-15	8.26E-23	1.98E-17	9.50E+10	9.52E-42	1.13E-22	4.27E-29
23	4.21E-11	1.21E-11	5.01E-17	1.21E-13	9.19E+10	4.00E-36	6.86E-19	2.59E-23
24	6.68E-07	7.16E-07	5.03E-10	6.66E-09	8.70E+10	6.92E-30	1.08E-14	7.44E-17
25	2.60E-06	3.01E-06	4.12E-09	2.60E-08	8.61E+10	5.21E-29	4.22E-14	6.09E-16
26	9.76E-06	1.29E-05	3.19E-08	9.74E-08	8.52E+10	3.69E-28	1.58E-13	4.70E-15
27	3.39E-05	5.58E-05	2.20E-07	3.38E-07	8.43E+10	2.34E-27	5.46E-13	3.23E-14
28	1.10E-04	2.45E-04	1.36E-06	1.09E-06	8.34E+10	1.33E-26	1.76E-12	1.99E-13
29	5.07E-04	1.95E-03	1.45E-05	5.00E-06	8.22E+10	1.27E-25	8.03E-12	2.12E-12
30	9.86E-04	5.04E-03	4.06E-05	9.73E-06	8.16E+10	3.34E-25	1.54E-11	5.88E-12
31	8.49E-04	3.95E-03	3.13E-05	8.26E-06	8.18E+10	2.57E-25	1.29E-11	4.46E-12
32	7.43E-04	3.23E-03	2.50E-05	7.23E-06	8.19E+10	2.03E-25	1.10E-11	3.47E-12
33	6.53E-04	2.66E-03	2.02E-05	6.36E-06	8.21E+10	1.61E-25	9.42E-12	2.73E-12
34	6.13E-04	2.45E-03	1.85E-05	6.06E-06	8.21E+10	1.44E-25	8.75E-12	2.43E-12
35	3.26E-04	8.72E-04	5.82E-06	2.90E-06	8.28E+10	4.73E-26	4.14E-12	7.54E-13
36	5.85E-05	9.10E-05	3.83E-07	5.27E-07	8.42E+10	3.15E-27	6.68E-13	4.41E-14
37	1.68E-05	2.06E-05	5.29E-08	1.53E-07	8.51E+10	4.29E-28	1.74E-13	5.48E-15
38	4.41E-06	4.68E-06	6.39E-09	4.04E-08	8.61E+10	5.16E-29	4.19E-14	6.02E-16
39	1.43E-06	1.43E-06	1.08E-09	1.32E-08	8.69E+10	8.60E-30	1.25E-14	9.33E-17
40	5.14E-07	4.99E-07	2.15E-10	4.77E-09	8.75E+10	1.68E-30	4.19E-15	1.71E-17
41	2.00E-07	1.91E-07	4.83E-11	1.86E-09	8.81E+10	3.73E-31	1.52E-15	3.58E-18
42	8.94E-08	8.52E-08	1.36E-11	8.38E-10	8.86E+10	1.03E-31	6.37E-16	9.39E-19
43	5.46E-08	5.20E-08	6.17E-12	5.14E-10	8.89E+10	4.51E-32	3.66E-16	4.00E-19
44	3.47E-08	3.30E-08	2.98E-12	3.27E-10	8.92E+10	2.11E-32	2.20E-16	1.82E-19
45	1.45E-08	1.31E-08	7.01E-13	1.30E-10	8.97E+10	4.93E-33	8.26E-17	4.04E-20
46	8.63E-09	7.70E-09	2.94E-13	7.68E-11	9.00E+10	1.92E-33	4.38E-17	1.52E-20
47	5.32E-09	4.76E-09	1.32E-13	4.75E-11	9.03E+10	7.91E-34	2.41E-17	6.08E-21
48	4.07E-09	3.80E-09	8.79E-14	3.79E-11	9.04E+10	4.79E-34	1.72E-17	3.62E-21
49	3.34E-09	3.17E-09	6.40E-14	3.16E-11	9.06E+10	3.29E-34	1.34E-17	2.46E-21
50	2.11E-09	1.83E-09	2.67E-14	1.82E-11	9.08E+10	1.34E-34	7.30E-18	9.73E-22
51	1.50E-09	1.34E-09	1.54E-14	1.34E-11	9.10E+10	6.82E-35	4.63E-18	4.84E-22
52	1.33E-09	1.28E-09	1.34E-14	1.27E-11	9.11E+10	5.35E-35	3.93E-18	3.76E-22
53	7.10E-10	5.82E-10	3.94E-15	5.81E-12	9.15E+10	1.57E-35	1.72E-18	1.06E-22
54	5.67E-10	5.34E-10	3.10E-15	5.33E-12	9.16E+10	1.03E-35	1.29E-18	6.85E-23
55	3.67E-10	3.22E-10	1.39E-15	3.22E-12	9.18E+10	4.44E-36	7.36E-19	2.88E-23
56	2.46E-10	2.21E-10	7.25E-16	2.21E-12	9.21E+10	2.08E-36	4.42E-19	1.32E-23
57	2.06E-10	1.95E-10	5.68E-16	1.95E-12	9.21E+10	1.48E-36	3.51E-19	9.29E-24
58	1.63E-10	1.53E-10	3.80E-16	1.53E-12	9.23E+10	9.50E-37	2.61E-19	5.88E-24
59	1.29E-10	1.20E-10	2.52E-16	1.20E-12	9.24E+10	5.97E-37	1.91E-19	3.65E-24
60	1.08E-10	1.03E-10	1.92E-16	1.03E-12	9.25E+10	4.29E-37	1.53E-19	2.59E-24
61	8.58E-11	7.99E-11	1.27E-16	7.99E-13	9.26E+10	2.73E-37	1.13E-19	1.63E-24
62	7.12E-11	6.73E-11	9.42E-17	6.73E-13	9.27E+10	1.90E-37	8.83E-20	1.12E-24
63	6.16E-11	5.85E-11	7.37E-17	5.85E-13	9.28E+10	1.42E-37	7.25E-20	8.31E-25
64	5.32E-11	5.06E-11	5.73E-17	5.05E-13	9.28E+10	1.06E-37	5.95E-20	6.13E-25
65								
66	eq.12				Pa		coble-rt 9b	glide,lft 9b
67	%	t(i-1)	t(i-1)	t(i-1)			fraction	fraction
68	e-coble	e(Ti,ti-1)	e-glide	e-coble	E	Tp Coe	Ec	Es-gl
69	6.23E-04	na	na	na	7.69E+10	3.97E-22	6.48E-09	9.47E-07
70								

Table II-7. Listing of Top Rows of Sheer: "Creep-WP"

	A	B	C	D	E	F	G	H	I	J	K	L	M	N	O
1	file = AMR-F0155-V1.xls														
2	**Sheet = creep-WP**														
3				**Temp range**	0.135006637										
4	figure 1 from cdf&stress														
5				Zone1	Zone1	Zone2	Zone2	Zone 3	Zone 3	Zone 4	Zone 4	Zone 5	Zone 5	Zone 6	Zone 6
6	**CDF**	**Case Number**	**Stress, Mpa**	**Temperature adj.**	**Creep**	**Temperature adj.**	**Creep**	**Temperature adj.**	**Creep**	**Temperature adj.**	**Creep**	**Temperature adj.**	**Creep**	**Temperature adj.**	**Creep**
7	100.00	278	146.34	0.928	99.000	0.998	99.000	0.992	99.000	1.004	99.000	0.933	99.000	1.015	99.000
8	99.95	1814	137.15	0.935	99.000	0.863	99.000	0.877	99.000	1.109	100.000	0.962	99.000	1.028	99.000
9	99.90	1653	131.40	1.030	99.000	0.929	99.000	0.998	99.000	1.036	99.000	1.048	99.000	1.072	99.000
10	99.85	1282	122.57	1.112	100.000	1.112	100.000	0.967	99.000	1.108	100.000	1.072	99.000	0.985	99.000
11	99.80	837	108.37	0.947	99.000	1.029	99.000	0.921	99.000	0.964	99.000	1.071	99.000	0.998	99.000
12	99.75	730	105.69	1.029	99.000	1.108	99.000	1.058	99.000	0.921	99.000	0.863	99.000	0.853	99.000
13	99.70	1368	105.12	1.007	99.000	1.032	99.000	0.962	99.000	0.906	99.000	1.074	99.000	1.003	99.000
14	99.65	51	98.11	1.085	99.000	1.095	99.000	0.884	99.000	1.103	99.000	1.022	99.000	1.069	99.000
15	99.60	1660	96.79	0.907	99.000	1.089	99.000	0.916	99.000	1.101	99.000	1.064	99.000	0.952	99.000
16	99.55	484	94.99	1.010	99.000	1.046	99.000	1.100	99.000	1.080	99.000	1.026	99.000	0.973	99.000
17	99.50	242	94.75	0.868	99.000	0.920	99.000	0.938	99.000	0.960	99.000	0.929	99.000	1.041	99.000
18	99.45	1675	93.75	0.939	99.000	0.961	99.000	1.088	99.000	0.855	99.000	1.050	99.000	0.987	99.000
19	99.40	346	92.04	0.912	99.000	0.935	99.000	0.935	99.000	1.021	99.000	1.057	99.000	0.878	99.000
20	99.35	756	91.45	0.988	99.000	1.090	99.000	1.027	99.000	1.064	99.000	0.872	99.000	0.935	99.000
21	99.30	994	89.98	0.936	99.000	1.121	99.000	0.958	99.000	1.034	99.000	1.077	99.000	0.834	99.000
22	99.25	881	89.81	0.893	99.000	0.971	99.000	0.896	99.000	0.951	99.000	1.029	99.000	0.895	99.000
23	99.20	860	87.96	1.006	99.000	1.066	99.000	0.943	99.000	0.951	99.000	0.910	99.000	1.054	99.000
24	99.15	1000	87.70	0.874	99.000	1.078	99.000	0.874	99.000	0.960	99.000	1.005	99.000	1.037	99.000
25	99.10	1848	87.17	1.103	99.000	0.899	99.000	1.068	99.000	1.075	99.000	0.940	99.000	0.819	99.000
26	99.05	1270	87.08	1.104	99.000	0.897	99.000	1.082	99.000	1.012	99.000	1.082	99.000	0.914	99.000
27	99.00	1418	87.07	0.879	99.000	1.022	99.000	1.110	99.000	1.056	99.000	0.851	99.000	0.976	99.000
28	98.95	1274	85.20	0.919	2.083	1.066	4.503	0.877	2.049	0.868	2.043	0.856	2.036	0.843	2.030
29	98.90	769	84.03	0.926	2.007	0.897	1.982	1.098	7.642	1.095	7.306	0.933	2.014	1.004	2.306
30	98.85	1289	83.59	1.032	2.716	0.986	2.132	0.955	2.018	0.988	2.142	0.969	2.054	0.900	1.956
31	98.80	1696	83.39	0.972	2.050	0.927	1.965	0.910	1.950	1.090	6.282	1.046	3.110	0.890	1.935
32	98.75	1502	83.14	0.994	2.144	1.026	2.550	1.103	8.085	1.110	9.561	1.028	2.584	0.985	2.089
33	98.70	1851	82.22	1.078	4.691	1.043	2.852	0.923	1.886	1.008	2.202	0.870	1.846	0.944	1.909
34	98.65	1051	82.15	1.014	2.266	1.083	5.153	0.943	1.904	0.890	1.855	0.861	1.837	0.881	1.849
35	98.60	258	80.42	1.044	2.666	1.009	2.069	1.031	2.365	1.024	2.243	0.861	1.732	1.061	3.266
36	98.55	1129	78.05	0.911	1.633	0.938	1.657	1.059	2.849	0.855	1.598	1.079	3.826	0.910	1.633
37	98.50	905	77.80	0.997	1.793	0.940	1.646	0.859	1.587	1.102	5.834	1.068	3.182	0.850	1.583
38	98.45	655	77.70	1.127	10.227	1.060	2.832	1.083	4.087	1.097	5.296	0.892	1.601	1.050	2.523
39	98.40	1065	77.59	0.989	1.742	1.012	1.884	0.892	1.595	0.904	1.604	0.939	1.633	0.975	1.693
40	98.35	1723	77.39	1.078	3.679	0.957	1.644	0.943	1.626	0.868	1.569	0.924	1.609	0.948	1.632

Table II-8. Listing of top Rows of Sheet: "Fail-Calc"

	A	B	C	D	E	F	G	H	I	J	K	L	M
1	file = AMR-F0155-V1.xls												
2	**sheet = fail calc**				Creep and SSC, table used for Figure 8				Creep only				
3				**Shift**	**WP Peak TC**	**Upper Limit**	**Mean fail fra.**	**Lower limit**	**Upper Limit**	**Mean fail fra.**	**Lower limit**		
4				**-150**	127	0.1942	0.0244	0.0105					
5				-100	177	0.1942	0.0244	0.0105	0.19415714	0.019552	0.001381		
6				-50	227	0.1949	0.0244	0.0105					
7				-25	252	0.2057	0.0258	0.0105					
8				-15	262	0.2156	0.0267	0.0105					
9				0	277	0.2479	0.0339	0.0106					
10				15	292	0.3264	0.0604	0.0120					
11				20	297	0.3628	0.0783	0.0133					
12				25	302	0.4080	0.0987	0.0173					
13				35	312	0.5052	0.1622	0.0370					
14				50	327	0.6379	0.3019	0.1067					
15				75	352	0.8227	0.5567	0.3424					
16				100	377	0.9553	0.7789	0.5920					
17				125	402	0.9970	0.9302	0.7986					
18				135	412	0.9985	0.9658	0.8720					
19					Above Table used for Fig. 8								
20													
21													
22	**Strain Uncertanty**	0.8	**Summary**	**0**	**277**	**0.2479**	**0.0339**	**0.0106**					
23	**Upper fail index**	0.4		Product		0.0053	0.0009	0.0002			0.0079	0.0014	0.0003
24	**lower fail index**	11.7		Weight		0.0191	0.0191	0.0191			0.0286	0.0286	0.0286
25				**Fail Fract.**		0.2790	0.0450	0.0105			0.2755	0.0495	0.0105
26				**Zone1**	Zone1	Zone1	Zone1	Zone1	**Zone2**	Zone2	Zone2	Zone2	Zone2
27		**Case Number**	**Stress**	**Creep**	Fail criteria	Upper Fail index	Mean fail index	lower fail index	**Creep**	**Fail criteria**	Upper Fail index	Mean fail index	lower fail index
28	**CCDF**	**Case Number**	**Mpa**										
29	100.00	278	146.34	99.00	0.95	1	1	1	99.00	8.97	1	1	1
30	99.95	1814	137.15	99.00	4.70	1	1	1	99.00	4.70	1	1	1
31	99.90	1653	131.40	99.00	2.16	1	1	1	99.00	4.70	1	1	1
32	99.85	1282	122.57	100.00	0.65	1	1	1	100.00	2.02	1	1	1
33	99.80	837	108.37	99.00	2.58	1	1	1	99.00	5.25	1	1	1
34	99.75	730	105.69	99.00	1.04	1	1	1	99.00	1.80	1	1	1
35	99.70	1368	105.12	99.00	2.40	1	1	1	99.00	1.10	1	1	1
36	99.65	51	98.11	99.00	0.79	1	1	1	99.00	9.44	1	1	1
37	99.60	1660	96.79	99.00	4.70	1	1	1	99.00	6.00	1	1	1
38	99.55	484	94.99	99.00	0.83	1	1	1	99.00	0.90	1	1	1
39	99.50	242	94.75	99.00	2.41	1	1	1	99.00	2.43	1	1	1
40	99.45	1675	93.75	99.00	1.01	1	1	1	99.00	4.37	1	1	1

Table II-9. Listing of Top Rows of Sheet: "Rand #"

	A	B	C	D	E	F	G	H	I	J	K	L	M	N	O	P
1	This sheet contains columns of random numbers used for the Fuel Rod Characteristics analysis.										file = AMR-F0155-V1.xls					
2	Each column is used for the calculation noted at the column title.										**Sheet = Rand #**			Test mean=		0.499266
3														Test median=		0.498918
4	**Temp C Zone 1**	**Temp C Zone 2**	**C Fail 1**	**C fail 2**	**C fail3**	**Temp C Zone 3**	**Temp C Zone 4**	**Temp C Zone 5**	**Temp C Zone 6**	**Creep Zone 1**	**Creep Zone 2**	**Creep Zone 3**	**Creep Zone 4**	**Creep Zone 5**	**Creep Zone 6**	**sample Numb.**
5	0.232125157	0.516956	0.898514	0.341278	0.252533	0.511765	0.5829651	0.372403	0.774887	0.907806	0.565085	0.78631	0.291068	0.008969	0.304836	278
6	0.260801258	0.013344	0.202301	0.325831	0.527147	0.080065	0.9805385	0.483736	0.827744	0.082132	0.156488	0.477543	0.877331	0.632386	0.522495	1814
7	0.611550437	0.260707	0.60249	0.961042	0.184783	0.532937	0.7045435	0.814733	0.997821	0.538518	0.795879	0.497769	0.025485	0.024826	0.676389	1653
8	0.916302715	0.942135	0.962604	0.856405	0.362758	0.417997	0.9748709	0.904772	0.658456	0.001064	0.642174	0.045457	0.446272	0.929563	0.921059	1282
9	0.303152686	0.633244	0.464965	0.313843	0.050209	0.245376	0.4313241	0.902375	0.707738	0.37262	0.800444	0.416413	0.337563	0.113341	0.489146	837
10	0.608346534	0.928968	0.860576	0.868715	0.571496	0.758004	0.2687656	0.10529	0.141523	0.801439	0.531167	0.694463	0.556408	0.709841	0.083036	730
11	0.525643003	0.645791	0.562003	0.642536	0.809432	0.398187	0.2128283	0.911822	0.729427	0.674119	0.837233	0.223768	0.974851	0.740532	0.542972	1368
12	0.814069086	0.878078	0.942233	0.120734	0.667336	0.108182	0.9557985	0.715991	0.985694	0.714568	0.147389	0.527129	0.468213	0.583775	0.009915	51
13	0.154437886	0.855915	0.204424	0.209041	0.862437	0.228251	0.9494977	0.875037	0.527814	0.589483	0.100436	0.041125	0.281319	0.57724	0.142589	1660
14	0.537888612	0.697416	0.931116	0.541668	0.418117	0.918156	0.87147	0.731154	0.609767	0.678485	0.347365	0.242657	0.302111	0.639761	0.817272	484
15	0.012881751	0.224804	0.523471	0.558834	0.174458	0.311268	0.4175848	0.359659	0.877115	0.840512	0.939072	0.99203	0.449321	0.419228	0.568701	242
16	0.272310328	0.380314	0.877117	0.088857	0.152823	0.872308	0.0213482	0.821689	0.667509	0.167748	0.327253	0.377774	0.527356	0.827036	0.011365	1675
17	0.173095511	0.282452	0.385406	0.57389	0.332895	0.299575	0.6460735	0.849652	0.239043	0.217598	0.393851	0.968861	0.46561	0.171292	0.892369	346
18	0.455396338	0.860426	0.220105	0.270136	0.729667	0.643266	0.8090247	0.141085	0.461249	0.173429	0.471333	0.048189	0.146099	0.960079	0.823007	756
19	0.262097141	0.974244	0.411747	0.358742	0.282369	0.384184	0.6968916	0.923988	0.064526	0.499425	0.370053	0.268013	0.293764	0.908877	0.852225	994
20	0.104180317	0.415629	0.817962	0.885715	0.273157	0.154268	0.3817272	0.741897	0.304504	0.662366	0.1651	0.38071	0.782422	0.280987	0.363107	881
21	0.523601867	0.770218	0.7902	0.472109	0.191046	0.330107	0.3839852	0.285223	0.928834	0.207384	0.519091	0.060718	0.954674	0.223067	0.586194	860
22	0.03158437	0.814461	0.486774	0.96999	0.683511	0.071018	0.4166439	0.650973	0.863908	0.266536	0.415849	0.027207	0.887569	0.091811	0.03196	1000
23	0.882318223	0.148933	0.428463	0.786398	0.801301	0.79784	0.8507878	0.400024	0.005518	0.866388	0.354817	0.844226	0.268876	0.111094	0.183474	1848
24	0.884378554	0.140584	0.059966	0.288652	0.727938	0.848031	0.6145644	0.944955	0.379771	0.264858	0.288673	0.696882	0.932439	0.348612	0.036161	1270
25	0.051703482	0.605217	0.459057	0.59192	0.056347	0.954266	0.7790187	0.058199	0.623037	0.076714	0.431409	0.285329	0.597299	0.555278	0.952178	1418
26	0.201558558	0.772629	0.859033	0.338219	0.679984	0.080997	0.0693279	0.078083	0.102318	0.861205	0.600412	0.254087	0.481931	0.413529	0.658711	1274
27	0.226445835	0.141331	0.059152	0.853156	0.680851	0.907389	0.9279805	0.372846	0.731816	0.9021	0.847846	0.523331	0.754028	0.690311	0.415791	769
28	0.617316359	0.474331	0.226888	0.000613	0.242927	0.373387	0.5228757	0.510876	0.326576	0.405368	0.553833	0.134339	0.720795	0.381479	0.501697	1289
29	0.39518612	0.25315	0.135734	0.505745	0.398258	0.205293	0.9070353	0.806201	0.285979	0.700445	0.742133	0.162156	0.067707	0.198539	0.138376	1696
30	0.476381941	0.622672	0.753326	0.573011	0.439503	0.925896	0.9826611	0.737173	0.657319	0.276697	0.57785	0.746092	0.642148	0.838553	0.891215	1502
31	0.788442292	0.684409	0.262751	0.63772	0.094331	0.253119	0.5999432	0.129762	0.496581	0.377893	0.674795	0.605688	0.578291	0.742935	0.903628	1851
32	0.553292172	0.835082	0.720968	0.003514	0.768129	0.329453	0.1537642	0.098457	0.251898	0.404138	0.031788	0.852339	0.692154	0.854748	0.815359	1051
33	0.662464615	0.56007	0.257341	0.857962	0.114005	0.657153	0.6566995	0.09525	0.954779	0.318068	0.343866	0.524909	0.427381	0.192976	0.212502	258
34	0.168922185	0.294365	0.197952	0.122797	0.274607	0.762047	0.0203188	0.931454	0.3647	0.390098	0.178208	0.207206	0.779757	0.029485	0.826781	1129

Table II-10a. Listing of Top Rows of Sheet: "TempC"

	A	B	C	D	E	F	G	H	I	J	K	L
1	file = AMR-F0155-V1.xls											
2	**Sheet = TmpC (Temperature, C)**											
3	Temperature Calculations				Components of below table shown on Fig. 2, Table 2							
4					radal zone	1	2	3	4	5	6	sum
5					Fraction	1.91E-02	2.86E-02	0.11429	2.10E-01	0.33333	0.29524	1.0000
6		average			TC Adj (inWP).	1	9.334E-01	0.887987	0.819805	0.660714	0.446429	
7					**TC adj (gross)**	**1**	**0.99334703**	**0.988804**	**0.981988**	**0.966086**	**0.944667**	
8	YMP-Time	WP Wall TC			inside WO Delta TC	Zone1, Center rod TC	Z 2	Z 3	Z 4	Z 5	Z 6	
9	0	24.61			38.20	62.81	60.27	58.53	55.93	49.85	41.66	
10	50	82.26			38.20	120.46	117.92	116.18	113.58	107.50	99.31	
11	50.2	176.54			33.90	210.44	208.18	206.64	204.33	198.93	191.67	
12	50.4	193.16			33.10	226.26	224.06	222.55	220.30	215.03	207.94	
13	50.6	209.79			32.80	242.59	240.40	238.91	236.67	231.46	224.43	
14	50.8	226.41			32.50	258.91	256.75	255.27	253.05	247.88	240.92	
15	51	243.03			32.20	275.23	273.09	271.63	269.43	264.31	257.41	
16	52	266.46			31.40	297.86	295.77	294.34	292.20	287.20	280.47	
17	**53**	**277.33**			**30.80**	**308.13**	**306.08**	**304.68**	**302.58**	**297.68**	**291.08**	
18	55	275.61			29.70	305.31	303.33	301.98	299.95	295.23	288.86	
19	57	273.88			28.90	302.78	300.85	299.54	297.57	292.97	286.78	
20	59	272.15			28.20	300.35	298.47	297.19	295.27	290.78	284.74	
21	60	271.29			27.90	299.19	297.33	296.06	294.16	289.72	283.74	
22	70	262.65			25.10	287.75	286.08	284.94	283.23	279.23	273.86	
23	80	238.65			23.00	261.65	260.12	259.07	257.50	253.84	248.92	
24	90	222.46			21.40	243.86	242.44	241.47	240.01	236.60	232.02	
25	100	206.28			19.90	226.18	224.85	223.95	222.59	219.43	215.16	
26	110	193.19			18.90	212.09	210.83	209.97	208.68	205.68	201.63	
27	120	181.91			18.00	199.91	198.71	197.89	196.67	193.80	189.95	
28	130	172.06			17.10	189.16	188.02	187.24	186.07	183.35	179.69	
29	140	164.01			16.30	180.31	179.23	178.48	177.37	174.78	171.29	
30	150	159.43			15.40	174.83	173.81	173.11	172.06	169.61	166.31	
31	160	154.86			15.03	169.89	168.89	168.20	167.18	164.79	161.57	
32	180	146.41			14.29	160.70	159.75	159.10	158.13	155.86	152.79	
33	205	141.57			13.37	154.94	154.05	153.44	152.53	150.40	147.54	
34	232	137.27			12.37	149.63	148.81	148.25	147.41	145.44	142.79	
35	250	134.99			11.70	146.69	145.91	145.38	144.58	142.72	140.22	
36	265	133.10			11.43	144.53	143.77	143.25	142.47	140.65	138.20	
37	310	128.79			10.62	139.41	138.70	138.22	137.49	135.80	133.53	
38	350	125.73			9.90	135.63	134.97	134.52	133.84	132.27	130.15	
39	365	124.58			9.71	134.29	133.64	133.20	132.54	130.99	128.91	
40	450	119.04			8.60	127.64	127.07	126.68	126.09	124.72	122.88	
41	480	117.09			8.30	125.39	124.84	124.46	123.89	122.57	120.79	
42	550	113.40			7.60	121.00	120.49	120.15	119.63	118.42	116.79	
43	615	109.97			7.15	117.12	116.64	116.32	115.83	114.69	113.16	
44	650	108.49			6.90	115.39	114.93	114.62	114.15	113.05	111.57	
45	695	106.59			6.59	113.17	112.73	112.43	111.98	110.94	109.53	
46	750	104.68			6.20	110.88	110.46	110.18	109.76	108.77	107.44	
47	790	103.29			5.96	109.25	108.85	108.58	108.17	107.22	105.95	
48	850	101.45			5.60	107.05	106.67	106.42	106.04	105.15	103.95	
49	900	99.91			5.40	105.31	104.95	104.71	104.34	103.48	102.32	
50	950	98.71			5.20	103.91	103.57	103.33	102.98	102.15	101.04	
51	1000	97.52			5.00	102.52	102.18	101.96	101.61	100.82	99.75	
52	Columns A,B E F used if Fig. 4											

Table II-10b. Listing of Rows 53 to 72 of Sheet: "TempC"

	A	B	C	D	E	F	G	H	I	J	K	L
53	file = AMR-F0155-V1.xls											
54	**Sheet = TmpC (Temperature, C)**											
55	WP wall shift TC	0.00E+00	(defined fail calc sheet)									
56		**Calculation of shaping factors for temperatures across WP**										
57	Location	Temperature	points averaged	Zone TC	delta TC from surface	reduction factor						
58	1	313.4	1	313.4	30.8	1						
59	2	309.3	1&2	311.35	28.75	0.9334416						
60	3	308.8	5&6	309.95	27.35	0.887987						
61	4	308.8	6&7	307.85	25.25	0.8198052						
62	5	309	9&10	302.95	20.35	0.6607143						
63	6	310.9	10&11	296.35	13.75	0.4464286						
64	7	304.8										
65	8	304.3										
66	9	304.1										
67	10	301.8										
68	11	290.9										
69	12	289.8										
70	13	283.4										
71	14	282.9										
72	15	282.6										

Table II-11a. Listing of Top Rows of Sheet: "TempC2"

	A	B	C	D	E	F	G	H	I	J	K	L	M	N	O	P	Q
1	file = AMR-F0155-V1.xls		**sheet = TempC2**														
2	Takes input temperatures for WP and interior and aligns them up to the same time steps																
3	Average Waste Package Surface Temp (C)																
4	RIP_Tavg_csnf_dsps_bc_bin20-60_mean			*Radial Temperature Distribution for EDA II (Axial Peaking Factor of 1.102)*													
5	Time(yr)	Bin Weight= 0.528528		Time (years)	WP Heat (W)	Node											
6	Time, Yr	T,C				1	2	3	4	5	6	7	8	9	10	11	12
7	0.0	24.6		50	4374.9	147.5	139.8	139.1	139.1	139.5	145.0	135.3	134.8	134.5	135.1	119.8	118.6
8	1.0	78.7		50.1	4369.5	236.9	231.5	230.9	231.0	231.2	234.4	226.9	226.5	226.2	224.9	212.5	211.4
9	2.0	87.2		50.2	4364.2	263.0	258.0	257.4	257.4	257.7	260.4	253.2	252.8	252.5	250.7	238.4	237.3
10	5.0	95.0		50.3	4359.0	273.0	268.1	267.5	267.6	267.8	270.4	263.4	262.9	262.6	260.8	248.8	247.6
11	30.0	90.6		50.4	4353.5	278.8	274.0	273.5	273.5	273.7	276.2	269.3	268.9	268.6	266.7	254.7	253.6
12	40.0	85.7		50.5	4348.3	282.9	278.1	277.6	277.6	277.9	280.3	273.4	273.0	272.7	270.7	258.9	257.8
13	50.0	82.3		50.6	4342.8	286.0	281.3	280.8	280.8	281.0	283.4	276.6	276.2	275.9	273.9	262.1	261.0
14	50.2	176.5		50.7	4337.6	288.7	284.0	283.5	283.5	283.8	286.1	279.4	278.9	278.6	276.5	264.9	263.8
15	51.0	243.0		50.8	4332.3	291.0	286.4	285.9	285.9	286.1	288.4	281.8	281.3	281.0	278.9	267.3	266.2
16	52.0	266.5		50.9	4327.1	293.0	288.5	288.0	288.0	288.2	290.4	283.8	283.4	283.1	281.0	269.4	268.3
17	53.0	277.3		51	4321.6	294.8	290.3	289.8	289.8	290.0	292.2	285.7	285.2	284.9	282.8	271.3	270.2
18	70.0	262.7		52	4269.1	306.3	302.0	301.5	301.5	301.7	303.7	297.4	297.0	296.7	294.4	283.3	282.2
19	80.0	238.6		**53**	**4217.0**	**313.4**	**309.3**	**308.8**	**308.8**	**309.0**	**310.9**	**304.8**	**304.3**	**304.1**	**301.8**	**290.9**	**289.8**
20	100.0	206.3		54	4165.8	317.9	313.9	313.4	313.4	313.6	315.4	309.4	309.0	308.7	306.4	295.7	294.7
21	110.0	193.2		55	4115.0	321.2	317.3	316.8	316.8	317.0	318.8	312.9	312.5	312.2	309.9	299.4	298.3
22	120.0	181.9		56	4064.8	323.4	319.6	319.1	319.1	319.3	321.0	315.2	314.8	314.5	312.2	301.9	300.9
23	130.0	172.1		57	4015.4	324.8	321.0	320.5	320.5	320.7	322.4	316.7	316.3	316.0	313.7	303.5	302.5
24	140.0	164.0		58	3966.5	325.7	322.0	321.5	321.5	321.7	323.4	317.7	317.3	317.1	314.8	304.8	303.8
25	160.0	154.9		59	3918.2	325.8	322.1	321.6	321.7	321.9	323.5	317.9	317.5	317.3	315.0	305.1	304.1
26	180.0	146.4		60	3881.0	325.4	321.7	321.3	321.3	321.5	323.1	317.6	317.2	316.9	314.7	304.9	303.9
27	205.0	141.6		70	3670.6	320.5	317.2	316.7	316.8	316.9	318.4	313.4	313.1	312.8	310.9	302.0	301.1
28	232.0	137.3		80	3481.2	309.7	306.6	306.2	306.2	306.4	307.8	303.2	302.9	302.6	300.9	292.8	292.0
29	265.0	133.1		90	3308.6	298.4	295.4	295.1	295.1	295.2	296.7	292.3	292.0	291.8	290.3	282.7	282.0
30	310.0	128.8		100	3152.7	287.9	285.1	284.7	284.7	284.9	286.3	282.2	281.9	281.7	280.4	273.3	272.6
31	365.0	124.6		110	2511.0	281.8	279.1	278.8	278.8	278.9	280.3	276.4	276.1	275.9	274.7	268.0	267.3
32	420.0	120.8		120	2369.0	275.9	273.3	273.0	273.0	273.1	274.5	270.7	270.5	270.3	269.2	262.8	262.2
33	480.0	117.1		130	2235.0	269.4	266.9	266.6	266.6	266.7	268.0	264.4	264.2	264.0	263.0	256.9	256.3
34	545.0	113.4		140	2108.6	262.3	259.8	259.5	259.5	259.7	261.0	257.5	257.3	257.2	256.3	250.4	249.8
35	615.0	110.0		150	1989.3	254.7	252.4	252.1	252.1	252.2	253.5	250.2	250.0	249.9	249.0	243.4	242.9
36	695.0	106.6		250	1448.6	222.7	220.8	220.6	220.6	220.7	221.8	219.2	219.0	218.9	218.5	214.2	213.8
37	790.0	103.3		350	1306.2	206.3	204.6	204.5	204.5	204.5	205.6	203.3	203.2	203.1	202.8	199.1	198.8
38	900.0	99.9		450	1193.2	194.9	193.4	193.3	193.3	193.4	194.3	192.3	192.2	192.1	191.9	188.7	188.4
39	1030.0	96.8		550	1101.5	185.5	184.1	184.0	184.0	184.1	184.9	183.1	183.0	183.0	182.8	180.0	179.7
40				650	1025.9	178.1	176.8	176.7	176.7	176.8	177.6	175.9	175.9	175.8	175.7	173.1	172.9
41				750	957.6	171.5	170.4	170.2	170.3	170.3	171.0	169.6	169.5	169.4	169.3	167.0	166.8
42				850	895.4	165.9	164.8	164.8	164.8	164.8	165.5	164.1	164.0	164.0	163.9	161.8	161.6
43				950	586.1	161.2	160.2	160.2	160.2	160.2	160.8	159.6	159.5	159.5	159.4	157.5	157.3
44				1050	539.9	157.5	156.6	156.5	156.5	156.6	157.2	156.0	155.9	155.9	155.9	154.0	153.9

Table II-11b. Listing of Rows 45 to 92 of Sheet: "TempC2"

	A	B	C	D	E	F	G	H	I	J	K	L	M	N	O
45	file = AMR-F0155-V1.xls		**sheet = TempC2**												
46	Time(yr)	Bin Weight= 0.528528	Tc, Interpolate	Time, WP internals	Internal del TC	Internal Delta Tc, Interpolated	WP Temp	Dellt Tc internal	Center Rod Temperature			Uncertainties			
47	Time, Yr	T,C, WP	T,C,WP	time, yr	Tc	Tc	Tc	Tc	Tc						
48	0.0	24.6		0	38.2		24.6	38.2	62.8			WP surface			
49	50.0	82.3		50	38.2		82.3	38.2	120.5			Max -avg		22.1	deg C
50	50.2	176.5		50.2	33.9		176.5	33.9	210.4						
51	50.4		193.1605	50.4	33.1		193.2	33.1	226.3			unceert interior		19.5	
52	50.6		209.785	50.6	32.8		209.8	32.8	242.6			air vs He			
53	50.8		226.4095	50.8	32.5		226.4	32.5	258.9				Sum	41.6	
54	51.0	243.0		51	32.2		243.0	32.2	275.2						
55	52.0	266.5		52	31.4		266.5	31.4	297.9			fraction uncert		0.135007	
56	53.0	277.3	277.333	**53**	30.8		**277.3**	**30.8**	**308.1**						
57	55		275.605706	55	29.7		275.6	29.7	305.3						
58	57		273.878412	57	28.9		273.9	28.9	302.8						
59	59		272.151118	59	28.2		272.2	28.2	300.4						
60	60		271.287471	60	27.9		271.3	27.9	299.2						
61	70.0	262.7		70	25.1		262.7	25.1	287.8						
62	80.0	238.6		80	23		238.6	23	261.6						
63	90		222.463	90	21.4		222.5	21.4	243.9						
64	100.0	206.3		100	19.9		206.3	19.9	226.2						
65	110.0	193.2		110	18.9		193.2	18.9	212.1						
66	120.0	181.9		120	18		181.9	18	199.9						
67	130.0	172.1		130	17.1		172.1	17.1	189.2						
68	140.0	164.0		140	16.3		164.0	16.3	180.3						
69	150		159.4335	150	15.4		159.4	15.4	174.8						
70	160.0	154.9		160.0		15.03	154.9	15.03	169.9						
71	180.0	146.4		180.0		14.29	146.4	14.29	160.7						
72	205.0	141.6		205.0		13.365	141.6	13.365	154.9						
73	232.0	137.3		232.0		12.366	137.3	12.366	149.6						
74	250		134.992364	250	11.7		135.0	11.7	146.7						
75	265.0	133.1		265.0		11.43	133.1	11.43	144.5						
76	310.0	128.8		310.0		10.62	128.8	10.62	139.4						
77	350		125.728091	350	9.9		125.7	9.9	135.6						
78	365.0	124.6		365.0		9.705	124.6	9.705	134.3						
79	450.0		119.042696	450	8.6		119.0	8.6	127.6						
80	480.0	117.1		480.0		8.3	117.1	8.3	125.4						
81	550.0		113.397704	550	7.6		113.4	7.6	121.0						
82	615.0	110.0		615.0		7.145	110.0	7.145	117.1						
83	650.0		108.490063	650	6.9		108.5	6.9	115.4						
84	695.0	106.6		695.0		6.585	106.6	6.585	113.2						
85	750.0		104.675474	750	6.2		104.7	6.2	110.9						
86	790.0	103.3		790.0		5.96	103.3	5.96	109.2						
87	850.0		101.446073	850	5.6		101.4	5.6	107.0						
88	900.0	99.9		900.0		5.4	99.9	5.4	105.3						
89	950.0		98.7139538	950	5.2		98.7	5.2	103.9						
90	1000.0		97.5151077	1000		5	97.5	5	102.5						
91	1030.0	96.8		1050	4.8										
92															

Table II-12. Listing of Top Rows of Sheet: "Unzip"

	A	B	C	D	E	F	G	H	I	J	K	L
1	file = AMR-F0155-V1.xls											
2	Sheet = Unzip											
3	velocity conversion =		0.0000219	cm/yr /(mg/m2-d)			Fuel length	366	cm			
4	**log10(rate) = a0 + a1/Tk + a2* PCO3 + a3* PO2 + a4 * pH**											
5			**Term=**	**a0**	**a1**	**a2**	**a3**	**a4**				
6	**Basic**	**pH>7**		**4.69**	**-1085**	**-0.12**	**-0.32**	**0**		E10 to E25 and L10 to L25		
7	**Acidic**	**pH< =7**		**7.13**	**-1085**	**0**	**-0.32**	**-0.41**		used in Figure 13		
8	**Example calculation**				**Tc**	**PCo3**	**PO2**	**pH**				
9	**dis Rate**	**log10(dis rt)**	**Acidic solution**	**Basic solution**	**Tc**	**PCo3**	**PO2**	**pH**	**M-CO3**	**Atm. O2**	**Velocity, cm/yr**	**yrs to unzip**
10	15.757	1.197	0.7175	1.1975	100	3	0.69897	8	0.001	0.2	1.38E-02	1.33E+04
11	14.387	1.158	0.6780	1.1580	95	3	0.69897	8	0.001	0.2	1.26E-02	1.45E+04
12	13.102	1.117	0.6373	1.1173	90	3	0.69897	8	0.001	0.2	1.15E-02	1.59E+04
13	11.902	1.076	0.5956	1.0756	85	3	0.69897	8	0.001	0.2	1.04E-02	1.76E+04
14	10.781	1.033	0.5527	1.0327	80	3	0.69897	8	0.001	0.2	9.44E-03	1.94E+04
15	9.739	0.989	0.5085	0.9885	75	3	0.69897	8	0.001	0.2	8.53E-03	2.15E+04
16	8.771	0.943	0.4631	0.9431	70	3	0.69897	8	0.001	0.2	7.68E-03	2.38E+04
17	7.875	0.896	0.4163	0.8963	65	3	0.69897	8	0.001	0.2	6.90E-03	2.65E+04
18	7.048	0.848	0.3681	0.8481	60	3	0.69897	8	0.001	0.2	6.17E-03	2.96E+04
19	6.286	0.798	0.3184	0.7984	55	3	0.69897	8	0.001	0.2	5.51E-03	3.32E+04
20	5.587	0.747	0.2672	0.7472	50	3	0.69897	8	0.001	0.2	4.89E-03	3.74E+04
21	4.947	0.694	0.2144	0.6944	45	3	0.69897	8	0.001	0.2	4.33E-03	4.22E+04
22	4.364	0.640	0.1599	0.6399	40	3	0.69897	8	0.001	0.2	3.82E-03	4.79E+04
23	3.834	0.584	0.1036	0.5836	35	3	0.69897	8	0.001	0.2	3.36E-03	5.45E+04
24	3.353	0.525	0.0455	0.5255	30	3	0.69897	8	0.001	0.2	2.94E-03	6.23E+04
25	3.834	0.584	0.1036	0.5836	35	3	0.69897	8	0.001	0.2	3.36E-03	5.45E+04
26	Variation in pH			H27 to H40 and L27 to L40 used for Figure 14								
27	55.412	1.744	1.7436	0.5836	35	3	0.69897	4	0.001	0.2	4.85E-02	3.77E+03
28	34.562	1.539	1.5386	0.5836	35	3	0.69897	4.5	0.001	0.2	3.03E-02	6.04E+03
29	21.558	1.334	1.3336	0.5836	35	3	0.69897	5	0.001	0.2	1.89E-02	9.69E+03
30	13.446	1.129	1.1286	0.5836	35	3	0.69897	5.5	0.001	0.2	1.18E-02	1.55E+04
31	8.387	0.924	0.9236	0.5836	35	3	0.69897	6	0.001	0.2	7.35E-03	2.49E+04
32	5.231	0.719	0.7186	0.5836	35	3	0.69897	6.5	0.001	0.2	4.58E-03	3.99E+04
33	3.834	0.584	0.5136	0.5836	35	3	0.69897	7	0.001	0.2	3.36E-03	5.45E+04
34	3.834	0.584	0.3086	0.5836	35	3	0.69897	7.5	0.001	0.2	3.36E-03	5.45E+04
35	3.834	0.584	0.1036	0.5836	35	3	0.69897	8	0.001	0.2	3.36E-03	5.45E+04
36	3.834	0.584	-0.1014	0.5836	35	3	0.69897	8.5	0.001	0.2	3.36E-03	5.45E+04
37	3.834	0.584	-0.3064	0.5836	35	3	0.69897	9	0.001	0.2	3.36E-03	5.45E+04
38	3.834	0.584	-0.5114	0.5836	35	3	0.69897	9.5	0.001	0.2	3.36E-03	5.45E+04
39	3.834	0.584	-0.7164	0.5836	35	3	0.69897	10	0.001	0.2	3.36E-03	5.45E+04
40	3.834	0.584	-0.9214	0.5836	35	3	0.69897	10.5	0.001	0.2	3.36E-03	5.45E+04